

UV-LED Lithography system using programmable light and tilt-rotational stage for 2D/3D  
microfabrication for micromachined RF devices

by

Sabera Fahmida Shiba

B.S., University of Dhaka, 2016

M.S., University of Dhaka, 2018

AN ABSTRACT OF A DISSERTATION

submitted in partial fulfillment of the requirements for the degree

DOCTOR OF PHILOSOPHY

Mike Wieggers Department of Electrical and Computer Engineering  
Carl R. Ice College of Engineering

KANSAS STATE UNIVERSITY  
Manhattan, Kansas

2022

## Abstract

In this dissertation, computer-controlled multidirectional UV-LED (Ultra-Violet Light Emitting Diode) lithography has been investigated for microscale three-dimensional (3-D) fabrication processes. The scalability, changeable light intensity, and multidirectional exposure capabilities of an array of UV-LEDs as a UV light source were described and investigated for the fabrication of both conventional semiconductor devices and advanced MEMS (Micro-Electro-Mechanical-Systems) devices. The UV-LED beam is diverging in nature and fades within a short distance. Therefore, commercial collimating equipment, like Fly's eye integrator is not suitable for the UV-LEDs. The primary contribution of this research is the development of a single lens collimation scheme for making a collimated UV-LED light source. A significant advantage of this scheme is that a high enough intensity is preserved even after collimation, facilitating millimeter-tall microfabrication. In the process of collimating the UV-LEDs individually, high contrast is observed, which is later compensated using a continuous rotation of the light source. Utilizing the independent control and the behavior of LED with the change of current and distance, additional features like regional control and adjustable intensities were added to the system.

The integration of a tilt-rotational sample holder introduces the opportunity to create 3D traces of the light on the target sample, which is unique among lithography systems. In addition, the adjustable intensities remunerate the non-uniformity of the intensity caused by the inclination of the sample. The light source combines 365 nm (i-line) and 405 nm (h-line), where the i-line spectrum is targeted for several hundred-micrometer tall microfabrication, and the h-line is targeted for millimeter tall microfabrication. With the functional scalability, a large-scale (8 inch<sup>2</sup>) light source has been demonstrated with two different optical designs, one using commercial Cabochons (Pandahall) as lenses and the other with customized hexagonal lenses.

The lithography system achieved collimation with a deviation of  $4.13^\circ$  with the commercial lens and a deviation of  $3^\circ$  with the hexagonal lens. An intensity of  $472 \text{ mW/cm}^2$  and  $258 \text{ mW/cm}^2$  were obtained from the H-line and I-line UV-LEDs respectively which is the highest so far. The high contrast of around 34% caused by the UV-LED matrix was minimized to around 2.5% by utilizing an orbital rotation of the LED arrays. The light source has been characterized for 8.5% uniformity. The 2D structures with a resolution of  $1.4 \mu\text{m}$  and the 3D vertical structures with a height of 3.14 mm have been demonstrated using different light profiles. Complex 3D microstructures like a flat bowtie, horn, bipod, tripod, open bowtie, double arrow, three-petalled flowers, and wind vanes were fabricated utilizing the programmable multidirectional functions.

A future direction of the research has been demonstrated where a self-tiltable UV-LED light source was built with an inclination range of  $+70^\circ$  to  $-70^\circ$ . This design helps eliminate the non-uniform exposure over an inclined sample and introduces a time-efficient complex 3D microfabrication method for liquid photoresists. An array of ultra-tall microstructure fabricated using the UV-LED lithography system showed the successful application as RF frequency-selective device in the 5G frequency range. Since the RF devices are strictly responsive to their parameters, a height of around several millimeters is needed for 5G device fabrication. The high intensity of the system was able to fabricate around 2.7 mm vertical pillars resonating to 27.8 GHz.

This lithography system can replace conventional UV lamps with higher and adjustable intensity ranges, larger exposure areas, multidirectional exposure, and user-friendly automatic lithography operations. In addition to tall and versatile 3D microfabrication, this system gives superior surface quality and higher production yield compared to similar technologies. With the versatile functionalities and demonstrated capabilities, this lithography tool has potential uses in bioMEMS, RF MEMS, sensors, and many other major semiconductor and MEMS applications.

UV-LED Lithography system using programmable light and tilt-rotational stage for 2D/3D  
microfabrication for micromachined RF devices

by

Sabera Fahmida Shiba

B.S., University of Dhaka, 2016

M.S., University of Dhaka, 2018

A DISSERTATION

submitted in partial fulfillment of the requirements for the degree

DOCTOR OF PHILOSOPHY

Mike Wieggers Department of Electrical and Computer Engineering  
Carl R. Ice College of Engineering

KANSAS STATE UNIVERSITY  
Manhattan, Kansas

2022

Approved by:

Major Professor  
Jungkwun 'JK' Kim

# Copyright

© Sabera Fahmida Shiba 2022.

## Abstract

In this dissertation, computer-controlled multidirectional UV-LED (Ultra-Violet Light Emitting Diode) lithography has been investigated for microscale three-dimensional (3-D) fabrication processes. The scalability, changeable light intensity, and multidirectional exposure capabilities of an array of UV-LEDs as a UV light source were described and investigated for the fabrication of both conventional semiconductor devices and advanced MEMS (Micro-Electro-Mechanical-Systems) devices. The UV-LED beam is diverging in nature and fades within a short distance. Therefore, commercial collimating equipment, like Fly's eye integrator is not suitable for the UV-LEDs. The primary contribution of this research is the development of a single lens collimation scheme for making a collimated UV-LED light source. A significant advantage of this scheme is that a high enough intensity is preserved even after collimation, facilitating millimeter-tall microfabrication. In the process of collimating the UV-LEDs individually, high contrast is observed, which is later compensated using a continuous rotation of the light source. Utilizing the independent control and the behavior of LED with the change of current and distance, additional features like regional control and adjustable intensities were added to the system.

The integration of a tilt-rotational sample holder introduces the opportunity to create 3D traces of the light on the target sample, which is unique among lithography systems. In addition, the adjustable intensities remunerate the non-uniformity of the intensity caused by the inclination of the sample. The light source combines 365 nm (i-line) and 405 nm (h-line), where the i-line spectrum is targeted for several hundred-micrometer tall microfabrication, and the h-line is targeted for millimeter tall microfabrication. With the functional scalability, a large-scale (8 inch<sup>2</sup>) light source has been demonstrated with two different optical designs, one using commercial Cabochons (Pandahall) as lenses and the other with customized hexagonal lenses.

The lithography system achieved collimation with a deviation of  $4.13^\circ$  with the commercial lens and a deviation of  $3^\circ$  with the hexagonal lens. An intensity of  $472 \text{ mW/cm}^2$  and  $258 \text{ mW/cm}^2$  were obtained from the H-line and I-line UV-LEDs respectively which is the highest so far. The high contrast of around 34% caused by the UV-LED matrix was minimized to around 2.5% by utilizing an orbital rotation of the LED arrays. The light source has been characterized for 8.5% uniformity. The 2D structures with a resolution of  $1.4 \mu\text{m}$  and the 3D vertical structures with a height of 3.14 mm have been demonstrated using different light profiles. Complex 3D microstructures like a flat bowtie, horn, bipod, tripod, open bowtie, double arrow, three-petalled flowers, and wind vanes were fabricated utilizing the programmable multidirectional functions.

A future direction of the research has been demonstrated where a self-tiltable UV-LED light source was built with an inclination range of  $+70^\circ$  to  $-70^\circ$ . This design helps eliminate the non-uniform exposure over an inclined sample and introduces a time-efficient complex 3D microfabrication method for liquid photoresists. An array of ultra-tall microstructure fabricated using the UV-LED lithography system showed the successful application as RF frequency-selective device in the 5G frequency range. Since the RF devices are strictly responsive to their parameters, a height of around several millimeters is needed for 5G device fabrication. The high intensity of the system was able to fabricate around 2.7 mm vertical pillars resonating to 27.8 GHz.

This lithography system can replace conventional UV lamps with higher and adjustable intensity ranges, larger exposure areas, multidirectional exposure, and user-friendly automatic lithography operations. In addition to tall and versatile 3D microfabrication, this system gives superior surface quality and higher production yield compared to similar technologies. With the versatile functionalities and demonstrated capabilities, this lithography tool has potential uses in bioMEMS, RF MEMS, sensors, and many other major semiconductor and MEMS application.

# Table of Contents

List of Figures .....	xii
List of Tables .....	xvii
Acknowledgements .....	xviii
Dedication .....	xix
Preface .....	xx
Chapter 1 - Introduction .....	1
1.1 Introduction to UV-LED lithography .....	1
1.2 Motivation .....	6
Chapter 2 - Advanced features of UV-LEDs for 3D microlithography .....	11
2.1 Introduction: Novel features of UV-LEDs .....	11
2.2 Novel features of UV-LED .....	11
2.2.1 <i>Selectivity of wavelengths</i> .....	12
2.2.2 <i>High and adjustable intensity</i> .....	17
2.2.3 <i>Scalability of the system</i> .....	19
2.2.4 <i>Multidirectional exposure capability</i> .....	20
2.3 Summary .....	21
Chapter 3 - Developing a UV-LED lithography light source set up for high resolution and millimeter tall microfabrication and its characterization .....	22
3.1 Introduction: The development of UV-LED lithography system .....	22
3.2 Concept of the UV-LED lithography light source .....	24
3.3 Design of the UV-LED lithography system .....	26
3.3.1 <i>UV-LED and PCB design</i> .....	26
3.3.2 <i>Collimating structure</i> .....	28
3.3.3 <i>Linear mask alignment stage</i> .....	29
3.3.4 <i>Overall chassis design</i> .....	30
3.4 Characterization .....	31
3.4.1 <i>Collimation</i> .....	31
3.4.2 <i>High intensity with a variable range</i> .....	32
3.4.3 <i>Light homogeneity</i> .....	34

3.5 Additional features of the lithography system .....	36
3.6 Results.....	37
3.6.1 High-resolution micron devices fabrication .....	38
3.6.2 High aspect ratio micron device fabrication .....	39
3.6.3 Millimeter-tall device fabrication .....	40
3.6.4 3D inclined microstructure fabrication .....	41
3.7 Summary .....	42
Chapter 4 - Developing multidirectional lithography system for traditional and complex 2D/3D microfabrication.....	44
4.1 Introduction: Multidirectional lithography for complex 3D microfabrication .....	44
4.2 Concept of the multidirectional lithography system.....	46
4.3 System design .....	47
4.3.1 Light source .....	48
4.3.2 Multidirectional system.....	51
4.4 Characterization .....	52
4.4.1 Collimation for the PCB embedded UV-LEDs .....	52
4.4.2 Adjustable intensity with individual UV-LED control .....	53
4.4.3 Thermal control with advanced waveguide design and additional cooling methods ..	55
4.4.4 Homogeneity with the orbital motion of the light source.....	57
4.5 Microfabrication method .....	62
4.6 Results.....	65
4.6.1 High-resolution microfabrication .....	65
4.6.2 High aspect ratio and ultra-tall micro-tower fabrication.....	66
4.6.3 Non-conventional multidirectional complex 3D microfabrication.....	67
4.6.4 High production yield .....	68
4.7 Summary .....	69
Chapter 5 - Developing an advanced programmable multidirectional UV-LED lithography system for large scale microfabrication.....	71
5.1 Introduction: Programmable UV-LED lithography system for large scale production.....	71
5.2 Concept of the programmable multidirectional UV-LED lithography.....	73
5.3 System design .....	75

5.3.1	<i>Dual-wavelength light source</i> .....	75
5.3.2	<i>Large scale light source</i> .....	76
5.3.3	<i>Integrated programmable tilt-rotational sample holder</i> .....	76
5.3.4	<i>Software and programs</i> .....	77
5.3.5	<i>Completed integrated system</i> .....	79
5.4	<i>Characterization</i> .....	80
5.4.1	<i>Programmable light intensity with individual control</i> .....	81
5.4.2	<i>Homogeneity with dual-wavelength light source</i> .....	83
5.4.3	<i>Uniformity with dual-wavelength light source</i> .....	86
5.4.4	<i>Light source stability over longer time periods</i> .....	88
5.4.5	<i>Thermal stability for large scale setup</i> .....	89
5.5	<i>Second version of the light source</i> .....	91
5.5.1	<i>Compact honeycomb arrangement</i> .....	92
5.5.2	<i>Advanced hexagonal collimating structures</i> .....	93
5.5.3	<i>Advanced collimation with customized lenses</i> .....	95
5.5.4	<i>Homogeneity with the honeycomb arrangement</i> .....	97
5.6	<i>Results</i> .....	100
5.6.1	<i>Improved resolution with 365 nm UV-LEDs and high aspect ratio microfabrication</i> .....	100
5.6.2	<i>Surface quality comparison with the existing 3D printing system</i> .....	102
5.6.3	<i>Large scale productions</i> .....	102
5.6.4	<i>Versatility of the system</i> .....	104
5.7	<i>Performance analysis</i> .....	106
5.8	<i>Summary</i> .....	110
<b>Chapter 6 - Tilttable UV-LED lithography system for 3D microfabrication for solid and liquid photoresists</b> .....		
		112
6.1	<i>Introduction to tilttable UV-LED lithography</i> .....	112
6.2	<i>Concept of the tilttable UV-LED lithography system</i> .....	113
6.3	<i>Tilttable UV-LED lithography system design</i> .....	115
6.3.1	<i>Optical setup</i> .....	115
6.3.2	<i>Mechanical and electric setup</i> .....	116

6.4 Characterization .....	119
6.4.1 Collimation with bigger lens and conical waveguide .....	119
6.4.2 Variable intensity with tilt functions .....	120
6.4.3 Homogeneity keeping the tilts intact .....	120
6.4.4 Comparison of uniformity with the existing tiltable systems .....	122
6.5 Fabrication method .....	123
6.5.1 Solid photoresist microfabrication .....	123
6.5.2 Liquid State microfabrication .....	124
6.6 Microfabrication results .....	125
6.7 Summary .....	126
Chapter 7 - 5G frequency-selective device fabrication utilizing micromachined 3D	
microstructures .....	128
7.1 Introduction .....	128
7.2 Concept of 3D micromachined frequency-selective device .....	129
7.3 Design of airlifted 3D microstructure .....	132
7.4 Fabrication method .....	134
7.5 Characterization .....	136
7.5.1 HFSS simulation .....	136
7.5.2 VNA analysis .....	137
7.6 Results .....	139
7.7 Summary .....	143
Chapter 8 - Conclusion .....	144
Bibliography .....	146

## List of Figures

Figure 2.1 Schematic of the transparency test. ....	14
Figure 2.2 Transparency test of the photoresist (a) Experimental setup for transparency test, (b) soft-baked SU8 sample placed on an intensity meter sensor, (c) The brown part and the transparent part showing the crosslinked and un-crosslinked part of the SU8. ....	15
Figure 2.3 Graph showing the transparency for different thicknesses of the SU8. ....	16
Figure 3.1 A collimating structure using a Fly’s eye integrator (Source- [Voetkel et. al.]). ....	23
Figure 3.2 Conceptual drawing of the UV-LED lithography system. ....	25
Figure 3.3 UV-LED Light source (a) Spectrum of the 405 nm UV-LED (Inset- 405 nm UV-LED (c) Schematic of the UV-LED light source.....	27
Figure 3.4 Collimating structures (a) Lens’s focal length measurement, (b) Waveguide model. ....	29
Figure 3.5 UV-LED lithography system.....	31
Figure 3.6 Collimation test (a) Illustration of light collimation using waveguide and lens, (b) Analysis of collimation using ImageJ (2018) software. ....	32
Figure 3.7 Intensity distribution with the change of current and distance (Inset- Intensity change from 20-45 mm). ....	33
Figure 3.8 Transforming high contrast illumination into homogenous light using rotational motion. ....	34
Figure 3.9 Light homogeneity (a) Matrix of UV-LEDs without rotation, (b) UV-LEDs with rotation, (c) Graphical representation of the light distribution over the intensity line.....	35
Figure 3.10 Reliability test of the UV-LED lithography system. ....	37
Figure 3.11 Micro device fabrication.....	39
Figure 3.12 High aspect ratio micron device. ....	40
Figure 3.13 Millimeter tall pillar fabrication (a-d) fabrication method of tall microstructure, (e) 2 mm tall micro towers. ....	41
Figure 3.14 3D inclined microdevice.....	42
Figure 4.1 Concept of the multidirectional lithography system. ....	47
Figure 4.2 Light source (a) Matrix of 25 UV-LEDs on the PCB with single waveguide, (b) Wavelength spectrum of the UV-LED (Inset- Unit UV-LED).....	48
Figure 4.3 Illustration of the waveguide. ....	49

Figure 4.4 Light source elements (a) Collimating glass lens, (b) Waveguide and lens assembled on the PCB. ....	50
Figure 4.5 Overall setup for the multidirectional UV-LED lithography system .....	52
Figure 4.6 Collimation test (a) Test setup, (b) Collimated light projected on a vertical screen. ..	53
Figure 4.7 Intensity variations with the change of current and distance. ....	54
Figure 4.8 Thermal behavior test with different cooling aids.....	55
Figure 4.9 Thermal control test on the PCB surface and Lens surface.....	56
Figure 4.10 Light source motion illustration (a) Rotational motion around the central axis, (b) Orbital motion around LED's own axis. ....	58
Figure 4.11 AutoCAD drawing of the UV-LED array (a) no rotation, (b) with orbital rotation..	59
Figure 4.12 UV-LED intensity profile (a) Single UV-LED, (b) Intensity distribution through the center and the periphery.....	60
Figure 4.13 Light homogeneity (a) 5 by 5 matrix of the UV-LED, (b) The UV-LED matrix with one rotation, (c) Intensity distribution of the light source with and without motion. ....	62
Figure 4.14 Microfabrication (a-f) 3D microstructure fabrication method, (g) Fabricated 3D microstructure. ....	65
Figure 4.15 High-resolution 2D patterning.....	66
Figure 4.16 Tall microstructures (a) High aspect ratio pillar, (b) 3 mm micro-tower.....	66
Figure 4.17 Unique 3D SU-8 structures (a) an array of 'chained triangular slab,' (b) millimeter-tall SU-8 tripod array, (c) large (1.5 mm tall) and small (200 $\mu\text{m}$ tall) 3D petal SU-8 structure on a single structure. ....	68
Figure 4.18 More than 2000 micropillar array in a one-inch glass.....	69
Figure 5.1 Concept of the programmable multidirectional UV-LED lithography system. ....	74
Figure 5.2 Light source matrix (a) 5 $\times$ 5 matrix of the waveguide with lenses, (b) 20 $\times$ 20 matrix of the light source.....	75
Figure 5.3 Tilt-rotational sample holder. ....	77
Figure 5.4 Program controlled operations. ....	78
Figure 5.5 Illustration of the programmable UV-LED lithography system.....	79
Figure 5.6 Programmable multidirectional UV-LED lithography system.....	80
Figure 5.7 The change of intensity with the change of distance and current (With lens and waveguide). ....	81

Figure 5.8 Brightness test (a) Graphical representation of the relationship between the brightness level and the intensity, (b) Graphical representation of the relationship between the brightness level and energy consumption. ....	82
Figure 5.9 Homogeneity test for the light source (a) 365 nm LEDs (stationary), (b) 365 nm LEDs (motion), (c) Graphical analysis of the intensity profile for 405 nm LEDs with and without motion, (d) 405 nm LEDs (stationary), (e) 405 nm LEDs (motion), (f) Graphical analysis of the intensity profile for 405 nm LEDs with and without motion, (g) Combined LEDs (stationary), (h) combined LEDs (motion), (i) Graphical analysis of the intensity profile for the whole light source with and without motion .....	84
Figure 5.10 Light source uniformity.....	86
Figure 5.11 Uniformity test (a) Test setup, (b) Table showing intensity measured at different days, (c) Graph showing the deviations of stability measurements.....	88
Figure 5.12 Thermal test (a) Temperature checked at different brightness levels, (b) Graph showing the changes of temperature with and without the heat sink.....	90
Figure 5.13 Light source arrangements (a) Matrix arrangement of UV-LEDs in parallel rows and columns, (b) Honeycomb arrangement of UV-LEDs. ....	91
Figure 5.14 Lens design considerations and an illustration of the hexagonal lens.....	92
Figure 5.15 Waveguide (a) Cross-section of the waveguide with lens seat and UV-blocker, (b) UV- blocker, (c) Waveguide unit.....	94
Figure 5.16 Micromachined stainless steel lens mold, (inset- the fabricated hexagonal lens). ....	96
Figure 5.17 collimation with hexagonal design (a) Divergent beam, (b) Illustration of the collimation with lens, (c) Collimation result. ....	96
Figure 5.18 Honeycomb light source (a) Hexagonal honeycomb arrangement, (b) All UV-LEDs on while rotating, (c) Alternate arrays are on while rotating.....	97
Figure 5.19 Homogeneity with honeycomb setup (a) Light source at a stationary position, (b) Light source with orbital movement, (c) Graphical analysis of the two states of the light source. ....	99
Figure 5.20 Microfabrication (a) High-resolution patterning, (b) High aspect ratio micro tower fabrication. ....	100
Figure 5.21 Surface quality (a) 3D vertical pillar printed using SLA printer (Formlabs), (b) Microfabricated pillar using multidirectional UV-LED lithography system.....	101

Figure 5.22 Production yield (a) Batch production of 3D vertical microstructures, (b) Graph showing a comparison of the production yield of microstructures with time for 3D printers and the UV-LED lithography system.....	103
Figure 5.23 Versatile microfabrication (a) Double inclined pillars, (b) Screwed vane structure, (c) 3D horn structure, (d) Quarter circle, (e) Double arrow, (f) 3 petal structures. ....	104
Figure 5.24 Performance analysis of some of the prominent lithography systems. ....	109
Figure 6.1 Concept of the tiltable UV-LED lithography system. ....	114
Figure 6.2 Waveguide design with lens housing (a) Side view, (b) Inside, (c) Lens and LED integrated.....	115
Figure 6.3 The light source with the tilting arrangement (inset- Unit waveguide with pivot joint). ....	116
Figure 6.4 Tiltable UV lithography system setup. ....	118
Figure 6.5 Collimation test result (a) Divergent illumination by the UV-LED, (b) Collimated light with lens and waveguide.....	119
Figure 6.6 Change of intensity with the change of distance and direct current.....	120
Figure 6.7 (a) Light source without rotation, (b) Light source with rotation, (c) Graphical comparison of intensity profile with and without rotation.....	121
Figure 6.8 Comparison of intensity distribution for an inclined light source with the tiltable sample holder. ....	122
Figure 6.9 Fabrication of SU8 structure: (a) Soft bake, (b) Inclined UV exposure at $+\Theta$ , (c) Inclined UV exposure at $-\Theta$ , (d) post-exposure bake, (e) Developing, (f) Fabrication result. ....	124
Figure 6.10 Microfabrication results (a) SU8 vertical pillars, (b) SU8 dual Inclined pillars, (c) SU8 3D triangle, (d) Liquid resin vertical microneedle, (e)Liquid resin dual microneedle, (f) Liquid resin multi-angled petal. ....	125
Figure 7.1 working principle of the micromachined air-lifted 3D frequency-selective device..	131
Figure 7.2 Comparison of solid and metal coated pillars (a) Solid metal pillar, (b) Metal coated polymer pillar.....	132
Figure 7.3 Parameter consideration for 3D vertical pillar designing.....	133
Figure 7.4 Fabrication procedure of 3D microstructure. ....	135
Figure 7.5 Experimental setup for an FSD resonance testing.....	139

Figure 7.6 Frequency selective device (a) Unit vertical pillar, (a) two adjacent pillars, (c) 4 -inch device. .... 140

Figure 7.7 HFSS simulation for the vertical pillar (a) HFSS simulation for a unit vertical pillar cell using Floquet port showing the  $S_{21}$  response, (b) The E-field distribution over the unit pillar, (c) The E-field vector over the vertical pillar. .... 141

Figure 7.8 Graph showing the response with the pillar frequency-selective device (inset-magnified view of the resonant frequencies). .... 142

## List of Tables

Table 5.1 comparison of the improvements on different UV-LED lithography systems discussed .....	107
Table 5.2 Comparison of different UV lithography systems.....	108
Table 7.1 Comparison between the simulated and the experimental result for the 3D vertical pillar FSD.....	143

## **Acknowledgements**

I want to express my deepest gratitude to my advisor Dr. Jungkwun ‘JK’ Kim, for his kind help and endless support throughout my tenure as a graduate student. He had been an incredible mentor throughout my Ph.D. journey. He has always supported and helped me overcome my challenges. It would be difficult for me to accomplish this dissertation without his help and support.

I owe my profound gratitude to my committee members Dr. Don Gruenbacher, Dr. Hongyu Wu, and Dr. Shih-Kang Fan, for their valuable time and support. Sincere gratitude to Dr. Amir Bahadori for serving as the chairperson of the examining committee for this Doctoral degree.

I would like to thank my collaborators from Samil Tech Co. Ltd., South Korea, for funding this project and helping me with everything for completing this project. I would like to thank my colleagues and lab mates, especially Jun Ying Tan, for being a good soul and always for helping and sharing ideas.

I would like to express my heartfelt thanks to my loving husband, Dr. Md Mahbubul Huq Riad, for his relentless love and unending support. I can’t thank him enough for always inspiring me to achieve my goals and staying by side through thick and thin. I am thankful to my mother, Ms. Kamrun Nahar, for inspiring me and for making me what I am now. I am thankful to my brother Md. Kamruzzaman Real for always supporting me in every way possible and for always being the shade over my head. I am grateful to my family members and my in-laws for always supporting me. Their prayers kept me going through my difficult times. I thank my ever-supportive friends, living both home and abroad, for always giving me the confidence and support I needed. Finally, all thanks to the Almighty for giving me the strength to reach this far and for all his blessings.

## **Dedication**

I dedicate this dissertation to my father Md. Mofazzal Hossain who dreamed a great life for me and my husband Md Mahbubul Huq Riad who always believed in me and helped fulfilling my father's dream.

## Preface

This dissertation, with the title “UV-LED lithography system using programmable light and tilt-rotational stage for 2D/3D microfabrication for micromachined RF devices” is submitted for the degree of Doctor of Philosophy in the Department of Electrical and Computer Engineering at Kansas State University. The research has been performed under the supervision of Prof. Jungkwun ‘JK’ Kim.

Most of the work is comprised of the following set of published or submitted peer-reviewed journal and conference papers:

- Peer-reviewed journal papers
  - S. F. Shiba, H. Jeon, J. S. Kim, J. E. Kim, J. Kim, 3D Microlithography using an Integrated System of 5-mm UV-LEDs with a Tilt-Rotational Sample Holder, *MDPI Micromachines* 2020, 11(2), 157
  - S. F. Shiba, J. Y. Tan, J. Kim, Multidirectional UV-LED Lithography using an Array of High-Intensity UV-LEDs and Tilt-Rotational Sample Holder for 3-D Microfabrication, *Springer Micro and Nano Systems Letters*, volume 8, Article number: 5, 20 April 2020.
  - S. F. Shiba, H. Jeon, H.-C. Jang, J.-S. Kim, J.-E. Kim, and J. Kim, Development of Programmable UV-LED Microlithography System for 3D Microfabrication, *IEEE Journal of Microelectromechanical Systems*, 5 Oct 2021
- Peer-reviewed conference papers
  - S. F. Shiba, J. Beavers, D. Laramore, B. Lindstrom, J. Broyles, C. Gaither, T. Hieber, and J. Kim, UV-LED Lithography System and Characterization, *IEEE Int’l Conference on Nano/Micro Engineered & Molecular Systems (IEEE-NEMS 2020)*, San Diego, USA, 27-30 Sept. 2020
  - S. F. Shiba, K. Wang, J. Kim, Tilttable UV-LED Lithography for 3D microfabrication, *The 21<sup>st</sup> Int’l Conference on Solid-state sensors, actuators, and microsystems, (Transducers 2021)*, 20-25 June, 2021.

- S. F. Shiba, J. Y. Tan, C. Kim, S. J. Kim, J. Kim, Ku- band frequency selective 3D vertical pillar array, The 21<sup>st</sup> Int'l Conference on Solid-state sensors, actuators, and microsystems, (Transducers 2021), 20-25 June, 2021.

# Chapter 1 - Introduction

## 1.1 Introduction to UV-LED lithography

UV lithography is an essential step in MEMS device fabrication. In UV lithography, a substrate is patterned by selective exposure to a UV light source for creating the desired circuitry. MEMS is the result of the evolution of integrated circuits (IC). The applied sectors of MEMS where UV lithography is a fundamental step, include bio MEMS [1], Optical devices like micro-lenses [2], high-efficiency communication devices [3], aerospace microdevices [4], implantable temperature sensors [5], micro-pressure sensors [6], wearable sensors [7]. Conventionally, mercury vapor lamps are used for IC fabrications or microdevice fabrications. Although MEMS technology is originated from IC devices fabrications, the modern MEMS covers almost every industry now. The range of MEMS devices can be from less than a micron to several millimeters.

The existing mercury vapor lamps with their limited exposure and functionality cannot cope with expanding MEMS technology. However, with the advancement of the diode manufacturing technology, the UV-LEDs' irradiance and power have improved and gained the ability to cure UV-sensitive materials and is used for photolithography applications [8] [9]. They have the superior ability to cure materials without involving any harmful chemicals. The narrower wavelength enables them to expose precisely, getting rid of the focal shift aberrations. UV-LEDs are getting also popular for lithography applications because they are compact, prompt-on, low maintenance, and reliable than traditional lamps [10]. Commercial companies are also relying on UV-LEDs for manufacturing UV light sources for lithography in recent times [11], [12], [13]. However, most of these UV-LED lithography systems are just a replacement of the mercury vapor lamps without any advancements. The UV-LEDs have some unique features which are not

common for the conventional lithography systems and can be utilized for developing an advanced lithography system.

The concept of 3D multidirectional structures fabrication using UV lithography is prevalent in MEMS society since the 1990s. C. Beuret *et al.* showed the use of an inclined rotating chuck to assign different inclination angles to get inclined microstructures using a positive photoresist [14]. By manually controlling the inclinations of the chuck they were able to get an inclination of around  $17^{\circ} \pm 3^{\circ}$  on a 100  $\mu\text{m}$  thick photoresist. This process achieved a very limited inclination due to the resist flow and the low transparency of the positive photoresist. The manual control of the exposure also gave rise to the non-uniformity of the structures fabricated on a single substrate. Later, around 1997, negative tone photoresist SU8 got popularity in MEMS applications due to its high transparency, more mechanical strength and low cost [15], [16]. Around 2003-2004, M. Han *et al.* showed the fabrication of inclined SU8 microstructures using a conventional light source, a contact stage, and a tilting stage. For making rotated SU8 microstructures, they used a turntable structure attached with the inclined stage [17]. With manual control, the contact stage is simply leaned against the tilting stage. At the same time, YK Yoon *et al.* also showed the application of inclined SU8 microstructures in vertical screen microfilter system [18]. Around 2006, YK Yoon *et al.* proposed another tilt-rotational microfabrication scheme which involves the use of a rotational stage placed under a fixed light source which can be tilted from  $0^{\circ}$  to  $\pm 90^{\circ}$  [19]. This system was preferable since both the rotation and the tilting could be controlled with a single setup. However, this system had some limitations since the stage was manually controlled and the tilting had to be fixed beforehand. In 2011, JK Kim *et al.* utilized the concept of the tilt-rotational stage and extended the scope of fabrications by introducing a computer controlled dynamic mode multidirectional lithography system where the tilting and the rotation is controlled with two

separate stepper motors [20]. In this system, the tilting range could be controlled from  $-90^\circ$  to  $90^\circ$ . Using a microcontroller and a computer, the tilting and rotational motion could be controlled simultaneously. In 2016, JK Kim *et al.* proposed the use of UV-LED arrays as a suitable light source for lithography [21]. This system showed the ability to fabricate complex 3D microstructures using a CNC controlled light motion synchronized lithography system. Since the UV-LED light is diverging in nature and no collimating structure is added, their intensity fades after traversing a very small distance. As a result, this system had a limited intensity and therefore limited microfabrication capability.

This research demonstrates the development of an advanced UV lithography system utilizing the unique features of the UV-LEDs and investigates the fabrication of 2D and 3D microstructures using the same. Lithography light source requires collimation for high resolution micro/nano fabrication. Traditional mercury vapor lamps use the standard collimating equipment like Fly's eye integrator that consists of several optical components like condensers, optical lenses, several sets of integrators, filters. A strong light is needed for travelling through all these components. However, a significant amount of light intensity is sacrificed in the process of collimation, and outputs a very low intensity. Due to the diverging nature of the UV-LED, the light fades within a short distance. Therefore, the standard or the commercial collimating equipment cannot be used for UV-LED collimation. For this reason, a single lens collimation scheme has been demonstrated in this research. This single lens gives good collimation giving a very high intensity as the output as the intensity is not sacrificed with the use of bulky optical setup. This high intensity helps create ultra-tall and 3D complex microstructures which are challenging to get using conventional lithography systems. While collimating each UV-LED with a single lens, a

high contrast is observed in the light source which is later minimized using a continuous rotation of the light source.

The UV-LEDs can be operated independently. This independent control of the UV-LED has been utilized for regional control of the light source. The LED intensity shows a linear change with the change of current and an exponential relationship with the change of distance. This behavior of the LED intensity has been utilized to get adjustable intensity. Since UV-LEDs can be arranged in different forms and sizes, a large-scale light source with a size of 8 inch<sup>2</sup> has been demonstrated with a combination of 365 nm (i-line) and 405 nm (h-line) UV-LEDs. The 365 nm is the recommended wavelength for SU8 fabrications within a several hundred micrometer heights, on the other hand, 405 nm with high transparency is recommended for processing millimeter thick photoresists. This lithography system adapted the use of both kinds of UV-LEDs to cover a wide range of microfabrication. A matrix arrangement of the UV-LEDs has been shown with commercial circular lenses and a more compact honeycomb arrangement has been shown with customized hexagonal lenses for getting better homogeneity with the alternate array orientation of dual wavelength light source.

Utilizing the findings of the CNC controlled light motion synchronized lithography system, a fully programmable tilt-rotational sample holder has been integrated with the UV-LED light source. This sample is moved in 3D spaces with different inclinations and rotations to fabricate complex 3D microstructures where the exposure energy is made uniform at different inclinations with the adjustable intensity functionality. Since the manual control of all these functions are challenging, this system has been made fully programmable using a C++ program. The selection of the light source pattern and the 3D movement of the sample are controlled precisely with the program commands. This dissertation is the representation of the third-generation multidirectional

lithography system and the second generation of the multidirectional lithography system using UV-LEDs.

Microfabrication using the solid photoresists require longer time since they involve multiple baking steps. Millimeter thick SU8 samples take 15-16 hours to bake on a hotplate and the baking might be non-uniform at different depths, which make the fabrication and developing challenging. The future direction of this research focuses on the fabrication of 3D microstructures with liquid 3D printing resins which does not require baking. Since the 3D movement of a liquid photoresist is challenging, a self-tiltable UV-LED lithography system prototype has been demonstrated which can tilt up to  $70^\circ$  keeping the sample stationary. This methodology solves the non-uniformity issue with the inclined sample and makes the microfabrication both time and cost efficient.

An application of the millimeter tall microstructure has been demonstrated in this dissertation. Since millimeter tall microstructures need more energy to be fabricated, it requires much more time with a low intensity light source. With a high intensity light source, the energy required for millimeter tall microstructures can be achieved with a shorter time. This high intensity has been utilized for high frequency RF device fabrication. The RF devices are responsive to the certain frequencies strictly corresponding to their parameters. The precisely controlled lithography functionalities can be utilized for RF applications. This dissertation shows the first ever application of the 3D microstructures in the 5G frequency selective device.

The fundamental contributions of this research are summarized as -

1. Developing a single lens collimation scheme for a high intensity UV-LED lithography light source for millimeter range 3D microfabrication.

2. Developing the first ever commercial version of the multidirectional UV-LED lithography system with integrated high precision tilt-rotational sample holder.
3. Developing a large scale fully programmable lithography system with regional control and adjustable intensity of the light source.
4. Introducing a self-tiltable UV-LED lithography system for facilitating both solid and liquid photoresist 3D microfabrication.
5. The demonstration of the first ever 5G frequency selective device using lithography.

## **1.2 Motivation**

The lithography process consists of some vital steps that involve UV radiation and chemicals. Most of these steps do not have any other alternatives, while training and safety measures are sufficient for them. However, some major hazards involving the harmful gases can be diminished by avoiding the use of mercury vapor lamps. The electricity passing through the mercury vapor in between two electrodes create ionization of the mercury vapor and UV light is emitted as the result. This mercury vapor can be harmful if the user is exposed. Some of the health hazards due to the mercury exposure may include eye and skin irritation, stomach inflammation, breathing difficulty, sleeping problem, physical weakness and exhaustion, headache, cough, irritability and weight loss [22]. Most of the mercury vapor lamps contain Argon gas to create a neutral medium for preventing the decay of Tungsten filament of the bulb. An exposure to the Argon gas can cause dizziness, nausea, vomiting, loss of consciousness. Excess amount of inhalation can be fatal for human [23]. Therefore, the use of mercury vapor lamps is not safe for the users. The UV-LEDs on the other hand operate using the electroluminescence property without the involvement of any gases. Therefore, The UV-LEDs are considered as a safer choice for lithography applications. Direct exposure to any UV light is harmful for human organs, skin and

eyes which can be fatal. However, these health risks can be prevented with proper shielding and careful handling.

On the other hand, UV-LEDs are being introduced in microfabrication for having similar spectra as the conventional mercury vapor lamps, cost-effectiveness, low power consumptions, and longer lifetime. In addition to that, UV-LED is also considered for environmental safety. However, these are not the only features of UV-LEDs that can be considered for a lithography system. The UV-LEDs have some novel features which are not common in conventional lithography systems.

The primary motivation of this research is to utilize the novel features of UV-LEDs like wide range of wavelength, scalability, individual control, multidirectional function for developing an advanced lithography tool replacing the conventional mercury vapor lamps. The novel features of the UV-LEDs for the advanced lithography system are discussed in detail in Chapter 2.

Collimation and homogeneity are two of the most important parameters that need to be characterized while designing the light source. Since UV-LEDs light is too weak to be collimated using the commercial collimators as their bulk system needs a strong light to be passed through until the output end. Therefore, a single plano-convex lens is used for individual collimation the UV-LEDs. On the other hand, due to the individual collimation, a high contrast is created between the neighboring UV-LEDs. A continuous motion of the light source is used for minimizing the contrast. The design of this unique collimating structures and the rotating structure along with a mask alignment setup has been discussed in Chapter 3.

The MEMS applications are expanding, and new devices are needed for the evolving technologies. As a result, the use of complex 3D microstructures is also increasing. A multidirectional exposure system is required to make complex 3D structures. The unique features

of the UV-LEDs combined with a multidirectional exposure system can make a vast range of microfabrication. A prototype of a multidirectional UV-LED lithography system has been shown in Chapter 4.

A large-scale UV lithography setup is required for batch production or industrial uses. An improved optical design of the collimating structures for efficient accommodation of the dual wavelengths have been presented here. An automated lithography system with advanced features like adjustable intensity, regional light source control, programmable 3D fabrication is all discussed in the chapter 5. An analysis of the performance as compared to the existing 3D printers and lithography systems have been discussed in brief.

The ongoing research focuses on implementing a unique control feature of the UV-LED for developing a self-tiltable UV-LED lithography system. This system will facilitate both baked and non-baked photoresist exposure with uniform illumination over a target area giving a wide range of microfabrication possibility. This research is briefly discussed in Chapter 6.

There are specific applications of the microstructures obtained through the process of lithography. The 2D and 3D microstructure fabrication have been demonstrated in chapter 3,4 and 5. While most of the microstructures have been shown for demonstrating the fabrication capability of the lithography system. They can have significant applications in the major semiconductor and MEMS devices with certain customization. The final research shows the practical implementation of the fabricated 3D microstructures in the field of RF MEMS as discussed in chapter 7. The 5G frequency range has been considered for this device fabrication.

Chapter 8 presents the concluding statement and the impacts of the research in the scientific fields.

The dissertation can be outlined as-

**Introduction:** to UV-LED lithography, research background, and motivation.

**Presenting the novel features of the UV-LEDs:** for developing a UV lithography system with the most advanced features.

**Developing a prototype of the high intensity UV-LED light source:** a high intensity UV-LED lithography light source using a single lens collimation scheme.

**Developing a multidirectional lithography system:** improved light source design and integrated tilt-rotational sample holder for complex 3D microfabrication

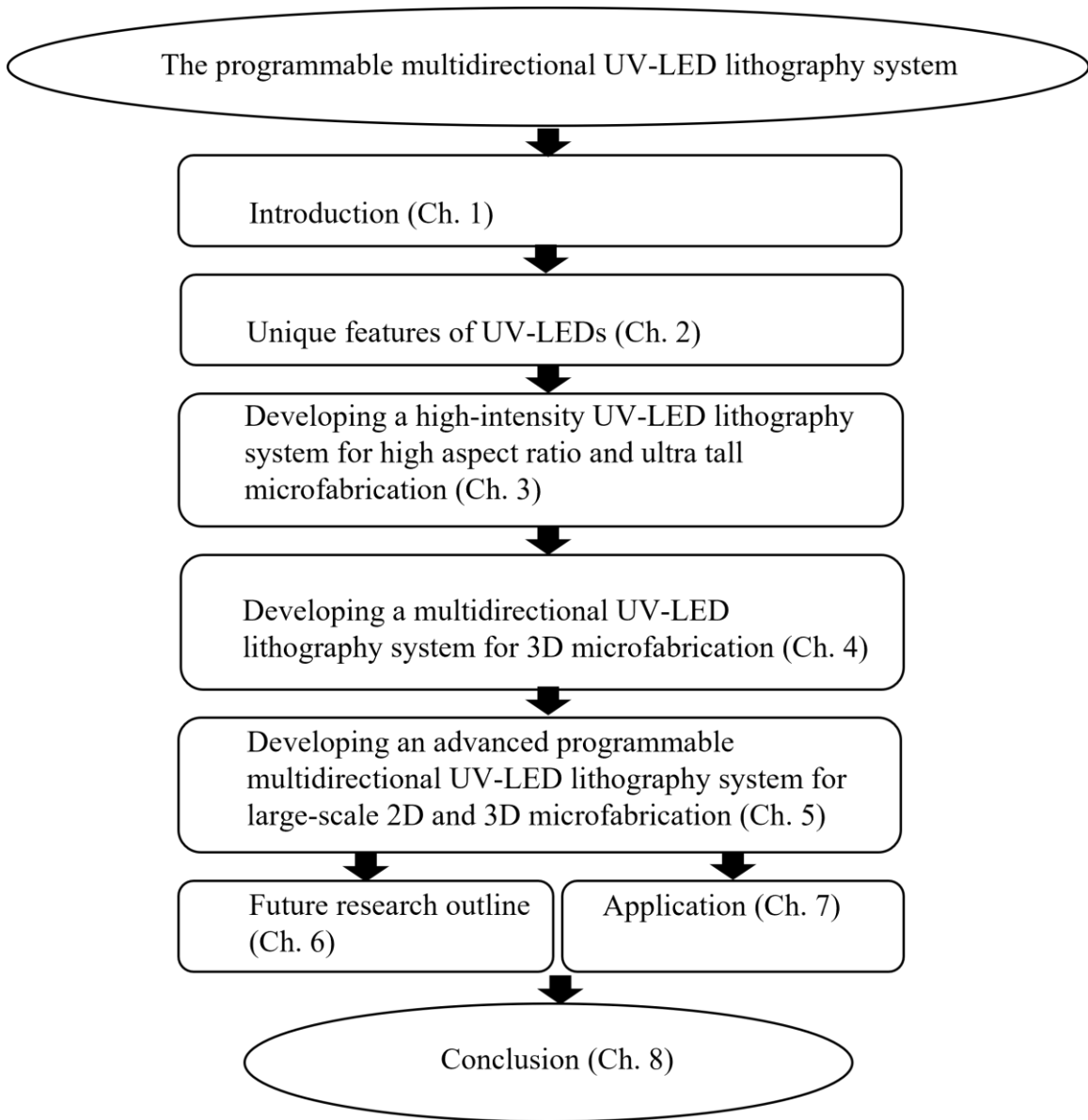
**Developing a large-scale programmable UV-LED lithography setup:** with advanced features and programmable operations for commercial uses in collaboration with Samil Tech, South Korea.

**Future research:** focusing on a self-tiltable UV-LED lithography system

**Application:** Utilizing the microstructures fabricated using the multidirectional UV-LED lithography system in RF frequency-selective device for 5G application.

**Conclusion:** concludes with the results and discusses the impact of this research in the scientific world.

The research has been organized as shown in the flow chart below-



# **Chapter 2 - Advanced features of UV-LEDs for 3D microlithography**

## **2.1 Introduction: Novel features of UV-LEDs**

Light-emitting diode (LED) is a significant invention of the modern semiconductor technology where a recombination of electrons and holes inside the semiconductor emit energy in the form of light. With the advancement of LED technology, many LEDs have been produced with different wavelengths and colors, including Ultraviolet (UV) wavelengths.

This advancement has started replacing the traditional mercury lamps in most of the applications but still follows the same operation principle as the mercury lamps. Not much advancement has been done on the UV-LED lithography systems that are available now. The existing light sources have limitations with wavelength and directivity. A significant amount of the original intensity is also lost in the process of making a collimation structure with multiple lenses, condensers, and integrators.

However, making use of some of the novel features available in UV-LEDs, it is not only possible to make a standard lithography system, but an advanced lithography system with the most advanced features can also be built. These advancements can make significant improvements in semiconductor and MEMS industry. This chapter discusses some of the unique features that can be utilized for modern and advanced UV lithography systems.

## **2.2 Novel features of UV-LED**

Some novel features of the UV-LEDs that have been utilized for UV microlithography have been discussed in the following sections.

### ***2.2.1 Selectivity of wavelengths***

Wavelength selection is important for lithography since different photoresists are responsive to different wavelengths depending on their chemical composition. Also, different wavelengths are useful for different thicknesses of photoresists. The near UV spectrum is used for lithography applications that starts from 315 nm. Broadband spectrum like the one used in mercury vapor lamps has the highest emissions at g (436 nm), h (405 nm), and i (365 nm)-lines of wavelengths that can be used for microstructure fabrications. One of the most popular negative tone photoresists used for microdevice fabrication is the epoxy based SU8. SU8 2000 series photoresist, with a refractive index of around 1.6, is widely used in MEMS applications because of its higher stability and robustness. Another photosensitive material that has been studied to be very promising for microstructure fabrication is the polymer-based 3D printing resin. In the following chapters, SU8 2025 and (Stereolithography) SLA 3D printing resin (Surgical guide resin, Formlabs) have been used in most of the fabrications. The wavelength selection has been discussed based on the characteristics of SU8 and 3D printing resin.

SU8 2025 (Microchem) is widely used as the negative tone photoresist, and 365 nm is recommended for the exposure of this resin [24] because of its high absorption capability. However, the standard datasheet provides information for only up to several hundred  $\mu\text{m}$  (around 225  $\mu\text{m}$ ) thickness of SU8 processing. The microstructures fabricated in the height range of several hundred microns are used in microfluidic channels [25], [26], electroforming applications [27], microdevices for lab-on-chip applications [28]. However, with the limitation of SU8 thickness, the flexibility of the design and other parameters also get limited. At the same time, taller 3D microstructures have the flexibility and option to enhance the performance of the microdevices. In recent times, several applied fields like advanced bioanalytic devices [29], energy harvesting

devices [30], micro inductors [31], [32] require ultra-tall SU8 structures. To meet the demands of the high-performance micro-devices, fabrication of the microstructures beyond the recommended thickness is needed. The energy requirement is high for a very tall microstructure, i.e., more than 300 microns or millimeter structures. In this case, the high absorption characteristic of 365 nm light doesn't contribute to crosslinking the thicker photoresist. Although higher wavelengths of a broad-spectrum work to crosslink the photoresist's more increased thickness, the absorption coefficients of different wavelengths create differences in the vertical sidewall of the ultra-tall microstructures. Due to their higher absorption coefficients, the shorter wavelengths tend to be absorbed in the closest area of the exposure, whereas the higher wavelengths penetrate more. For example, the absorption coefficient of 365 nm is around four times that of 405 nm. As a result, most energy gets absorbed near the patterned area, and the structures become non-uniform. The vertical profile of the tall microstructure is affected by these several different absorptions at different heights, which causes distortions and makes these structures unsuitable for the applied fields where smooth sidewalls are needed. On the other hand, higher wavelengths may contribute to higher diffractions, which is another important parameter to be optimized for tall microfabrication. That is why higher wavelengths like the g-line (436 nm) are not recommended for the elevated microstructure fabrication. Therefore, 405 nm UV light is more suitable for ultra-tall microstructure fabrication because of its high transparency through SU8 compared to 365 nm and lower diffraction compared to 436 nm [33] [34]. Therefore, a necessity to filter out the unwanted wavelengths rises if a broadband spectrum is used. However, instead of using different filters for eliminating different wavelengths, only specific UV-LEDs having specific wavelengths can be used for lithography applications. If a particular wavelength LED is used, filtering is

unnecessary, and the problem with the multi-peak distortion can be solved. And this choice has been made in making the lithography systems discussed in this dissertation.

Both 405 nm and 365 nm UV-LEDs have been discussed for their significant roles in fabricating microstructures with SU8 photoresists of different size ranges. The small prototypes have been built with just single wavelength UV-LEDs, whereas the final system contains a combination of both 365 nm and 405 nm UV-LEDs. An experiment was conducted to show the intensity profile of the UV light after passing through different thicknesses of photoresists, which is termed as the transparency test. Figure 2.1 shows the schematic of the transparency test experiment. The light is placed underneath an acrylic board with a hole to direct to confine the target area within the hole. The sample is the baked photoresist on a thin slide glass. The intensity meter sensor is placed just above the target area of the photoresist. The brown color shows the changing of the photoresist color with a long-time exposure.

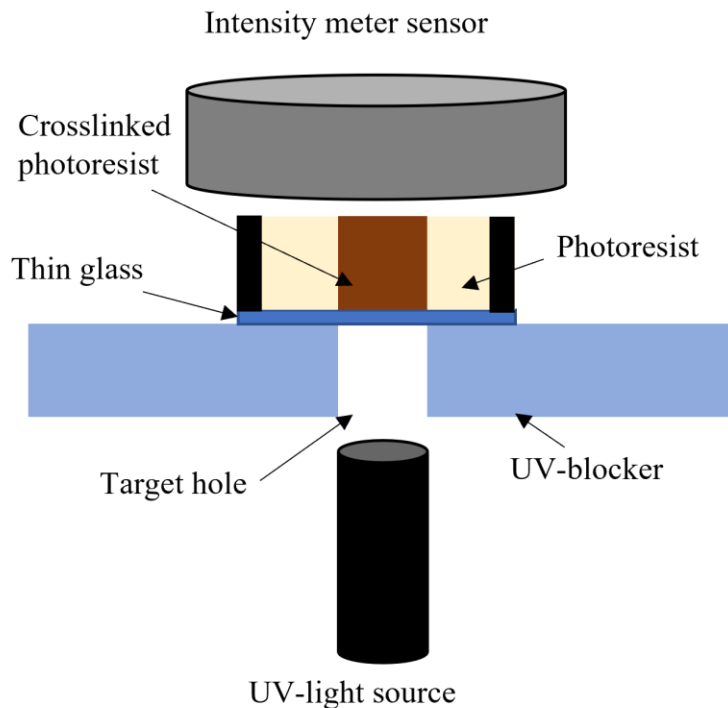


**Figure 2.1** Schematic of the transparency test.

Figure 2.2 shows the transparency test of the 405 nm light for fabricating tall microstructures. The transparency test has been conducted for 405 nm only since 405 nm wavelength has been verified for taller microstructure fabrication compared to 365 nm as 405 nm wavelength shows only 38% attenuation while 365 nm wavelength shows 96% attenuation at around a thickness of 2.5 mm [35].

Here, the term transparency has been used to represent the fact that the un-crosslinked SU8 allows the passage of UV light, or in other words, the un-crosslinked SU8 acts as a transparent medium for UV light. However, with the starting of cross-linking, the color of the SU8 gradually changes to darker shades of brown and then makes it opaque for UV light passing. This characteristic of the SU8 has been considered in this experiment for checking the cross-linking capability of different thicknesses of SU8 for 405 nm UV light.

Figure 2.2 (a) shows the experimental setup, Figure 2.2 (b) shows the sample placed on a sensor, Figure 2.2 (c) shows the brown circles on the SU8 showing the cross-linking. The casting method was used here which is the direct pouring of photoresists on the microscope slide glass sample. For confining the liquid photoresist, a 3D printed frame was utilized.

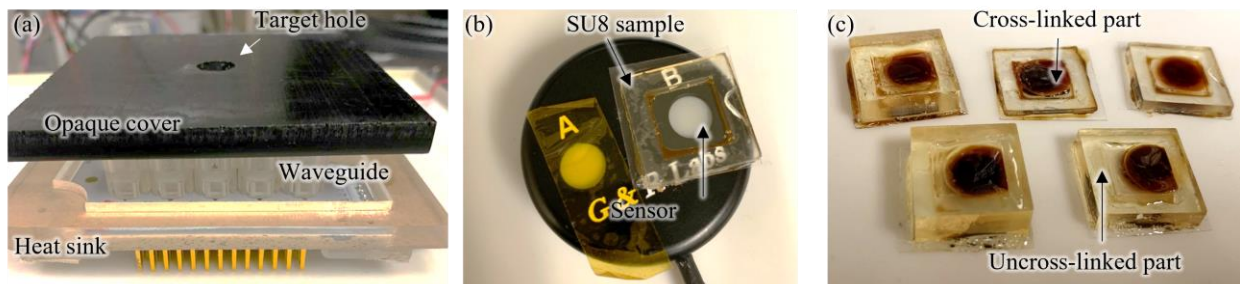


**Figure 2.2** Transparency test of the photoresist (a) Experimental setup for transparency test, (b) soft-baked SU8 sample placed on an intensity meter sensor, (c) The brown part and the transparent part showing the crosslinked and un-crosslinked part of the SU8.

For testing the transparency of SU8, different thicknesses of SU8 were cast directly on a transparent glass and soft baked at 95 °C. After baking for 10-15 hours, depending on the thickness. Since the gentle baking helps evaporate the solvent part, it was considered that the thick SU8 sample is fully evaporated. The sample was placed underneath the UV-LED (405 nm) and the light intensity at the opposite side of the sample was measured with the intensity meter (Model 202, G&R Labs).

Figure 2.3 shows transparency data of the SU-8 with various thicknesses ranging from of 0.5 mm to 7 mm. Most samples showed a similar attenuation rate of the light intensity in the exposure time range of 10 to 100 as the intensity dropped by 30 to 40 % after 100 seconds of exposure. The light intensity was significantly decreased after 1000 seconds (about 17 minutes) where 10% or lower than the initial intensity.

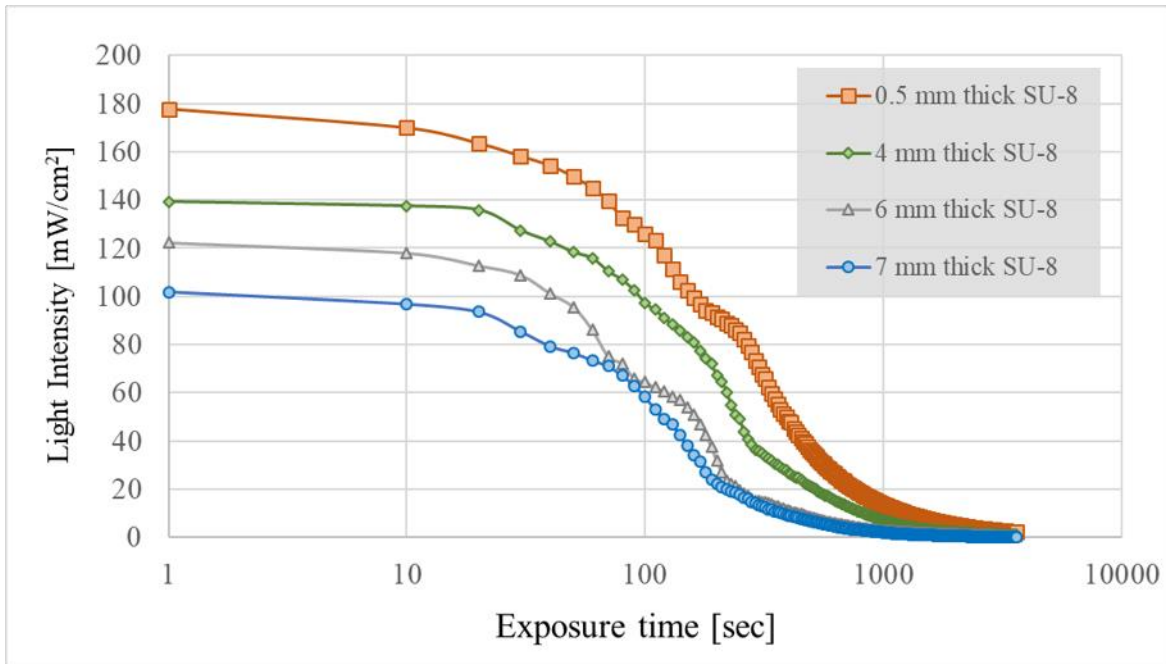


**Figure 2.3** Graph showing the transparency for different thicknesses of the SU8.

As the intensity of the UV-LED light source was set at 200 mW/cm<sup>2</sup>, the suggested exposure time for the UV-LED is up to 600 seconds (10 minutes), where the light intensity still shows higher than 10 mW/cm<sup>2</sup>, which is enough to crosslink SU-8 with small thicknesses.

The advantage of using a high-intensity light source is that, even after dropping the intensity to around 10% due to long time exposure, there remains a high enough intensity to perform the crosslinking.

### ***2.2.2 High and adjustable intensity***

Epoxy-based photoresists like SU8 are usually used in stable microstructure fabrication since this material can crosslink to form stable bonds and form an insoluble structure once exposed to UV light. When exposed to UV light, polymerization starts to create the crosslinked network. The exposure dose defines the energy required for photoresist exposure. This exposure dose can be represented as –

$$\text{Exposure dose} = \text{Intensity} \times \text{time} \quad (2.1)$$

While the intensity is defined by mW/cm<sup>2</sup>, time is measured in seconds. The exposure dose varies as a function of the thickness of the photoresist.

The manufacturer usually indicates the consistency required for a definite thickness. Since the intensity of the traditional lithography setups is constant, therefore the dose is a function of time. Thicker photoresists need higher exposure time. In addition to that, if selective wavelength filters are used, some of the intensity is attenuated depending on the material and the filter's thickness, which increases the exposure time. To fabricate a millimeter tall microstructure, a standard mercury vapor lamp takes several hours since the intensity is low. In addition to that, a long-time exposure can increase the diffraction effect on the photoresist, which again causes

unexpected enlargement of the exposed area. This results in the non-uniformity of the sidewall profile [32]. Therefore, the challenge of dealing with optimizing this exposure dose is manifold.

This lithography light source gives the highest intensity among the commercially available lithography systems so far. The 405 nm UV-LED showed an intensity of  $472 \text{ mW/cm}^2$  and the 365 nm UV-LED showed an intensity of  $258 \text{ mW/cm}^2$ . Among the available lithography systems, the highest intensity available recorded from a 405 nm UV lithography system was  $90 \text{ mW/cm}^2$  (Suss-MA300 Gen 2) and for a 365 nm, it was around  $50 \text{ mW/cm}^2$  (Idonus EXP 100). Therefore, the demonstrated UV-LED lithography system has an intensity that is more than five times that of the available lithography systems and the mask aligners.

To facilitate all ranges of microfabrication, a UV-LED light source can be used because the intensity of the UV-LED is a direct function of the current. With the increase of current, the intensity as measured by an intensity meter increases and vice-versa. The intensity of a UV-LED is also variable with the change of linear distance. In this study, these two UV-LED intensity characteristics have been utilized to get a variable light source. This is beneficial for the fabrication in two major ways. Firstly, since using a particular wavelength eliminates a filter, the initial intensity can be preserved. Secondly, with the variation of current and distance, a wide range of powers or exposure doses can be achieved, significantly improving the fabrication of all kinds of microstructures. For example, the lower thickness of the photoresist can be crosslinked using lower intensities by lowering either the current or increasing the linear distance between the light source and the target sample. On the other hand, higher currents can get higher intensities, making the crosslinking of thicker photoresists possible with a shorter amount of time. Moreover, by assigning different values to different UV-LEDs, multiple variations of microfabrication can be done with a single exposure. Therefore, microfabrication becomes more straightforward and time efficient.

For multidirectional lithography, a tilt-rotational sample holder is used for creating the 3D traces of the light. Since the linear distance changes with the change of inclinations, the intensity also varies. In this case, the adjustable intensity can have a vital role. The intensity of UV-LEDs can be adjusted to keep a uniform intensity on the target surface. This adjustable intensity feature can be programmed for automatic operations.

### ***2.2.3 Scalability of the system***

Starting from the integrated circuit (IC) fabrication to the RF MEMS fabrication, good production yield is the aim of a system. For industrial or large-scale productions of microstructures, it is essential to ensure good quality with a good production yield, which indicates the amount of usable or quality products out of a system. A good light source is a fundamental requirement for microfabrication, and for mass production, a more comprehensive light source is required. The traditional light sources with mercury vapor lamps have a limited light source size and a limited target area. Therefore, the number of microstructure fabrication becomes limited. However, frequent mass production is needed with the increasing demand for microstructures in MEMS. Since microfabrication is a time-consuming process and every operation needs all the steps strictly, it is desirable that many microstructures can be fabricated at once following the same fabrication steps, which saves time and maintains uniformity well.

In this case, UV-LEDs can be the option for lithography since every UV-LED can be independently dealt with, and any orientation size is possible with the system's efficient design. One most common setup is the matrix arrangement of UV-LEDs, which allows any number of LEDs with the proper amount of power supply. In addition to that, the light source can be made to be current-controlled or voltage controlled by changing the type of connection based on the availability of the power supplies. On that note, the power consumption of the UV-LEDs is around

60-70% less than that of a UV lamp [37]. Therefore, a more comprehensive scale light source can be designed with UV-LEDs with the same power availability, and a higher production yield can be achieved.

#### ***2.2.4 Multidirectional exposure capability***

Although UV lithography was initially aimed for 2D micro/nanopatterning on thin films deposited on a wafer, the evolution of MEMS technology has made rooms for 3D microstructures in a lot of applications. With the increasing demand for 3D microstructures, the improvisation of a microfabrication system is also required. There are several ways to make 3D microstructures that use different technologies like LASER 3D microfabrication that directly adds or subtracts material on a bulk sample [38], [39], 3D projection stereolithographic, which forms the microstructures by depositing layers on predefined locations [40], multiphoton lithography where the focal point of a LASER is moved around in 3D spaces to create 3D microstructures [41], [42]. However, the use of tilt rotational sample holder is one of the most used techniques of microfabrication that directly utilizes the standard lithography techniques [43], [44]. This multidirectional sample holder is mainly introduced for 3D microfabrication as the light sources are usually one-directional. Therefore, the sample is rotated or inclined to make the 3D traces of light. Since UV-LED is discussed here as the light source for lithography applications, many modifications are possible to make with them.

In addition to the discussed advantages of the UV-LEDs so far, another essential benefit of UV-LEDs is that they can be controlled individually. Although the traditional way of using a UV-LED is to connect them with a PCB, they can function fine even without a PCB. Therefore, more freedom is there to customize a light source when UV-LED is used. For example, with an efficient design, a UV-LED can be made to move in 3D spaces and create 3D light traces without needing

any multidirectional sample holder. Therefore, the sample can stay at the stationary position and 3D microfabrication is possible only by moving the light. This kind of flexibility is not available in the existing lithography systems for 3D microfabrication. This feature of the UV-LED is also beneficial to introduce liquid state photoresist exposure for complex 3D microstructure fabrication, which has been discussed in the ongoing research project.

### **2.3 Summary**

The unique features of the UV-LEDs to make an advanced lithography system has been discussed in this chapter. With the advancement of LED technology, the UV-LED can be the ultimate future for UV lithography where desirable monochromatic LEDs are available. In addition to all the features magnified here, there are other undeniable advantageous features like prompt-on functionality, low maintenance, longer lifetime, cost-effectiveness, compactness, and last but not the UV-LEDs are a safer choice for the environment. However, the UV-LEDs are not ready for precise micro fabrications. Theoretical considerations and the efficient design of optical and mechanical parameters are vital for making a standard lithography suitable light source. Other customizations are also required for 3D micro fabrications. The following chapters discuss the development of a standard light source prototype, a multidirectional UV-LED lithography system prototype for 3D microfabrication, a large-scale setup for mass production with advanced features. The ongoing research and one application of the advanced multidirectional lithography system are also discussed in this dissertation.

# **Chapter 3 - Developing a UV-LED lithography light source set up for high resolution and millimeter tall microfabrication and its characterization<sup>1</sup>**

## **3.1 Introduction: The development of UV-LED lithography system**

UV-LEDs have been shown to be a great replacement for the conventional mercury lamp for their ability to process microfabrication as well as advanced features like a prompt on functionality, longer lifetime, low maintenance, and environmental safety [45], [46], [47]. Nowadays, UV-LED lithography is used in applications like microfluidic devices [48], [49], surface acoustic wave devices [50], micro-lens fabrication [51]. However, UV-LED light is divergent and the illumination fades within a short distance. Therefore, collimating structures are necessary to create a focused and consistent illumination. The designing and the implementation of the UV-LED for lithography can be challenging for the makers. Getting homogenous illumination from a collimated light source while preserving high-intensity irradiance can be critical. Researchers presented several designs and models to use the UV-LEDs as the lithography tool. One lithography model shows the L-shaped arrangement of two UV-LED arrays with a checkerboard half-mirror arrangement to get uniform exposure [52], an automatic UV-LED exposure system shows the system setup using a combination of a light mixing system, a beam splitter, an optical lens system, a sensor and a controller [53]. Another UV-LED lithography model shows the use of Köhler illuminator optics in order to get rid of the non-uniformity caused by the array arrangement of the UV-LEDs [45]. A commercial setup of UV-LED exposure system also uses the Köhler integrator to homogenate the irradiance and uses a set of condenser lenses and

---

<sup>1</sup> This chapter is reformatted and slightly version of our article [69]

mirrors to get collimated exposure [54]. The use of Köhler integrator or the Fly's eye integrators and a set of reflectors is a very common practice for obtaining the collimation and uniformity [55] [56].

Figure 3.1 shows an example of the typical collimated structure in a commercial UV-LED lithography system using Köhler integrator or Fly's eye integrator. They use arrays of lenses to collimate the light. The precise alignment of the light source and the other integrating elements is very challenging in these systems. Although these arrangements can achieve good homogeneity and collimation, the combination of all these elements makes the system bulky. In the way of collimating with this complex setup, intensity is sacrificed. Here, in the case of the setup shown in Figure 3.1, only  $46 \pm 6\%$  of power reaches the output reflector. The UV-LED light diverges rapidly, and this intensity is not enough to pass through the bulky system of this collimator. As a result, this collimator is not a good fit for UV-LED collimation. Another concern for the integrator systems is the routine calibration of the optical arrangement.

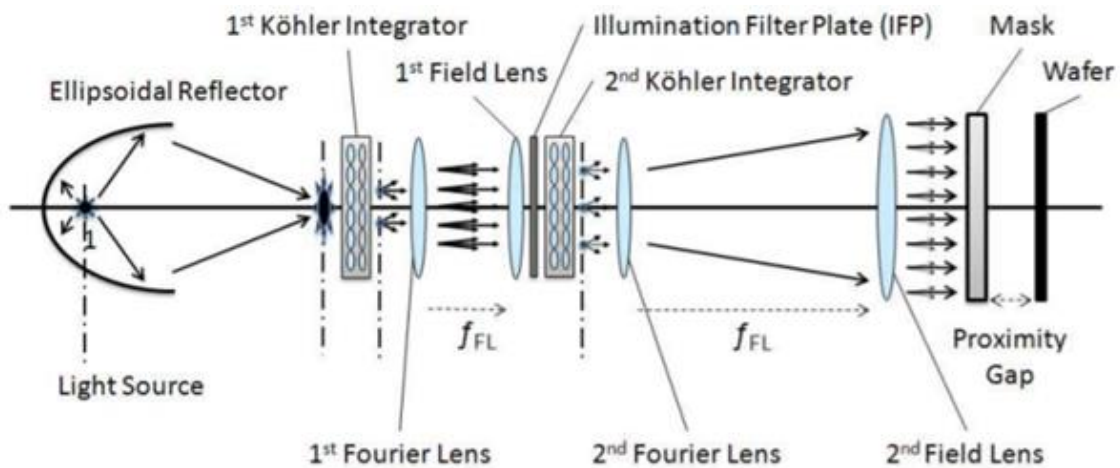


**Figure 3.1** A collimating structure using a Fly's eye integrator (Source- [Voetkel et. al.]).

However, there are less complicated lithography setups as well where the rows of UV-LEDs are used with a rotational gear to get homogeneous exposure [57]. This setup is more straightforward to operate but they do not have any proper optimization for collimation. Also, due to the use of the current limiting circuit, each UV-LED only allows up to 30 mA current, and the intensity is limited to only 50 mW/cm<sup>2</sup> which limits the microfabrication capability.

This chapter presents a UV-LED lithography light source setup where a single lens has been used for collimation, 3D printed structures have been used for guiding the light and accommodating the lens. The single lens makes the system compact and preserves a high enough intensity to process thick photoresists. On the other hand, the intensity is adjustable with the change of current and distance which makes the system unique with a wide range of options. Continuous rotation of the light source is used to get homogenous illumination. The system has been characterized for collimation, very high and adjustable intensity, and homogenous illumination. The microfabrication capability has been demonstrated with high resolution and high aspect ratio microstructures.

### **3.2 Concept of the UV-LED lithography light source**

The concept of the UV-LED lithography system is the use of UV-LED arrays as a UV source, where each UV-LED is equipped with only a single lens for collimation without using integrators and multiple lenses. As a result, higher intensity is preserved which is usually lower for other lithography caused by the bulk arrangement of the collimating structure.

As each UV-LED is individually collimated, a gap is created in the array arrangement of the light source. The gaps create a high contrast illumination over the target area and causes inconsistencies in the microfabricated structures.

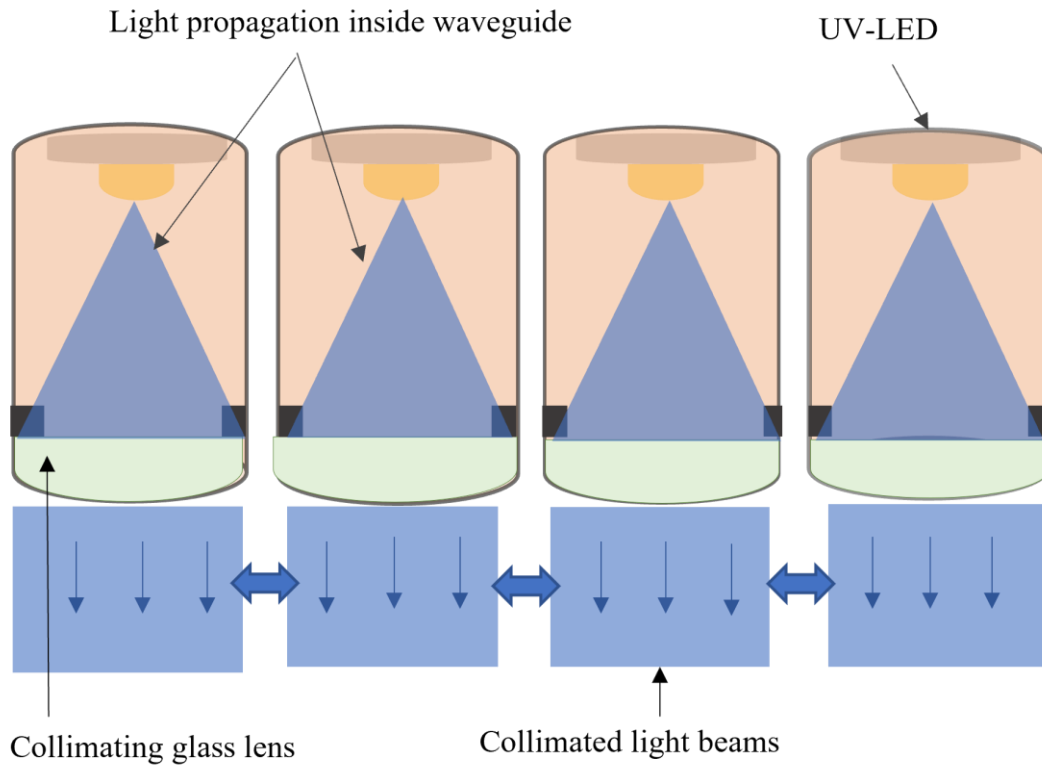


**Figure 3.2** Conceptual drawing of the UV-LED lithography system.

The setup presented here uses the rotational motion to compensate for the gap in between the individually collimated lights. Figure 3.2 shows a conceptual drawing of the UV-LED lithography system where UV-LEDs emit diverging lights.

This diverging beam is targeted on a plano-convex lens from a distance equivalent to its focal length, that converts the diverging light into a collimated one. The lenses are placed inside 3D printed light-guiding structures or waveguides and are arranged in arrays.

Thus, a collimated light source can be achieved without involving complex or expensive structures without sacrificing intensity. The rotational motion helps to cover up the high contrast created by the gaps in between adjacent LEDs.

### **3.3 Design of the UV-LED lithography system**

The UV-LED lithography system has been specially designed for tall microstructure fabrication in millimeter ranges as these structures have particular applications like high-frequency RF antennas, micro inductor fabrication [58] [59]. High intensity is important for thick photoresist processing and this system is customized for preserving high intensity while adding advanced features like adjustable intensity, mask alignment, and compact arrangement. The design of the system has been explained in detail in the following sections.

#### ***3.3.1 UV-LED and PCB design***

Surface-mounted UV-LEDs (Chanzon, 10DGL-DZ-3W-405) were chosen as the unit of the photolithography light source. The 405 nm wavelength has been selected as this is recommended for high aspect ratio microstructure fabrication. The spectrum was analyzed using a spectrum analyzer (BLUE- Wave, Stellar Net Inc.) and Spectrwarz software (2018). Figure 3.3 (a) shows the spectrum of the UV-LED used, and the inset shows the LED itself. The graph shows that the intensity achieves its peak at 405 nm only. There is no other significant peak within the range between 350 nm to 600 nm. Also, the peak starts from around 390 nm and extends up to around 430 nm, giving it a narrow spectrum eliminating the need for a filter. To eliminate the gaps between the consecutive UV-LEDs, the PCB was designed to accommodate the LEDs in a very compact manner. A single-layered Aluminum board has been used as the PCB. The dielectric used in a single-layered Aluminum PCB is about 5 to 10 times as thermally conductive as the traditional epoxy-based PCBs. The thickness is also reduced to about one-tenth. To provide more heat dissipation, thermal paste is added to the footprint of each UV-LED before soldering. This setup of the PCB helps to maintain the structural integrity and maintains high heat dissipation. Thus, it helps to keep the components safe from thermal damages. The PCB board is a thin rectangular

board with 5.5" x 6.5" dimensions accommodating 100 UV-LEDs with a 10 x10 matrix arrangement. Figure 3.3 (b) shows the schematic of the UV-LED arrangement. The LED matrix is arranged in two strings of fifty UV-LEDs in series, adding up to one hundred total components. The LEDs are rated for a voltage of 3.3 V, with a maximum allowed current of 500 mA, which results in maximum power demand of 165 W for 100 UV-LEDs. To supply the required power for two strings of UV-LEDs, two separate 100W Mean Well HLG-100H-C constant current LED driver was used, giving a maximum of 500 mA of constant current output.

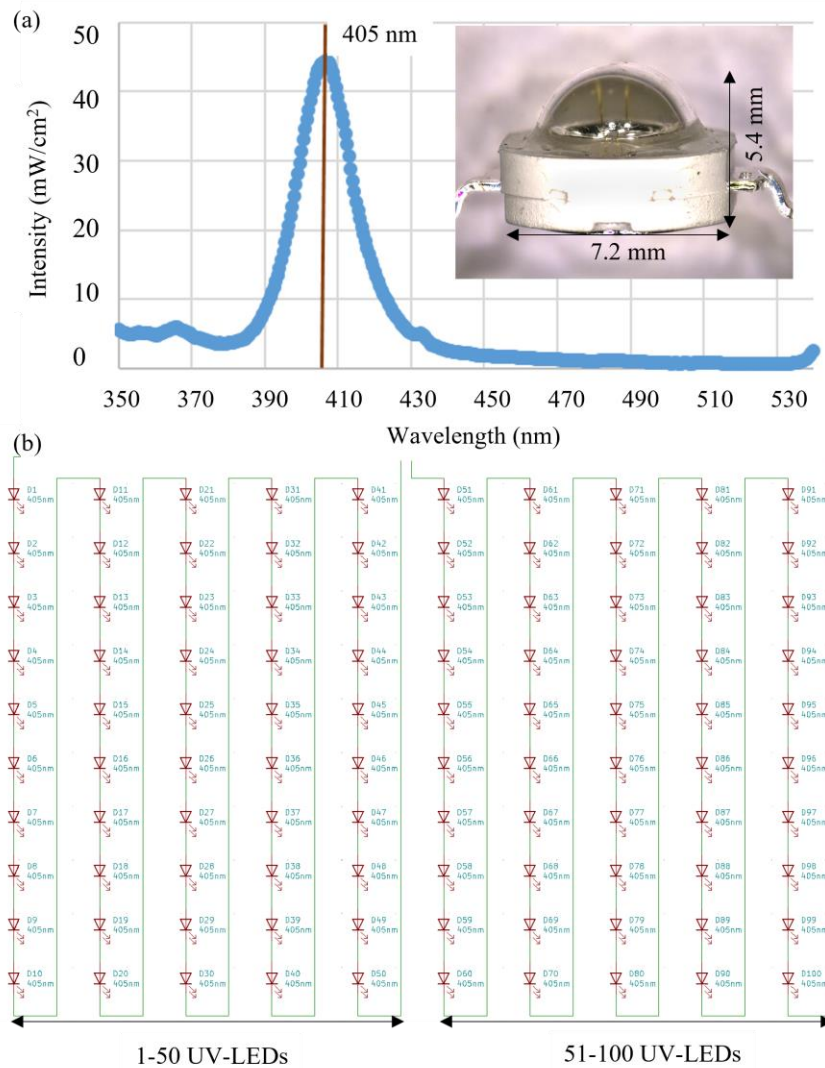


**Figure 3.3** UV-LED Light source (a) Spectrum of the 405 nm UV-LED (Inset- 405 nm UV-LED (c) Schematic of the UV-LED light source.

### 3.3.2 Collimating structure

A divergent light is not suitable for lithography applications since nano/micropatterning requires a focused or collimated light beam. Collimation is important for keeping the exposure confined within a target area and getting a good resolution and. Converging lenses are used to focus any form of diverging light to control the precise level of lithography patterning. The lens's focal length is accounted for to collimate and focus light from the LEDs. The appropriate combination of waveguide and lens is of paramount importance for guiding the light in a particular path and getting a focused beam. Multiple lenses and reflectors are ubiquitous for UV light sources. In this UV lithography setup, one lens has been utilized per UV-LED to obtain the necessary collimation, and 3D printed customized structures have been used as waveguides. A commercially available cabochon (Pandahall), which has a plano-convex shape with a diameter of 10 mm, was chosen to be the lens after testing its ability to collimate the diverging light.

The Lens-Maker's Formula was used to calculate the theoretical focal length of the lens-

$$1/f = (n-1)(1/R) \quad (3.1)$$

Where  $f$  is the focal length,  $R$  is the radius of curvature, and  $n$  is the refractive index of the material of the lens. Figure 3.4 (a) shows the verification test of the focal length of the lens used. A collimating light was sent to the lens and the height at which the light focuses clearly was noted by observing the projection on the surface. The theoretical calculation and the experimental measurement were matched well, and the focal length was finalized. Figure 3.4 (b) shows a single unit of waveguide model drawn in AutoCAD. The cylindrical structure is the main waveguide structure here.

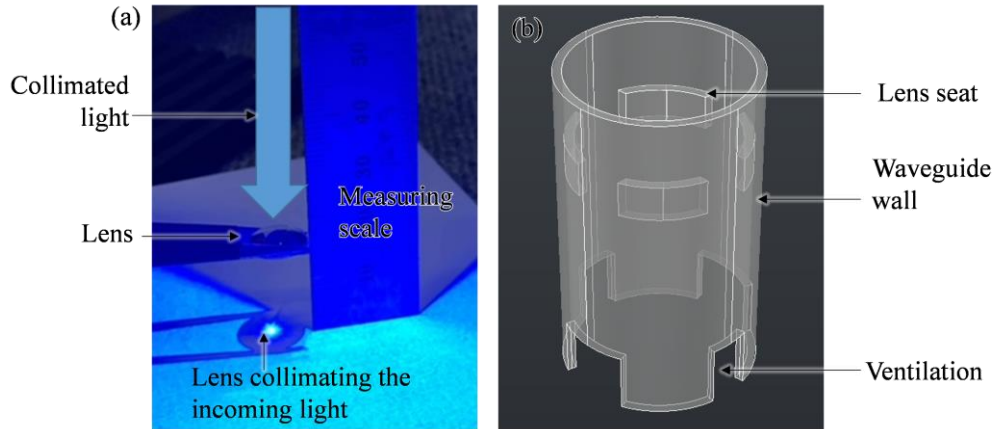


**Figure 3.4** Collimating structures (a) Lens's focal length measurement, (b) Waveguide model.

Considering the expansion of the designed model after 3D printing due to resolution limitation, the waveguide hole was designed to be 400 microns wider than the actual diameter. The inner diameter of the waveguide cylinder was designed to be 10.4 mm to accommodate the lens.

The four small sections seen in the middle of the cylinder provide a seat for the lens which is exactly at a height of the focal length from the LED tip. Ventilations are provided on the lower sides of the waveguide so that convective heat dissipation is possible. Thus, each LED is provided with a waveguide and a lens that makes the collimating structure.

Since the focal length is 14.5 mm, the lens was placed at a distance of 14.5 mm from the LED tip inside the waveguide. The total height of the waveguide was made considering the focal length plus the height of the lens and the height of the LED itself. When the diverging light hits the lens on its planar side, the rays are converted to parallel rays after passing through the lens.

### ***3.3.3 Linear mask alignment stage***

A sample holder is a platform where the target sample is placed for UV exposure and aligned with the pre-patterned mask. Proper adjustment of the sample is required for ensuring micron-level precision. For obtaining precise control over the X, Y, Z, and  $\theta_{xy}$  adjustment, a simple

linear positioning stage (MAXYZ-40R XYZ), and an in-plane rotation stage (MAR-40L-P) are used. For holding the sample flat, a rigid pedestal is used, which is fastened to the  $\theta_{xy}$  stage. A laser-cut Acetal plate was placed above the sample holding stage. The mask is then placed in a slot on the plate, which holds the mask in place. The alignment needs to be monitored visually. An optical microscope is used to align the wafer to the mask. This design allows moving the exposure system in linear trails while the exposure system is in an idle state. Utilizing this movement, the light source is moved to the other side of the housing, and the microscope is placed to observe the mask and sample alignment. After the alignment is done, the microscope is set beside the system, and the exposure system is moved back to its default position and ready for UV exposure.

### ***3.3.4 Overall chassis design***

The chassis of the UV-LED lithography system is made of laser-cut Acryl sheets, small 3D printed parts and multiple Aluminum extrusions. Figure 3.5 shows the overall setup of the UV-LED lithography light source. To make the intensity controllable, two potentiometers were used that serve as dimmers to control the light output. The timer/relay also controls the exposure time interval.

A separate switch for the motor is used for rotation. This motor must be turned on before beginning the exposure. The power supplies necessary for lighting up the LEDs and running the other electronic devices are accommodated inside the chassis. The chassis walls are made of Acryl sheets cut in precise sizes. The front Acryl sheets hold the operating switches, including the dimmer switches. The movement of the light source is made over the Aluminum extrusion trails. A 3D printed holder holds the PCB, the UV-LEDs, waveguides, and the lenses. This holder can be rotated with the help of a motor, as shown in the right inset of Figure 3.5. The connecting wires to the power supply are inserted through the upper hole and soldered with the PCB.

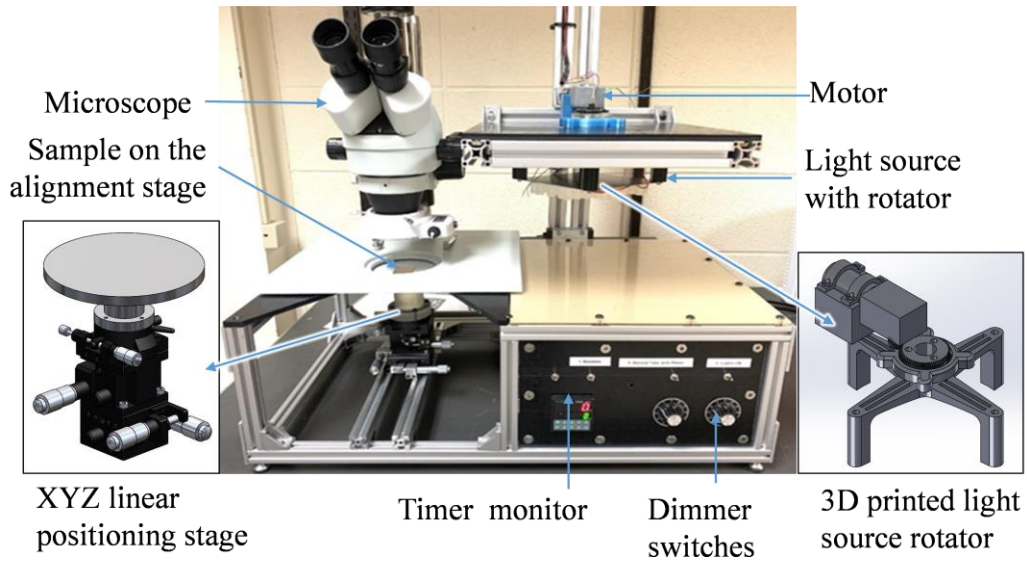


**Figure 3.5** UV-LED lithography system.

Four holes were drilled on the PCB board to insert the screws for holding it with the 3D printer rotator.

The waveguides were placed above the LEDs with a little amount of glue. All the power supplies and visible wires were paced inside the acryl housing to keep them secured and organized.

### **3.4 Characterization**

#### **3.4.1 Collimation**

As discussed in the earlier sections, a single lens and a waveguide have been discussed as the collimating structure. Figure 3.6 (a) shows the illustration of the placement of the lens at a distance equivalent to the focal length.

The lens converts the divergent light from the UV-LED into a collimating light. On the other hand, the waveguide keeps the light within its boundary and acts as a UV-blocker. Figure 3.6 (b) shows the image of the actual collimated light after completing the arrangement with the lens and the waveguide. The collimation of the light was analyzed with ImageJ (2018) software.

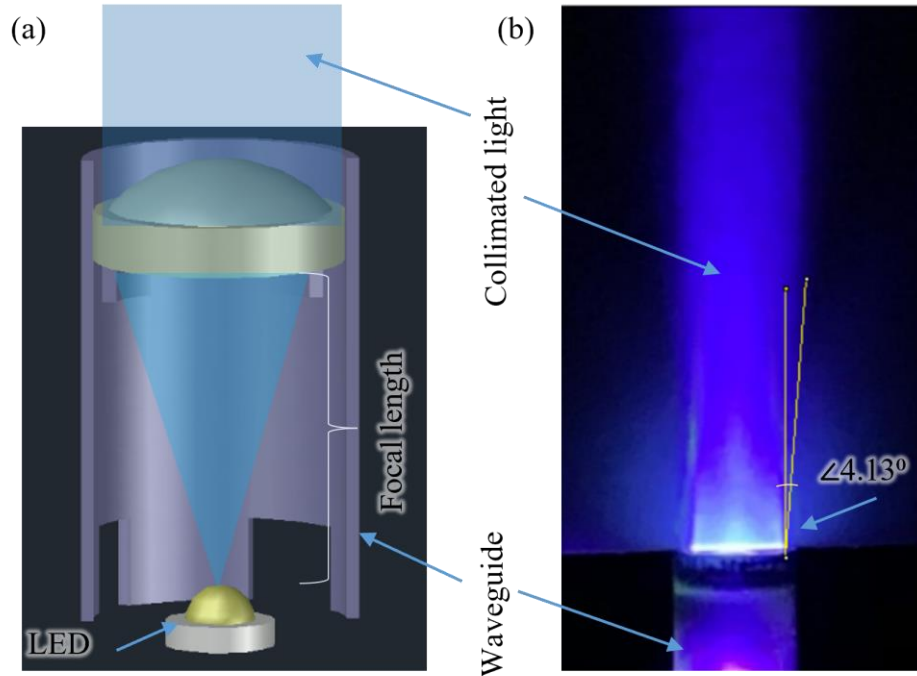


**Figure 3.6** Collimation test (a) Illustration of light collimation using waveguide and lens, (b) Analysis of collimation using ImageJ (2018) software.

After analyzing, the deviation from a perfectly collimated light was found to be  $4.13^\circ$ . In lithography systems, a deviation within an angle of  $5^\circ$  is acceptable. This collimation was obtained with a single lens suitable for lithography without involving any complicated optics.

### 3.4.2 High intensity with a variable range

Intensity is the measure of the power emitted from a UV light source for photoresist processing. Different photoresists' thicknesses require different exposure doses to cross-link the target thickness. Most of the existing exposure systems lose their initial intensity due to their bulk optical structures. Modern MEMS devices are emphasizing both micron level structures as well as millimeter levels of microstructures. Moreover, complex 3D microstructures require more exposure dose than the simpler ones. Since the exposure dose is defined by the product of intensity and time, generally, longer time is expected with low-intensity exposure systems for exposing taller and complex 3D microstructures. However, if the intensity is more, the time can be

minimized for those applications. Intensity as high as  $448 \text{ mW/cm}^2$  was recorded just above the LED surface at 140 mA current on a single UV-LED. This intensity is much higher than the commercially available lithography systems. The fabrication of tall and complex 3D microstructure becomes easier utilizing this level of UV intensity.

On the other hand, micron and sub-micron levels of microstructures require a much lower dose of UV exposure. A variable intensity light source would be beneficial to keep up with all kinds of microfabrication. The intensity of the UV-LED used in the system changes with current change and longitudinal distance. The change of intensity is exponential with the change of distance, and the change is linear with DC change. This characteristic of the UV-LEDs has been utilized for getting adjustable intensity for different applications.

Figure 3.7 shows the intensity distribution over a distance of 0 to 60 mm, while the inset shows the intensity over the distances of 20 mm to 45 mm. Even at a 10 mm distance, the intensity is  $178 \text{ mW/cm}^2$ , which is good enough to get millimeter range microstructures and complex 3D microstructures. On the other hand, an intensity of about  $35 \text{ mW/cm}^2$  is obtained at only 20 mm. Two dimming switches are connected to two power supplies to control the intensity.

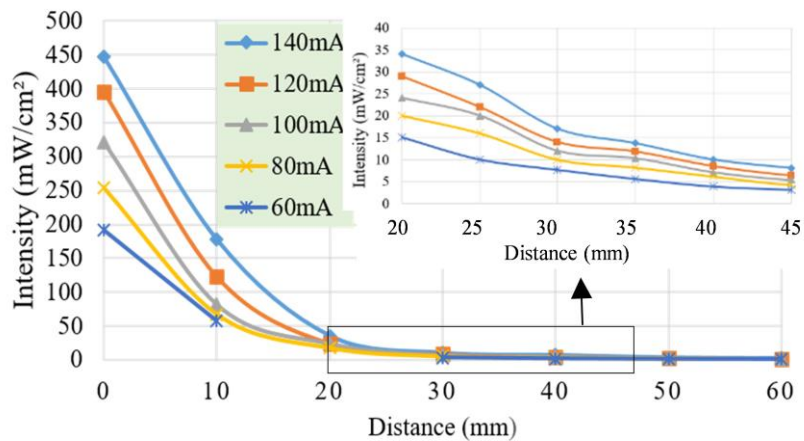


**Figure 3.7** Intensity distribution with the change of current and distance (Inset- Intensity change from 20-45 mm).

These dimming switches utilize the change of intensity with the change of current. The light source can be moved up and down along an aluminum trail and the desired intensity can be achieved by adjusting the vertical distance as well. This adjustable intensity functionality makes the light source a good tool for a wide variety of micro-fabrications.

### 3.4.3 Light homogeneity

Microfabrication involves the fabrication of hundreds of thousands of microstructures on a substrate. Uniformity of the structures is required for most of the applications like RF devices or biosensors. Due to the physical structure of the UV-LEDs and electrical connection spacing, there remains a small gap even if the UV-LEDs are arranged in compact matrices. On the other hand, the waveguides need a minimum thickness to be survivable with 3D printing. The thickness should also be enough to block any other scattering and interferences. These gaps create some dark regions, which may create inconsistencies in microfabrication. The rotational movement of the light source has been utilized in this setup to prevent the high contrast exposure created by the inter UV-LED gaps.

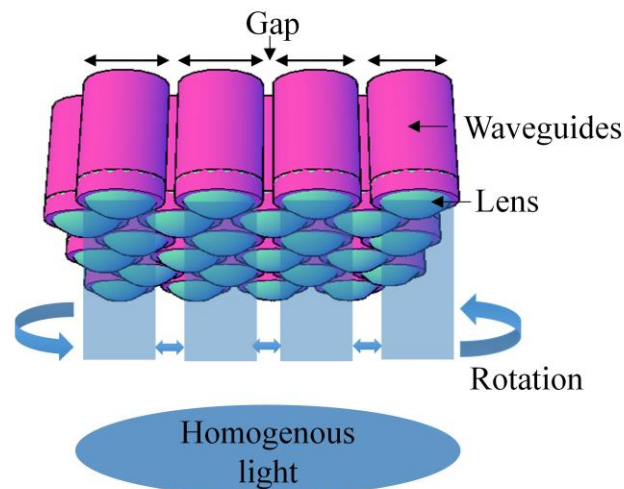


**Figure 3.8** Transforming high contrast illumination into homogenous light using rotational motion.

The principle is that each UV-LED covers its adjacent gap and creates a circular path while rotating around a central axis. Every UV-LED creates its circular path, and all the gaps are eventually covered, and overall circular illumination is obtained. Figure 3.8 shows the principle of how the matrix of UV-LEDs is converted to a homogenous circular light.

The CAD drawing shows the arrangement of the UV-LED along with the waveguides and lenses, leaving a gap in between the adjacent ones. The rotational movement is shown with arrows resulting in the homogenous distribution of the UV light.

This system has been characterized for homogeneity which has been shown in Figure 3.9. Figure 3.9 (a) shows the matrix arrangement of the UV-LEDs at its stationary position when the light source is ON,

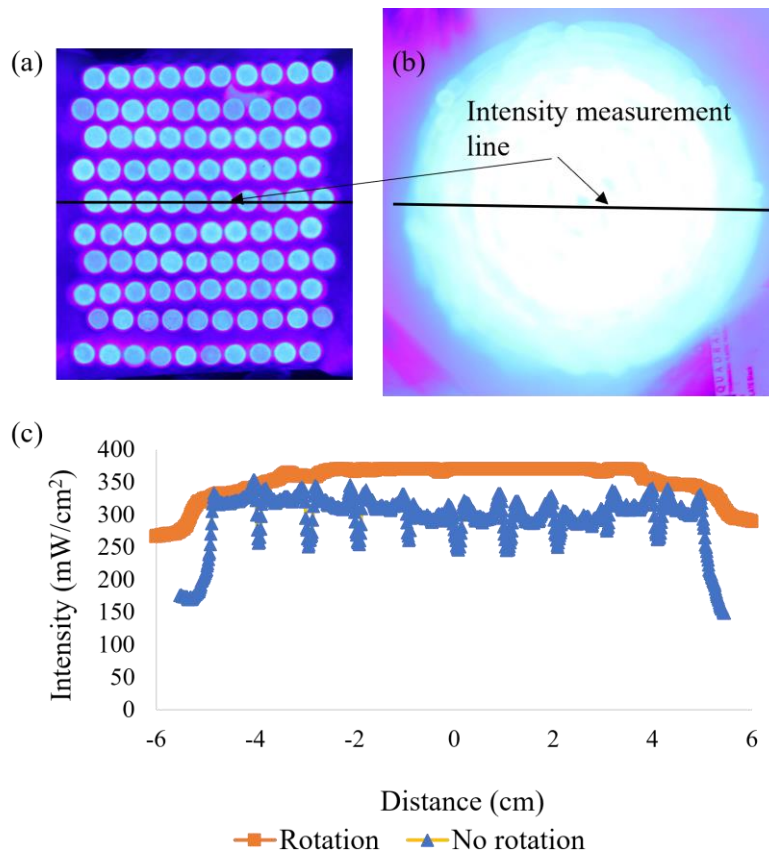


**Figure 3.9** Light homogeneity (a) Matrix of UV-LEDs without rotation, (b) UV-LEDs with rotation, (c) Graphical representation of the light distribution over the intensity line.

Figure 3.9 (b) shows the light distribution when the light source is rotated, 3.9 (c) shows the graphical analysis of the light distribution over the central intensity lines as shown in Figure 3.9 (a) and (b). This graph shows that the highest intensity obtained from a single LED without rotation was noted at 336 mW/cm<sup>2</sup> and the lowest intensity in the dark area was 244 mW/cm<sup>2</sup>. A contrast of 15% was obtained without rotation.

The contrast is calculated using the equation,

$$\text{Contrast (\%)} = \frac{\text{Highest intensity} - \text{Lowest intensity}}{\text{Highest intensity} + \text{Lowest intensity}} \times 100 \quad (3.2)$$

Whereas the intensity variation is in between 367 to 354 mW/cm<sup>2</sup> reducing the contrast up to 1.8%.

### **3.5 Additional features of the lithography system**

This system is reliable for continuous operations. Lithography is a continuous process that needs continuous operations. On the other hand, the system needs to keep on for a long time for millimeter thick SU8 structure fabrication or complex 3D microstructures fabrication. Therefore, the system needs to be checked for compatibility and stability with long-time operations. For testing the reliability, the light source was kept turned on for 100 hours without a break to check the compatibility. The intensity was being monitored by using a monitoring software (i-Spyconnect, 2018).

An intensity meter was used where the sensor reads the intensity in the range of 400 nm, and the monitor shows the intensity in mW/cm<sup>2</sup>. For keeping the sensor safe from heating up, it was placed at a far distance (30 mm) from the light source, and the intensity was monitored continuously. Figure 3.10 shows the intensity monitored over 100 hours.

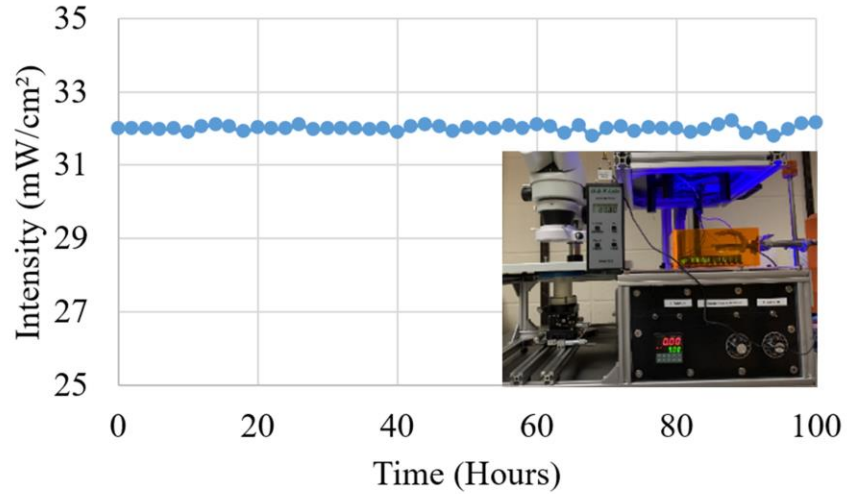


**Figure 3.10** Reliability test of the UV-LED lithography system.

The average intensity noted at this distance remains between 31 mW/cm<sup>2</sup> to 33 mW/cm<sup>2</sup>. The experimental setup has been shown in the inset of Figure 3.10. Considering the system's stability over a long span of 100 hours proves the reliability of this system for tall as well as complex microstructure fabrication.

### 3.6 Results

A lithography light source is primarily judged based on the highest resolution it can achieve. Resolution is a measure of the minimum feature size that can be patterned or transferred to a photoresist coated substrate. The resolution of a lithography system can be defined from the equation [60]

$$R = \sqrt{K\lambda s} \quad (3.3)$$

Where,  $\lambda$  is the wavelength of the light source, K is a constant which is considered to be around 1 and s is the air gap between the mask and the wafer. The smaller the wavelength, the smaller the resolution it can achieve. Since, the wavelength of a system is chosen beforehand, in

this case 405 nm, and for contact lithography,  $s$  is zero, the resolution depends on the wavelength of the system. The theoretical resolution of the system with a 405 nm UV-LED is around 20 nm.

However, the contact lithography faces some defects owing to the uneven gap created due to the deposition of particles and the surface plasmon interference between the mask and the wafer. On the other hand, the demonstrated UV-LED light source is not a point source which could be the ideal light source for lithography. As a result, the practical resolution of the system is degraded. Practically, around 0.5  $\mu\text{m}$  resolution can be obtained from a standard contact lithography system [61] depending on the wavelength and the thickness of the photoresist. As the UV light passes through thicker photoresists, more diffraction occurs changing the patterning resolution.

Among the several standard ways of getting higher resolution, reducing the wavelength of the light, avoiding hard contact of the mask and the wafer, multiple -exposure, off-axis illumination can be used. Positive photoresists also give better resolution due to their smaller polymer sizes. However, since the wavelength was chosen primarily for high aspect ratio microstructures and the negative photoresists of around 30-40  $\mu\text{m}$  thickness have been used for stable device fabrication, a deviated resolution is obtained from the theoretical one. But this is not the limit of the lithography system rather it is possible to get higher resolution with thinner photoresists and minimizing the deposition of particles for ensuring a perfect contact.

### ***3.6.1 High-resolution micron devices fabrication***

The microstructures having a diameter of 1-200  $\mu\text{m}$  are classified as micron devices. Resolutions as low as several microns are hard to achieve without highly collimated light sources. Figure 3.11 shows an example of micron-level device fabrication where small feature sizes as small as 3  $\mu\text{m}$  was achieved.

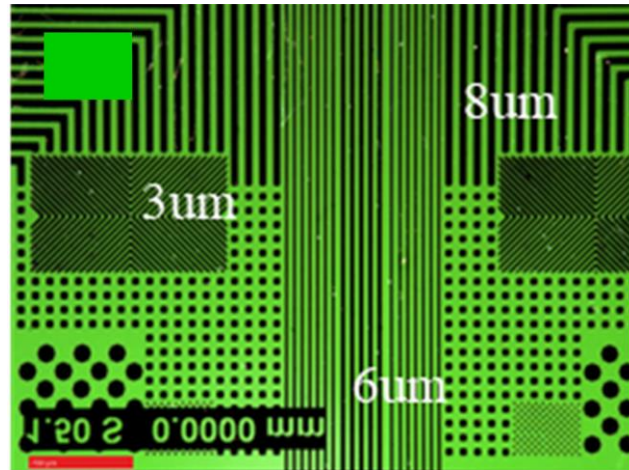


**Figure 3.11** Micro device fabrication.

For fabricating this structure, SU8 2025 was spin-coated on a patterned Chromium coated glass at a speed of 2000 rpm to get around 40  $\mu\text{m}$  thickness. After soft baking for 5 minutes at 95° on a hotplate, it was exposed at an intensity of 75  $\text{mW}/\text{cm}^2$  for 2 minutes.

After that, the sample was post-exposure baked and developed in SU8 developer with mild agitation for 1 minute. For its narrow-patterned characteristic, it has potential uses in microfluidic channels. The single substrate having different sizes of patterns signifies those different resolutions on the same sample can be obtained with optimized exposure and controlled developing.

### ***3.6.2 High aspect ratio micron device fabrication***

The aspect ratio is defined as the ratio between the diameter and the height of the microstructure. It is challenging to get micromachined structures with small diameters and longer heights. Highly collimated light with sufficient intensity is required to get a good resolution and thick photoresist crosslinking.

Figure 3.12 shows the example of a 1370  $\mu\text{m}$  tall pillars with a pattern diameter of only 34  $\mu\text{m}$ , giving it an aspect ratio of around 1:40. The intensity used was 175  $\text{mW}/\text{cm}^2$  for 15 minutes.

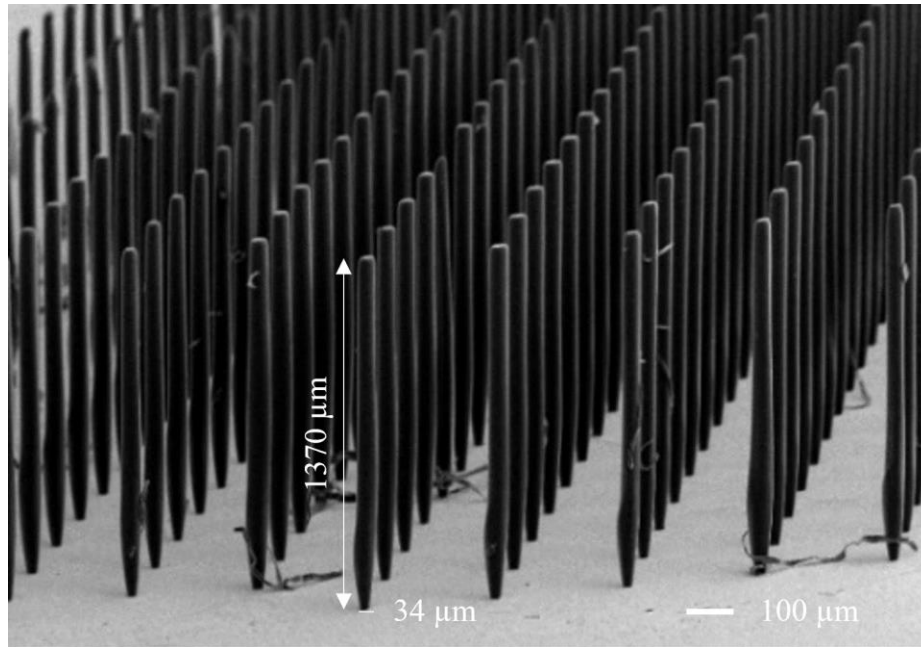


**Figure 3.12** High aspect ratio micron device.

Since the light passes through small diameters, diffraction effects are seen at the bottom of the structures since these parts receive the maximum exposure throughout the time. These vertical standing microstructures have potential uses in RF MEMS and communication devices.

### ***3.6.3 Millimeter-tall device fabrication***

Millimeter tall microstructures are very challenging to get by using UV lithography, as a lot of energy is required for cross-linking a millimeter thick photoresist through small diameters. Since most of the existing UV lithography sources have lower intensities, a very long-time exposure is required for tall microfabrication. Figure 3.13 (e) shows a matrix of 2 mm high micro-towers with its fabrication method since this method is slightly different from the traditional ones. Figure 3.12 (a-d) shows the fabrication method for millimeter tall microstructure fabrication. Since photoresists thicker than several hundred microns cannot be spin-coated, it is directly cast on the patterned Chromium glass sample.

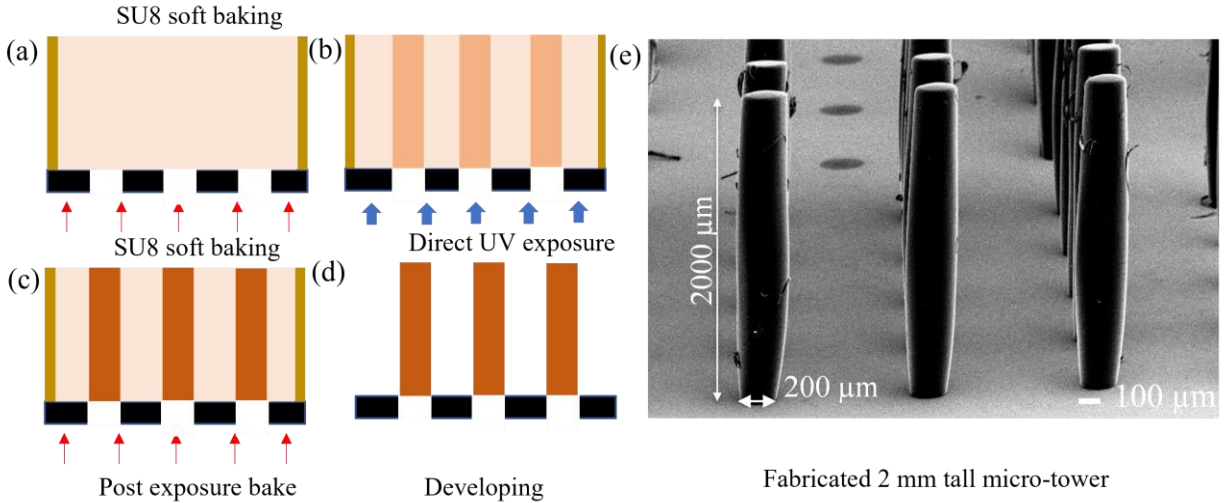


**Figure 3.13** Millimeter tall pillar fabrication (a-d) fabrication method of tall microstructure, (e) 2 mm tall micro towers.

A 3D printed boundary is used for keeping the photoresist within a given height and for avoiding spilling. The sample was soft baked for 15 hours at a temperature of  $95^{\circ}$ . It was cooled down naturally and was UV exposed following a top-down setup.

The intensity was around  $190 \text{ mW/cm}^2$  and the exposure time was 10 minutes to get these 1:10 aspect ratio millimeter tall micro-towers. After one-hour post exposure baking, it was developed in SU8 developer solution with mild agitation. Figure 3.13 (e) shows the fabricated 2 mm micro-towers. The surface quality of the side walls is also good. These structures have the potentiality to be used as RF antennas, airlifted frequency-selective devices.

### 3.6.4 3D inclined microstructure fabrication

The modern MEMS devices are getting compact, and multiple functions are being integrated into a single device. As a result, complex 3D microstructures are becoming increasingly popular for integrating multi functionalities together. Figure 3.14 shows an example of the complex 3D microstructure fabrication where adjacent inclined pillars are made to form a chained structure.

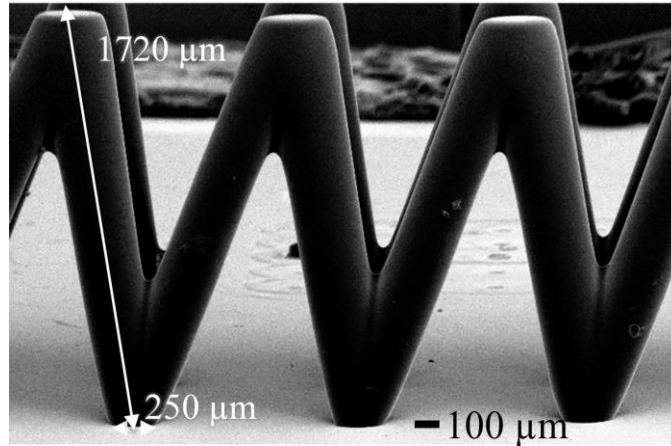


**Figure 3.14** 3D inclined microdevice.

This was done by keeping the sample inclined at an angle of  $70^\circ$  with respect to the light source at an intensity of  $175 \text{ mW/cm}^2$  for 18 minutes for each inclined pillar.

The two inclined pillars are  $90^\circ$  out of phase. Although the light source can give one-directional exposure only, the sample can be arranged at different angles to get complex 3D microstructures. This observation made from this light source prototype can be utilized in the next prototypes for complex 3D microfabrication.

### 3.7 Summary

A UV-LED lithography system has been demonstrated with single-lens collimation giving high and adjustable intensity and homogenous illumination. This system can show traditional micro-fabrications and difficult-to-get micro-fabrications such as high-aspect-ratio or millimeter tall microstructures. The exposure system has a narrow bandwidth, negating the need for a filter while giving high intensity as high as  $448 \text{ mW/cm}^2$ . The intensity can be varied by changing the current and the distance, giving the system the versatility of fabricating structures within a range of a few microns to a few millimeters, which is superior to the conventional lithographic systems. The uniform distribution of the collimated light with high intensity gives this system the ability to

replace the traditional lithographic systems with easy maintenance. The system is reported to give resolutions up to 3 microns for the demonstration and can give about 2 mm tall SU8 micro-pillars. These parameters were chosen for demonstration only, however the system is not limited to these parameters only. The introduced system has the potential to give higher resolutions and taller micro-structures. The results fabricated using this system hold great potential in the micro-fluidic channel and RF micro antenna fabrications. While this setup only demonstrates a prototype of a one-directional UV lithography light source, the findings are valuable in the way of building a modified and advanced lithography system.

# **Chapter 4 - Developing multidirectional lithography system for traditional and complex 2D/3D microfabrication<sup>2</sup>**

## **4.1 Introduction: Multidirectional lithography for complex 3D microfabrication**

3D microstructures have application in different research and applied fields like high aspect ratio bioMEMS [63], cytometry devices for biomedical applications[64] RF antennas and filters [65], fiber optic devices [66]. Some of the older methods of 3D microfabrication were done by a combined micro-stereolithography and thick resist UV lithography [67], single-photon absorbed photopolymerization [68], two-photon absorbed photopolymerization [69], [70]. Among the recent 3D microfabrication systems, Contact liquid photolithographic polymerization is one method that demonstrates layer-by-layer photopatterning with a fine movement of the sample stage with x-y-z direction to form 3-D microfluidic device [71], moving mask lithography [72], micro-stereolithography using layer by layer photopolymerization [73] are notable. Similarly, a stereolithographic approach was introduced for photopatterning of metal molding using a positive photoresist [74]. A focused UV light stayed at a fixed position with an on-and-off function is synchronized with an x-y-z movable sample holder to draw a pattern by layers to form a 3-D structure. A method of high-resolution projection micro stereolithography (PμSL) using a spatial light modulator as a dynamic mask which enables a parallel fabrication of highly complex 3D microstructures [75]. A prism-assisted lithography was introduced to change the light exposure angle to photo-pattern a slanted sidewall of the 3-D microstructure [76]. A backside UV exposure and multiple layer stacking method with the aid of a fine alignment system was also introduced to form several hundred micron 3-D structures for cell culture scaffold application [77]. Mask-less

---

<sup>2</sup> This chapter is a reformatted and slightly modified version of our article [62]

lithography methods using digital micromirror (DMD) and liquid crystal display (LCD) were also introduced and have become the basis of today's DMD or LCD 3-D printer [78], [79].

Several 3-D microlithography methods have utilized a layer-by-layer stage control to form 3-D photo-patternable structures. The nature of the layer-by-layer fabrication method creates multiple steps on an inclined structure, which often becomes a challenge to be used as RF or optical microdevices due to the high surface roughness. A multidirectional UV lithography has been introduced for 3-D microfabrication where a sample holder was tilt-rotational to create 3-D microstructures with a single direct exposure [44], [80]. Since the tilt-rotational sample holder could introduce various inclined angles tangent to the light source with a microcontroller command, various 3-D inclined structures such as horns, tilted pillar, and triangle shapes have been freely able to photo-pattern. This method is superior for the surface quality of the inclined sidewall over the prism-assisted lithography or lay-by-layer lithography method. With an automated multidirectional lithography system, complex 3-D microstructures such as a letter horn and a ribbon horn [81], and nanoscale 3-D structures [82] were presented as advanced 3-D structures. Also introducing various refractive index mediums in the automated multidirectional lithography extended 3-D projectable volume by increasing the tilt-able angle [83] and millimeter height pillar was introduced by increasing the exposure time by demonstrating 3-D toroid inductor [84].

Recently, the multidirectional UV lithography has been further advanced with the UV-LEDs as its light source [85] [86]. The versatility of the UV LEDs includes the ease of control of individual LED in terms of an on-off switching as well as intensity variation. Based on the analysis of UV-LEDs as lithography light sources [87], a higher power but smaller surface mount type UV-LEDs were tested for the multidirectional UV-LED lithography system. This chapter presents a

computer-controlled multidirectional UV-LED lithography system for 3-D microfabrication. The presented lithography system has been designed for complex 3D microfabrication with the help of an integrated tilt-rotational sample holder. The light source has adopted adjustable or programmable high-intensity UV-LEDs as a light source for photopatterning both several microns thin and several millimeter thick SU-8 photoresist processes. The prototype of the proposed system comprises of 5-by-5 surface-mounted type UV-LEDs. It is equipped with a collimation lens, a 10 cm tilt-rotational sample holder for introducing multidirectional light exposure, and a computer-control asset for synchronized controls of the light source and the sample holder. With the tilt-rotational sample holder, the multidirectional UV-LED lithography system can fabricate various 3-D microstructures in a wide range of photoresist film thicknesses. An orbital rotation method was introduced for homogenous light distribution and ease of control and configuration of the UV-LEDs. The system has been characterized for collimation, homogeneity, uniformity, multidirectional exposure. The 3-D microfabrication result includes an array of micro triangle slabs, a 3D tripod array, 3 mm micro-towers, the different scale same 3-D geometry structures on the same substrate.

#### **4.2 Concept of the multidirectional lithography system**

The UV-LED lithography system demonstrated in this chapter is based on the matrix arrangement of high-intensity UV-LEDs. An orbital movement of the light source is utilized to make a homogenous light source, and the tilt-rotational sample holding system was utilized for creating 3D ray tracing. This system is designed to fabricate complex 3D microstructures by moving the sample holder in different tilt angles and rotations in 3D directions. This sample holder, along with the high-intensity lights, makes this system suitable for very high aspect ratio vertical and inclined 3D structures.

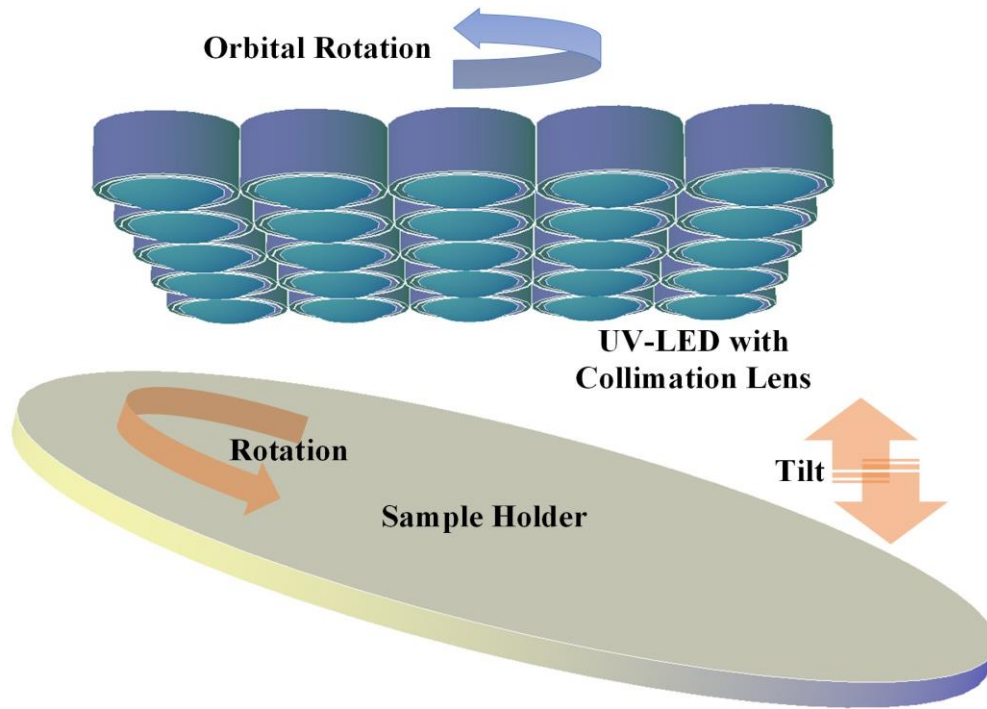


**Figure 4.1** Concept of the multidirectional lithography system.

Figure 4.1 shows an illustration of the multidirectional UV-LED lithography system. The compact matrix of UV-LEDs and the waveguides and collimating lenses perform a continuous rotational motion. The circular sample holder is placed directly under the light source, keeping it at a definite distance to tilt and rotate simultaneously without hitting the light source.

### 4.3 System design

The system has been designed based on the unique features of UV-LEDs and the integration of the tilt-rotational sample holder. Although this system describes a small prototype, the scientific findings and significant results can be beneficial for designing large scale and improved setups later. The significant design considerations are described in the following sections.

### 4.3.1 Light source

The UV-LEDs used in this system are surface-mounted type LEDs. The chosen UV-LED (LEDUVA35T01VL00, LG) has a width and height of 3.4 mm by 3.4 mm. This LED has been chosen for its high intensity and narrow bandwidth. Each of the chosen UV-LEDs can handle the current up to 500 mA with 3.4 V voltage, and a total power of 1.15 W. A prototype of the UV-LED lithography system has been built comprising 25 UV-LEDs in a matrix form of 5 rows and 5 columns. Since one problematic UV-LED can affect the whole UV-LED light source is connected in series, the UV-LEDs in this system have been made to be connected in parallel so that each UV-LED can be controlled individually. Individual control over the UV-LEDs decreases the chance of overall damage and allows creating a variation of UV-LED parameters, including intensity and wavelength. Figure 4.2 (a) shows the matrix of 5 by 5 UV-LEDs placed on the PCB. Figure 4.2 (b) shows the LED's spectrum analysis, which was measured with an optical spectrum analyzer (BLUE-Wave, StellarNet Inc.). The intensity profile reaches its peak at 405 nm, and the 50% intensity bandwidth ranged from 396 to 416 nm, which is a narrow bandwidth for eliminating the need for an expensive optical filter. All the 25 UV-LEDs in this prototype are 405 nm UV-LEDs, however, there are scopes to customize the UV-LEDs.

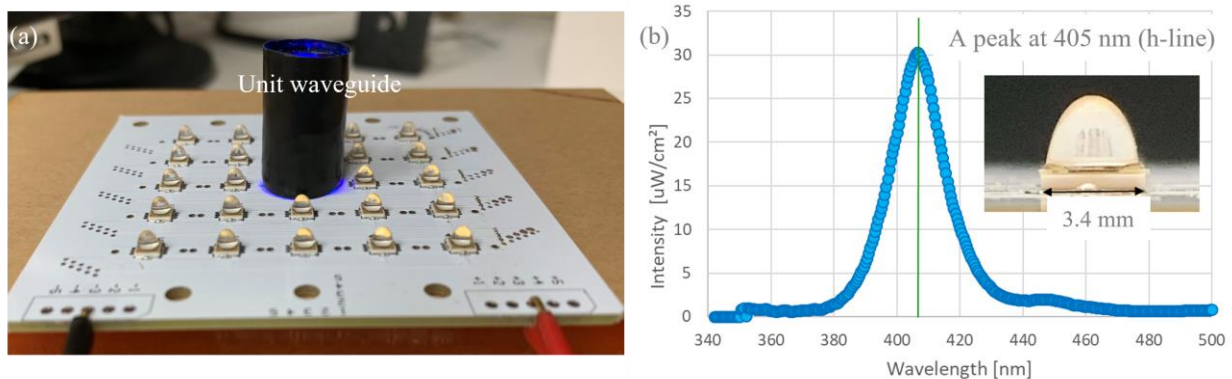


**Figure 4.2** Light source (a) Matrix of 25 UV-LEDs on the PCB with single waveguide, (b) Wavelength spectrum of the UV-LED (Inset- Unit UV-LED).

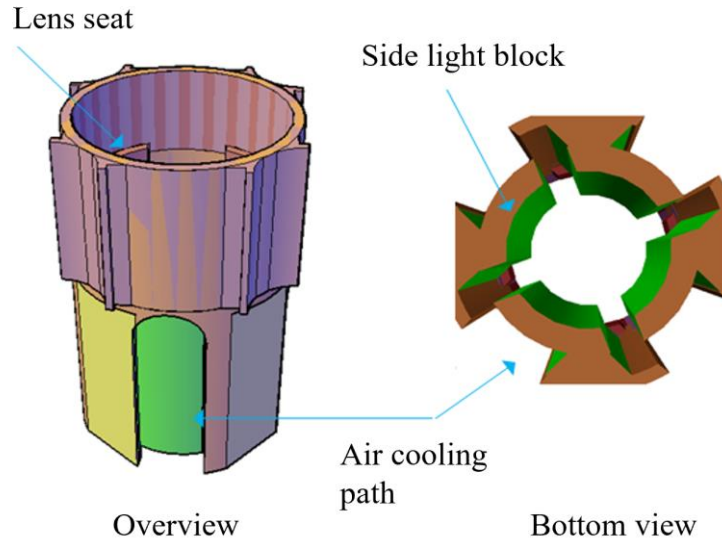


**Figure 4.3** Illustration of the waveguide.

A 3D printed waveguide and a cabochon glass were used as the collimating structure. The waveguide was customized for guiding the divergent beam having a diverging angle of  $55^\circ$ , and it was built to accommodate the lens with minimum loss of light and maximum heat dissipation by creating curved ventilations. The waveguide was designed in AutoCAD (2018) and printed with a Form 2 (Formlabs) SLA 3D printer. Figure 4.3 shows an illustration of the waveguide design. A large amount of heat is produced from turning on the LEDs, which can melt or deform the 3D printed structures if filaments or standard printing resin are used. Therefore, high-temperature resin (RS-F2-HTAM-02, Formlabs) was used, which can handle up to  $238^\circ$ , giving the structure thermal stability and preventing it from thermal damages created from the light source itself. One more advantage of using the high-temperature resin is that it can print with a resolution of 25 microns, suitable for printing small features and details.

The waveguide wall thickness was optimized to minimize the shadow area and get a robust structure after 3D printing. Considering the resolution and the robustness, a thickness of 0.5 mm

was chosen for the outer walls. A seating arrangement was designed to be thick enough to hold the lens but not too thick to block a significant amount of light. The opening hole was designed to hold the lens tightly, and no light is leaked through the periphery of the lens. Overheating inside the waveguide can create a smoking effect on the lenses, damaging the fabrication quality. Therefore, small windows were created at the bottom of the waveguide to channel the heat out. However, there remains a chance of light leakage through the windows or, in other words, ventilations. To prevent this leaking, a UV blocker was created surrounding the LED, ventilating holes with a ‘C’ like a pathway to channel the heat. This UV blocker and the waveguide wall create a complete structure that guides the light directly towards the lens, helping dissipate the heat and preventing light leakage. As the printing resin is transparent, the waveguides may scatter some light, affecting the fabrication. Therefore, the waveguides were dyed with high-temperature black enamel paint (241169, Rust-Oleum) all over after developing properly with clean IPA. A cabochon glass lens (PH PandaHall, Inc.), as shown in Figure 4.4 (a), was adopted for light collimation. The lens has a diameter of 10 mm, an offset thickness of 1.3 mm, and a curvature thickness of 2.2 mm respectively. Figure 4.4 (b) shows the assembled waveguide and lens. For printing and setting convenience, all the 25 waveguide units were combined and printed together.

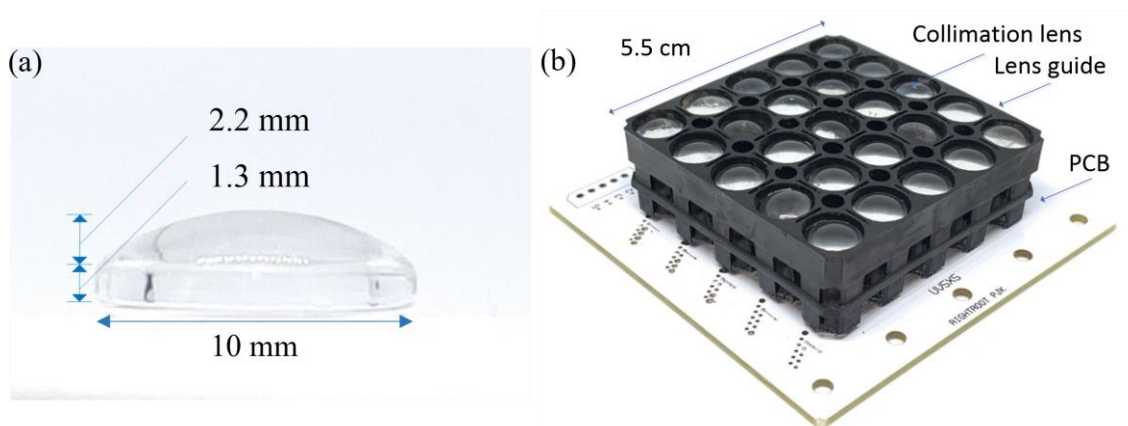


**Figure 4.4** Light source elements (a) Collimating glass lens, (b) Waveguide and lens assembled on the PCB.

### ***4.3.2 Multidirectional system***

The light source was designed to have an orbital motion where each UV-LED rotates around its axis to compensate for the high contrast illumination. In the preceding chapter, a circular motion around a central axis was used to obtain homogenous illumination where each UV-LED rotates around a central axis and covers up the gap adjacent to it. In this new setup, an orbital motion was used so that each UV-LED rotates around its own axis and each UV-LED can be controlled individually. As a result, each UV-LED covers up all the gaps surrounding it and none of their motion disturbs the overall profile. In this structure, the rotating plates were made by LASER cutting Acryl sheets, and the gears were 3D printed using Photon (Anycubic) 3D printer. Since these structures are supposed to face many frictions and might break, a tough resin (Anycubic) was used to get more robust structures. A DC motor (12V, 600 rpm) and small metal bearings (22 mm diameter) were used to create the orbital motion. This sample holder is connected to two stepper motors, one of which controls the 360° rotation and the other controls the tilting along the Y-axis. These motors are controlled using a microcontroller and the programming software All-motion software (EZ4AXIS, All Motion, Inc.). The tilt-rotational sample holder was introduced to create multidirectional ray tracing with the light source. The sample holder consists of a metal disc of 10 cm diameter suspended freely. In the final setup, the light source was set on one piece of Acryl plate, rotatable in an orbital motion. This Acryl sheet and another stationary acryl plate that holds the motor are both suspended to an Aluminum extrusion frame. This whole arrangement was set on a firm wooden board. Figure 4.5 shows the overall setup of the multidirectional UV-LED lithography system. This benchtop setup is lightweight and can be moved easily. The powers are connected externally, and a UV protection shield is used separately as this system does not have an integrated UV shield.

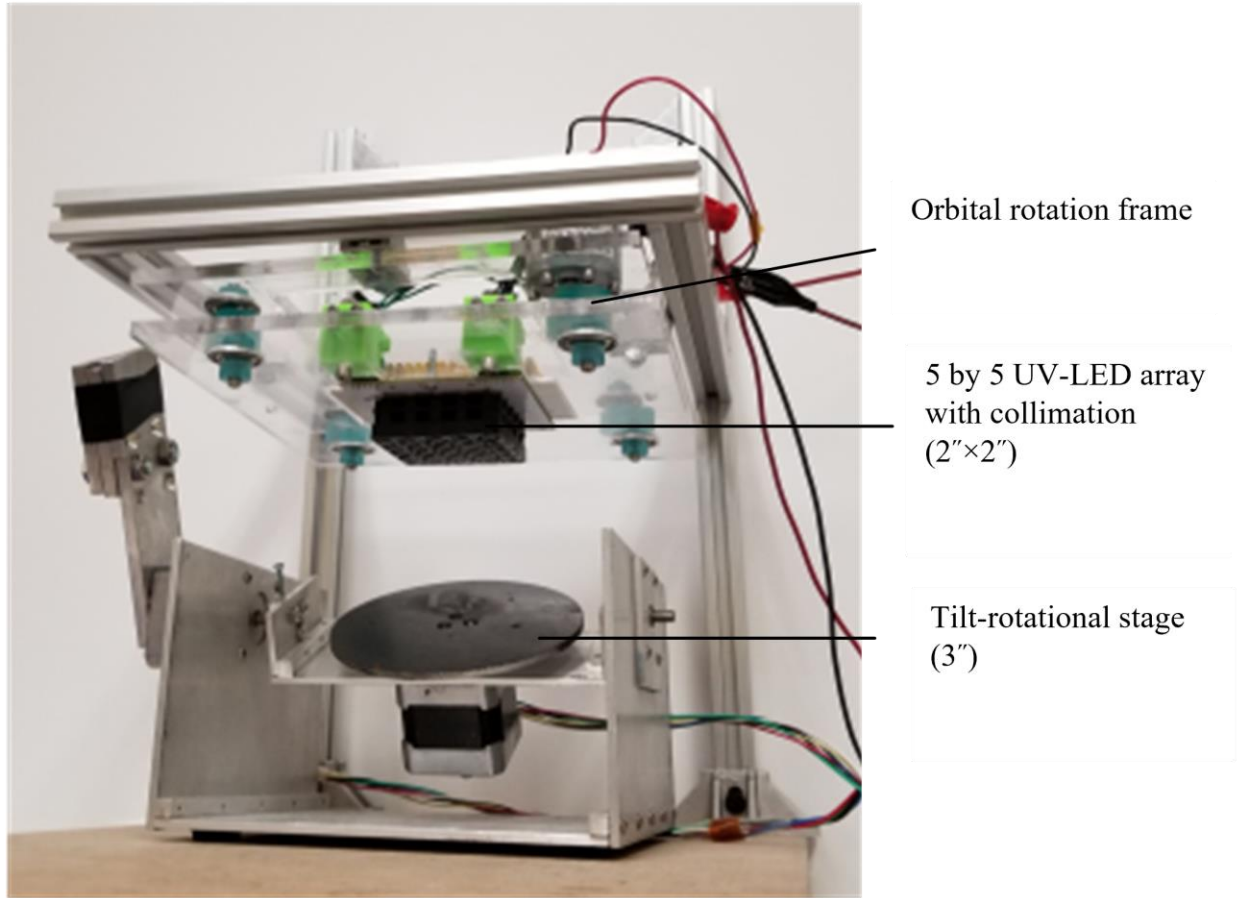


**Figure 4.5** Overall setup for the multidirectional UV-LED lithography system

#### **4.4 Characterization**

The 5 by 5 UV-LED lithography system has been characterized for the features like light collimation, adaptive intensity, thermal optimization, and uniformity of the light distribution.

##### ***4.4.1 Collimation for the PCB embedded UV-LEDs***

The glass lens was placed at a distance equivalent to the focal length from the UV-LED. The lens receives the beam diverging at an angle of  $55^\circ$  and converts it into parallel beams. Figure 4.6 (a) shows the experimental setup with the array of UV-LEDs with waveguides and lenses and shows how a vertical screen was placed above the light source to check the collimation.

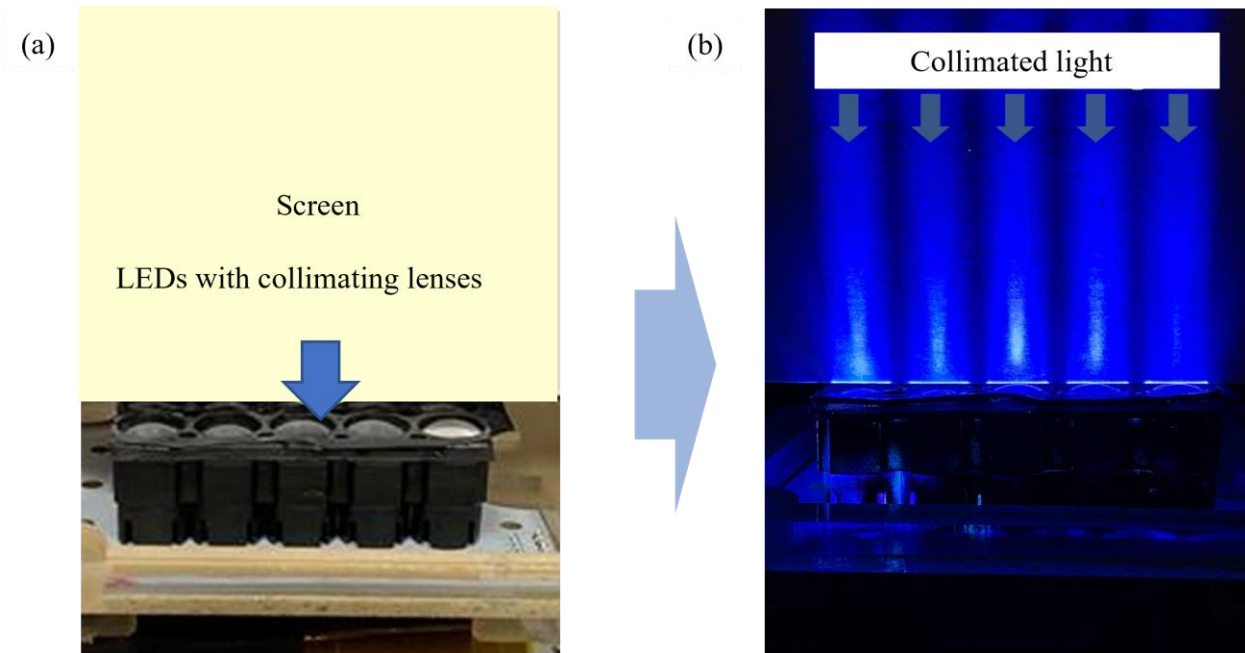


**Figure 4.6** Collimation test (a) Test setup, (b) Collimated light projected on a vertical screen.

The five consecutive UV-LEDs were powered up and the light was projected through the white screen in the darkroom. Figure 4.6 (b) shows the result for collimation. The projected collimation angle was measured at the sidewall of the light propagation column using software, ImageJ (2018). It showed  $4.13^\circ$  divergence from the perfect collimation. Since the divergence is within  $5^\circ$ , this setup is acceptable for the photolithography purpose.

#### ***4.4.2 Adjustable intensity with individual UV-LED control***

A unique feature of the multidirectional UV-LED lithography system is the adaptive intensity. Since the UV-LED lithography system is designed for a variety of microfabrication starting from several microns to several millimeters, the intensity needs to be perfectly set for all kinds of fabrications without changing other parameters. On the other hand, since the tilt-rotational sample holder is introduced, the intensity can be different for different inclinations. The ability of the UV-LED to adjust with different amounts of current passing through it was utilized for making the light source adaptive to get uniform intensity over the target sample.

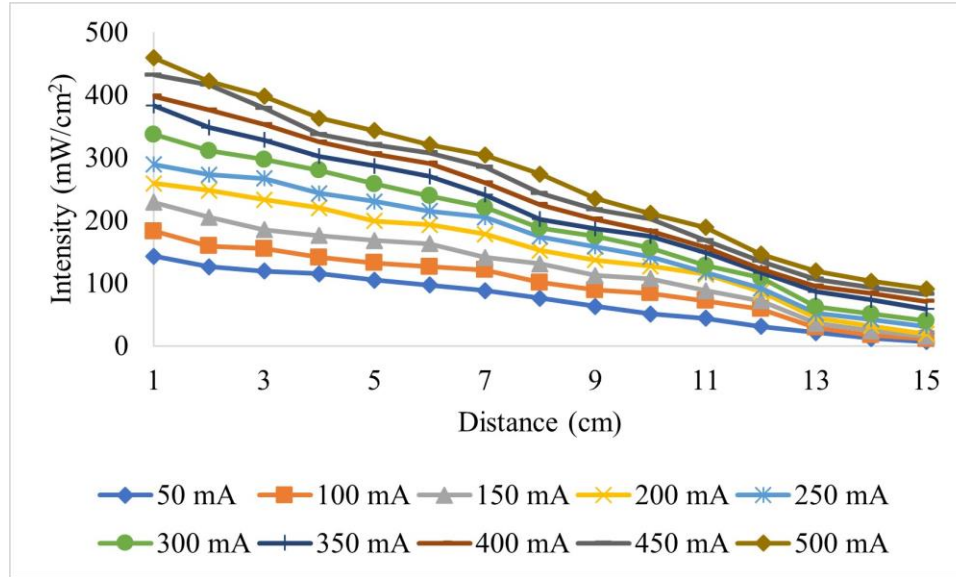


**Figure 4.7** Intensity variations with the change of current and distance.

This adjustable intensity can also be utilized for getting different microstructures on a single sample with a single exposure. Figure 4.7 shows the measurement result of the UV-LED light intensity. The maximum allowed current for each LED was indicated as 500 mA from the manufacturer. The light intensity was measured at distances of 1 to 15 cm. The intensity graph shows the highest intensity achieved with 500 mA current at a distance of 1 cm from the light source, which is 452 mW/cm<sup>2</sup>. This high intensity is beneficial for millimeter-high microfabrication. The light intensity at the distance of 15 mm still showed around 15 mW/cm<sup>2</sup>, which is still high enough for the thin SU-8 process. Since the system was designed for tilt rotational sample exposure, the intensity was adjusted for tilted exposure. While the diameter of the sample holding disc was 10 cm, there should be enough space for the safe movement of the disc while exposing. The distance of around half of the circular disc is also secured for the tilt-rotational sample holder's space, and the intensity is sufficiently preserved. On the other hand, as shown with lower current values, the lower intensities are suitable for cross-linking lower thicknesses of photoresists and are beneficial for several micron microstructure fabrications.

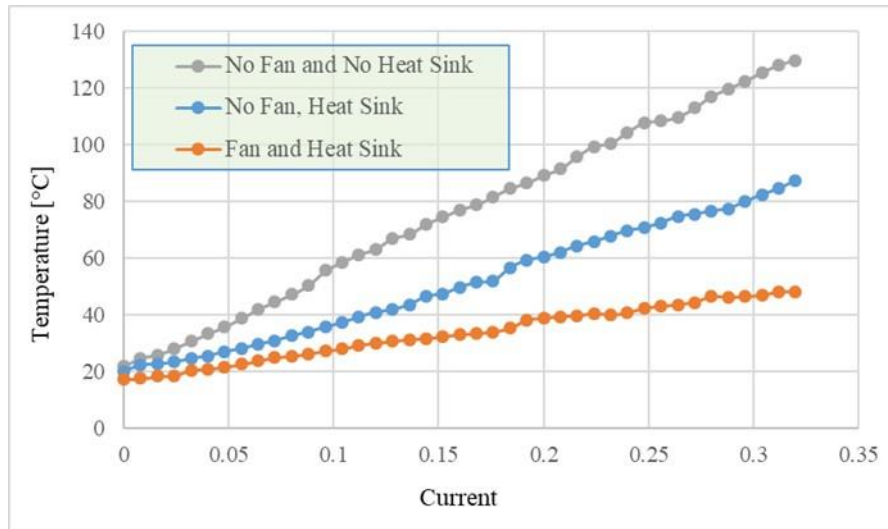


**Figure 4.8** Thermal behavior test with different cooling aids.

Either of the parameters can be changed for obtaining the desired intensity. The measured data of the variable light intensity can be a reference later for a programmable light exposure system.

#### **4.4.3 Thermal control with advanced waveguide design and additional cooling methods**

As the current flows through each LED, the electron flow creates some excitement on the LED which causes some heating on the UV-LED and its adjacent surfaces. If the heat is not minimized, it can affect the LED itself and the other optical elements. The applied current to each LED was increased up to 320 mA with every 8-mA step and the thermal behavior of the LED was observed. The first observation was conducted without any heat management tool. Starting from room temperature, where each LED was heated up to 129.7°C at 320 mA, which is high enough to damage the LED. The same test was performed after adding an aluminum heatsink (BNTECHGO, Inc.) to the backside of the UV-LED PCB board. Figure 4.8 shows the change of temperatures with and without the cooling methods on the surface of the LED. The heat increment was proportional to the current applied, and the highest temperature was observed at 87.3 °C.

Based on the recommended temperature for the LED from the manufacturer, the 87.3 °C was marginally acceptable, but any increase could affect the system. Therefore, an external fan was added, and the same temperature experiment was conducted. While observing the slow increment of the temperature, the highest temperature obtained was 48 °C at 320 mA. The lens receives the heat from the UV-LED through convection and is placed in a confined area, overheating can create smoking effects on the lens as well. The PCB is in direct contact with the UV-LED and holds the soldering and other optical components. Overheating on the PCB may de-solder the connections, affecting the whole setup. Therefore, the temperature on the lens and PCB surface with and without an external fan was measured as well. Figure 4.9 shows the temperature changes with and without the fan in the lens surface and the PCB surface. The reading shows that the PCB temperature reaches a highest of around 62° at a current of around 250 mA/LED. The heat reduces to around 45° after adding the fan. The lens, on the other hand, reaches a temperature of 82° and is reduced to around 50° with the addition of the fan.

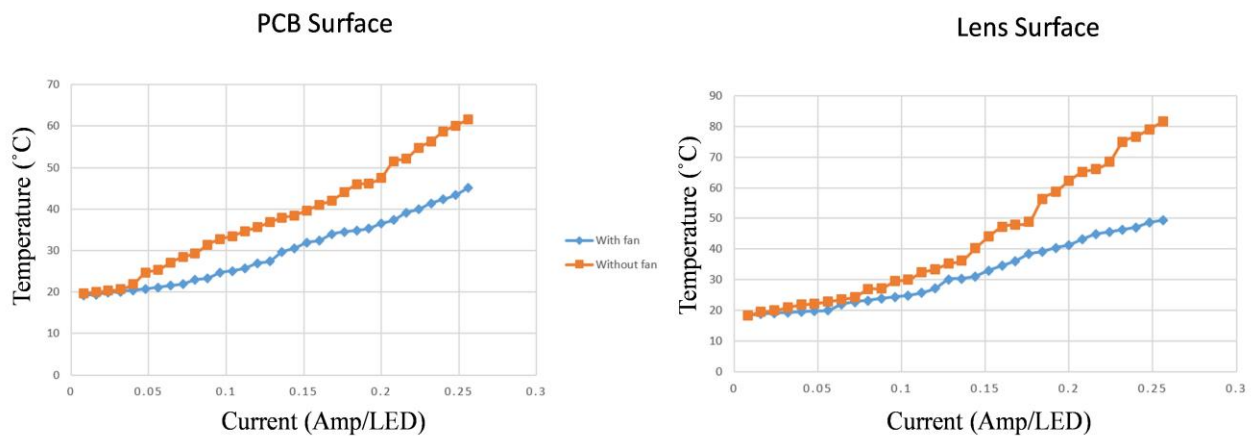


**Figure 4.9** Thermal control test on the PCB surface and Lens surface.

To be noted here, although the PCB is adjacent to the LED, it is less heated than the lens because of the temperature-friendly Aluminum PCB board and the metal heat sink used beneath the PCB board. This test implies that suitable cooling systems will be required for similar prototypes and bigger setups.

#### ***4.4.4 Homogeneity with the orbital motion of the light source***

Homogenous light distribution is significant in microfabrication for consistent microfabrication. Consistency must be maintained among the microstructure parameters and characteristics. A lack of consistency and uniformity can adversely affect the applications like RF antennas where the periodicity of the same structure is required. A high contrast illumination can change the microstructures features as the exposure dose can vary in different regions. Since the UV-LEDs are arranged in a parallel matrix on the PCB, a high contrast illumination is created. Therefore, the light source of this system was designed to have an orbital rotation which is advantageous for regional LED control as the location of each LED remains fixed even with the rotation.

Slip ring is a mechanical component used in devices where a 360° rotation is needed. In the UV-LED lithography setup discussed in chapter 3, the PCB containing all the UV-LEDs was connected to the motor through a slip ring so that the motor rotation can rotate the PCB along with the UV-LEDs. In this setup, the whole light source rotates around one central axis. As a result, each UV-LED must rotate around the whole area to cover up the gap in between the adjacent UV-LEDs. In the first setup of the UV-LED lithography light source, same kind of UV-LEDs were connected in series and was centrally controlled. When the slip ring rotates each UV-LED rotates around the central axis and covers up the gaps. Since, all the UV-LEDs are same, the movement of it around the central axis does not affect the adjacent UV-LED exposed area.

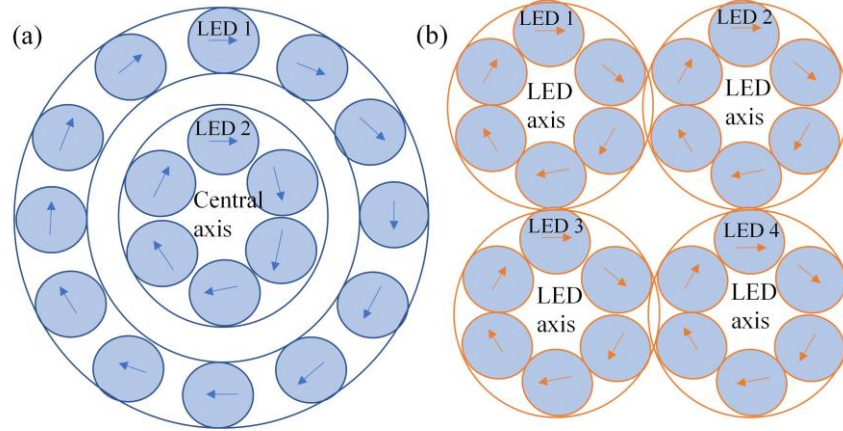


**Figure 4.10** Light source motion illustration (a) Rotational motion around the central axis, (b) Orbital motion around LED's own axis.

However, for the other setups of the UV-LED lithography systems, an individual or regional control the UV-LEDs is aimed. Mixed wavelengths can also be used if an orbital rotation is used

Figure 4.10 shows a comparison between two types of rotations of the light source. The rotational movement is shown in Figure 4.10 (a), where each LED has changed its position to complete a rotation around a central axis. Figure 4.10 (b) shows the orbital movement where each LED traverses around its own imaginary axis without changing position.

As in orbital rotation, each UV-LED rotates around its own axis, each UV-LED can be controlled individually without affecting the exposed area corresponding to the neighboring UV-LED. As a result, the homogeneity and the regionality is preserved.

In addition to that, orbital rotation is the method where only one side of the light source is connected to a motor with a gear, other sides are connected only with bearings and 3D printed connectors. Therefore, the wiring gets simpler, and the rotation gets smoother for this system since it is not controlled by a central axis.

The orbital rotational structure is made with a combination of a DC motor, bearings, and 3D printed parts. Only a single motor is used to control the mechanical movement. The motor shaft is connected to a 3D printed gear which is connected to another similar gear that initiates the rotational motion. The rotational structure is made of two rectangular acrylic plates, one of which holds the motor and remains stationary, while the other one holds the light source. The offset with which the light source will rotate is designed in such a way that each UV-LED covers up the adjacent gaps.

The homogeneity of the UV-LED light source is the measure of how well the gaps between the adjacent rows and columns can be covered and the contrast is minimized. Since the UV-LEDs have been arranged in rows and columns and each UV-LED has an individual waveguide and a lens for getting collimated light beams, a gap is resulted by the matrix arrangement and the waveguide walls. For minimizing the contrast created by the inter LED gaps, an orbital motion is employed where each UV-LED rotates around its own axis and covers the gap between the rows and columns. The mechanism of how the orbital rotation works to cover the gaps can be visualized from the AutoCAD drawing shown in Figure 4.11.

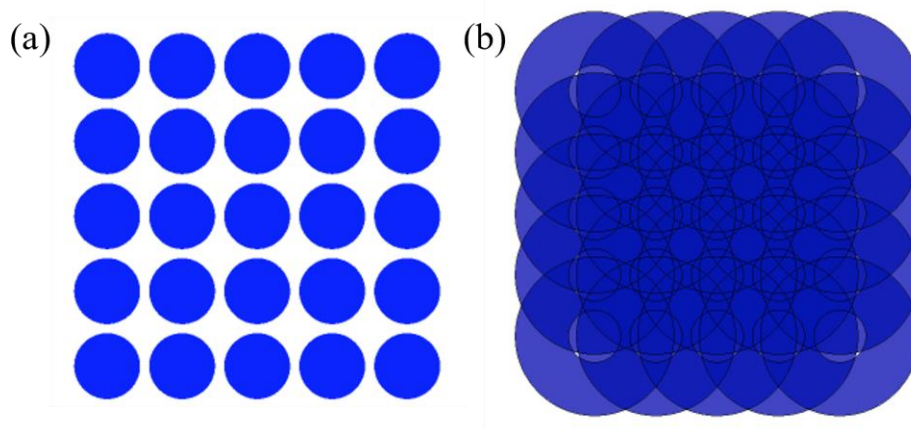


**Figure 4.11** AutoCAD drawing of the UV-LED array (a) no rotation, (b) with orbital rotation.

Figure 4.11 (a) shows the UV-LED matrix where each UV-LED is shown as a 10 mm circle as each LED uses a 10 mm lens for collimation. The distance between the adjacent UV-LEDs is 11.5 mm and the figure shows a matrix of 25 UV-LEDs. This matrix when rotates with the help of an orbital rotator with an offset of 10 mm, the phenomenon can be visualized as the one shown in Figure 4.11 (b). In this orbital motion, only one motor is used at one corner of the arrangement, and the other corners are connected by 3D printed connectors and gears. All the other three corners follow the motion of the single motor and create a synchronous motion all over the light source area. Since the offset of the primary gear is 9.8 mm corresponding to the motor shaft all the other connectors are designed with the same offset. Figure 4.11 (b) shows the movement of each UV-LED around that 9.8 mm offset and the gaps being covered giving a homogenous light distribution.

However, the UV-LED doesn't have a uniform light distribution all over the diameter of the lens rather it has a gaussian distribution of the intensity. The center is typically around 10% brighter than the periphery and the edges are around 2% brighter than the periphery. Figure 4.12 (a) shows the image of an illuminated UV-LED and Figure 4.12 (b) shows the intensity distribution of the UV-LED through the center and the periphery.

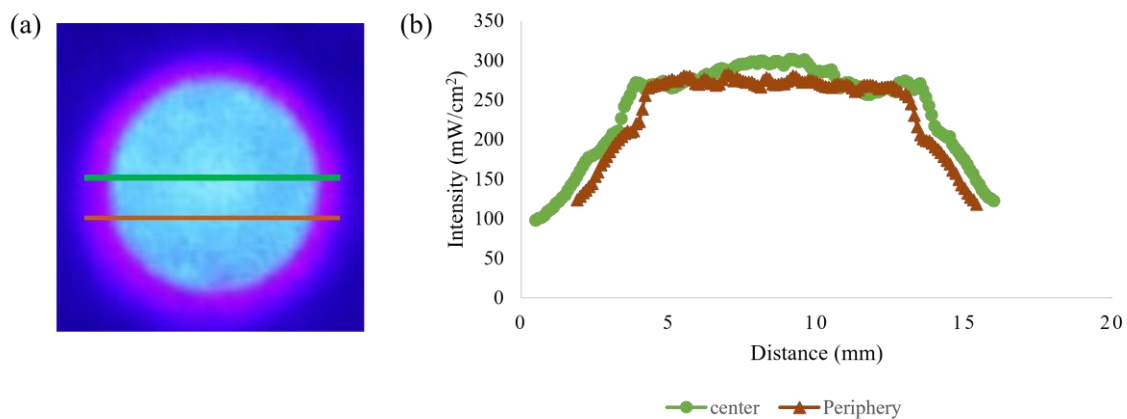


**Figure 4.12** UV-LED intensity profile (a) Single UV-LED, (b) Intensity distribution through the center and the periphery.

Due to the continuous orbital rotation, this Gaussian profile gets flattened to a certain percentage. The practical implementation of this phenomenon has been shown in Figure 4.13 with the actual light source and a long exposure photo to show one complete rotation using the orbital rotation. Figure 4.13 (a) shows the light source when all the UV-LEDs are ON, and the light source is stationary. Figure 4.13 (b) shows the light source when it is in orbital rotation and the camera captures one complete rotation of the light source with 1 second exposure. The gaps are seen in Figure 4.13 (a) and are seen to be covered in Figure 4.13 (b). An analysis of how much contrast is minimized using this method is explained in Figure 4.13 (c). Figure 4.13 (c) shows the graph where the blue line shows the intensity distribution over the line drawn through the center of the light source at its stationary position. The yellow line shows the intensity distribution of the 5 UV-LEDs with their gaussian profiles. The orange line shows the intensity distribution of the light source when it's in orbital motion. These graphs were obtained by analyzing the images using the software ImageJ (2020). The graph for the stationary light source shows that the intensity around the edge of the UV-LED is around 246 mW/cm<sup>2</sup>, at the center it is around 250 mW/cm<sup>2</sup> and at the gap it is around 117 mW/cm<sup>2</sup>. Therefore, the contrast is around 36% between the periphery and the gap. The contrast is calculated using the equation shown below-

$$Contrast (\%) = \frac{Highest\ intensity - Lowest\ intensity}{Highest\ intensity + Lowest\ intensity} \times 100 \quad (4.1)$$

In the graph for the rotational light source, the highest intensity is around 295 mW/cm<sup>2</sup> and the lowest is the 286 mW/cm<sup>2</sup> giving a contrast of around 1.54% only. Since the image analysis detects an overlap of the two adjacent UV-LED rotations, it detects this difference of intensity.

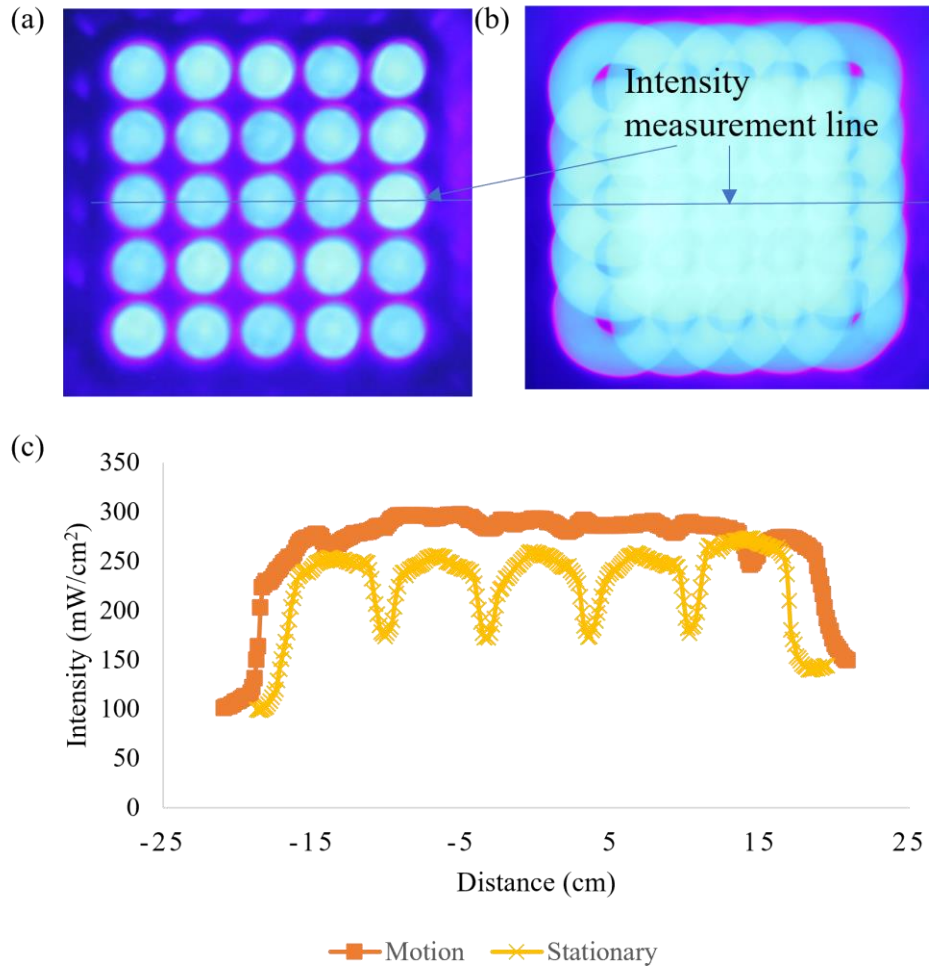


**Figure 4.13** Light homogeneity (a) 5 by 5 matrix of the UV-LED, (b) The UV-LED matrix with one rotation, (c) Intensity distribution of the light source with and without motion.

This analysis is a visualization of the phenomenon, in the actual case, this overlap doesn't occur, and the UV-LED simply covers the gaps in its locus and all the target area receives equal exposure. For analyzing the homogeneity, the central area is mainly focused since the surrounding blank spaces of the LED matrix create some additional contrast at the edges.

#### 4.5 Microfabrication method

Most of the steps of the SU-8 microfabrication are like the conventional procedure, there are a few differences for processing the thick SU-8 photoresist. For 1000  $\mu\text{m}$  or thicker photoresist,

the conventional spin coating process is not recommended firstly because the achievable thickness by the spin coating method is limited to a couple of hundred microns only unless running multiple spinning processes. Secondly because most of the applied photoresist to the substrate is wasted during spinning. The thicker the photoresist, the more is the waste. One practical solution for the thick film coating is to use a dry SU-8 film where the pre-manufactured film needs to be attached to the substrate. Although the dry SU-8 film process is convenient and saves long soft baking time, the user's requirement might not align with the preset thickness of the manufacturer's sample. Therefore, for thick SU-8 film coating, a weigh and pour method is introduced, where a relationship between the weight and the given thickness was measured and the photoresist was directly cast on the sample. A 3D printed wall was placed on the substrate before applying the SU-8 to prevent overflowing. The overflowing barrier wall was 3-D printed using a stereolithography type printer (Form 2, Formlabs, Inc.) where the acrylic resin has 100% fill inside the structure and can bear with 95 °C temperature. Since there are two baking steps involved at a temperature of 95 °C, materials that can handle high temperatures are only recommended for making the barrier. The wall is also advantageous for estimating the final SU-8 film thickness during the soft baking process. During the exposure, the substrate is flipped for the backside exposure, the barrier then also acts as a standing platform for the sample. Since the SU-8 2025 includes more solvent (around 75%) than the photoresist, the initial poured amount of the SU-8 is higher, and it is gradually reduced as the solvent evaporates.

This UV-LED lithography system has been characterized for both traditional and complex 3D microfabrication by integrating a multidirectional sample holder. The sample holder can tilt in between +180° to -180° in Y-direction and rotate from 0° to 360°. The fabrication process for 3-D SU-8 photoresist includes sample cleaning, photoresist coating, soft baking, UV exposure, post-

exposure baking, and developing. The fabrication of a complex 3D structure has been briefly pictured as shown in Figure 4.14. Two inclined pillars like 'V' shape and a reverse triangle slab were UV-projected through a single micro hole shown in Figure 4.14 (a-b-c-d). The 405nm UV light source was chosen, and the light intensity from the 1-inch distance was set at 194 mW/cm<sup>2</sup>. The first inclined pillar was exposed for 30 minutes where the tilt position of the sample holder was set at 60°, as shown in Figure 4.14 (b). The sample holder was rotated for 120° for the second pillar exposure position. The second pillar was exposed for the same energy with the same tilt angle as shown in Figure 4.14 (c) The sample holder was again rotated for 120° for the exposure of the reverse triangle slab. The continuous UV exposure was performed while the rotation angle oscillated from +20° to -20° for 60 minutes, as shown in Figure 4.14 (d). The sample was baked at 95 °C for the post-exposure baking for an hour and cooled down to room temperature after baking, as shown in Figure 4.14 (e). Then the sample was dipped into the SU-8 developer solution (MicroChem, Inc.) for 45 minutes and cleaned with isopropyl alcohol, as shown in Figure 4.14 (f). During the development process, the SU-8 photoresist side was facing down. This accelerated the process as the unexposed SU-8 was down by gravity during the developing process. The sample was cleaned with isopropyl alcohol (IPA) and dried to complete the fabrication. Figure 4.14 (g) shows an SEM image of the fabricated 3-D structure where the fabrication process followed the steps as shown in Figure 4.14 (a-f). The 3-D structure shows two inclined pillars with one reverse triangle shape from one single origin. The photomask pattern was a 50- $\mu$ m diameter hole. The diameter of the cross-section of the pillar was larger than the 50  $\mu$ m which was caused by the overexposure dose. Due to the high intensity exposure for a long time, diffractions affected the original size of the microstructure. The measured height of the 3-D structure was 1200  $\mu$ m which was well aligned with the predicted height, that is equivalent to the height of the 3D printed barrier.

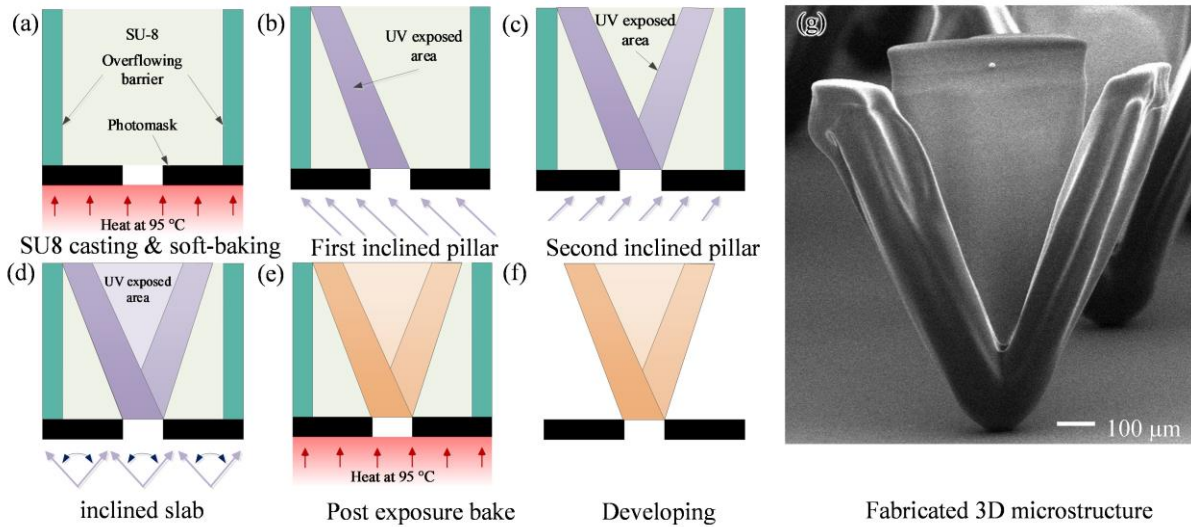


**Figure 4.14** Microfabrication (a-f) 3D microstructure fabrication method, (g) Fabricated 3D microstructure.

## 4.6 Results

Some significant microfabrication results are demonstrated below.

### 4.6.1 High-resolution microfabrication

Considering the highest resolution available, the contact lithography method has been used in all the demonstrated micro-fabrications. Figure 4.15 shows some micropatterns obtained on SU8 with a thickness of 40  $\mu\text{m}$  and with no air gap. The highest resolution obtained from this sample is 3.5  $\mu\text{m}$ . The narrow lines are 3.5  $\mu\text{m}$ , and the broad lines are 8  $\mu\text{m}$  and 13  $\mu\text{m}$ , where the patterns were made of SU-8 2025. The demonstrated 3.5  $\mu\text{m}$  feature size shows good compatibility with the conventional UV lithography uses. Versatile sizes of micropatterns on the single sample show the compatibility to fabricate dynamic ranges of microfabrication as well. Again, as the thickness of the photoresist increases, the resolution tends to degrade. Conventional microfabrication as shown in Figure 4.15 includes the microstructures fabricated using a one-directional UV light source.

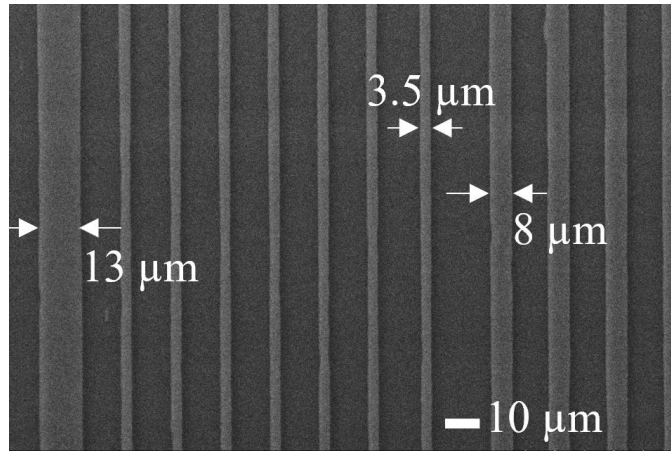
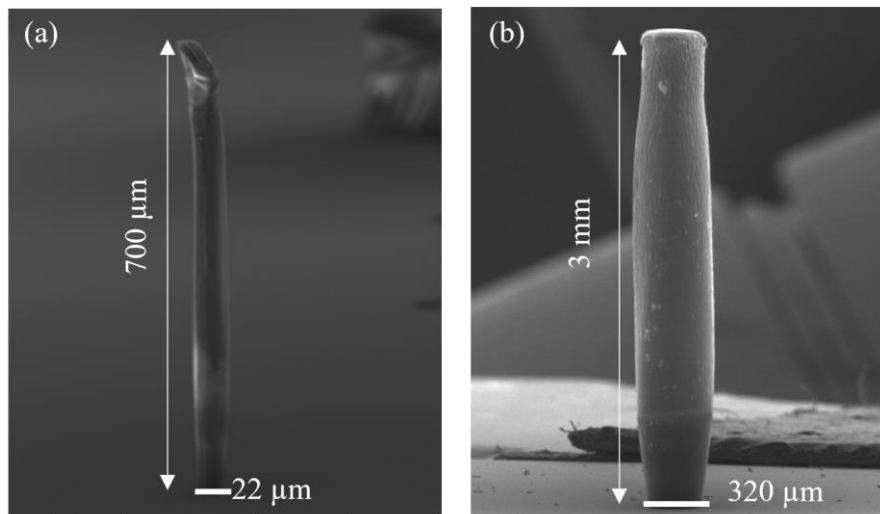


**Figure 4.15** High-resolution 2D patterning.

This kind of microstructure does not require a customized sample holder as one-directional exposure is sufficient for the fabrication. This micropattern requires low intensity since the thickness is only around 30-40 μm.

#### 4.6.2 High aspect ratio and ultra-tall micro-tower fabrication

For very tall microstructure fabrication, very high intensity is required. This system shows an intensity of around 452 mW/cm<sup>2</sup> which is very high and is suitable for several millimeter tall micro-fabrications.



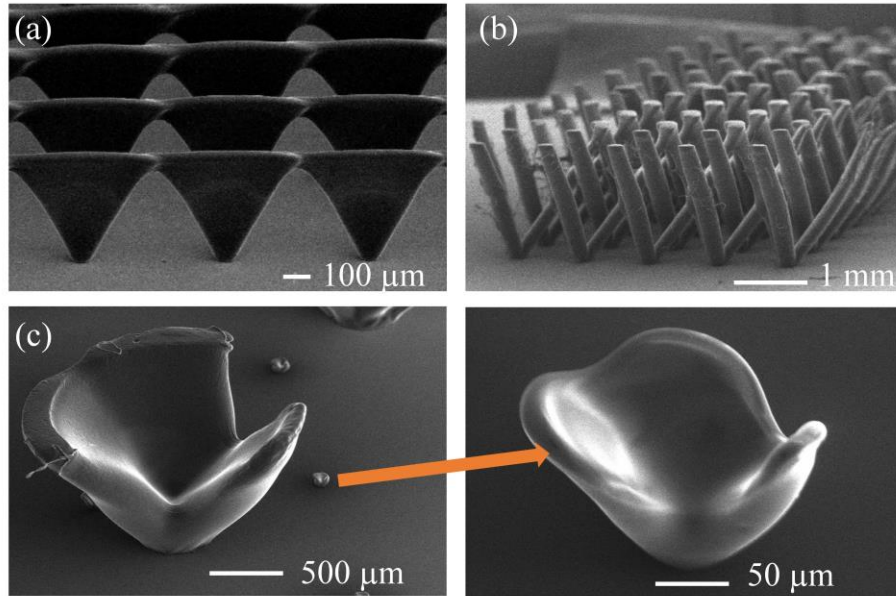
**Figure 4.16** Tall microstructures (a) High aspect ratio pillar, (b) 3 mm micro-tower.

Figure 4.16 (a) shows a 700  $\mu\text{m}$  tall microstructure with an aspect ratio of around 34. Figure 4.16 (b) shows 3-mm tall SU-8 pillar which is very challenging to get with low intensity light sources. The SU8 pillars are extremely tall as compared to the conventional SU-8 structures. The diameter of the pillar was 300  $\mu\text{m}$  and therefore the aspect ratio of the pillar shows 10. In this 3-mm tall SU-8 pillar fabrication, a total UV-exposure time of 10 minutes was applied at an intensity of 200  $\text{mW}/\text{cm}^2$ .

The extended height of the SU-8 structures has an excellent potential for RF/microwave antenna devices with high frequencies.

#### ***4.6.3 Non-conventional multidirectional complex 3D microfabrication***

The 3D structures that required tilting and rotation for their fabrication have been termed as complex 3D microstructures here. Since it is not possible to get these structures using the conventional lithography setup, they have been called non-conventional structures as well. Figure 4.17 shows various 3-D SU-8 structures fabricated using the UV-LED light and the tilt-rotational stage. Figure 4.17 (a) shows an array of ‘chained triangular slabs.’ An array of the 30- $\mu\text{m}$  hole on chromium glass was utilized as a substrate and a backside exposure photomask. 300- $\mu\text{m}$  thick SU-8 was coated on the substrate and baked for 95°C. The tilt-rotation sample holder was programmed to continuously move the tilt angle from -70° to +70° while the rotation angle was fixed. The light intensity was set at 200  $\text{mW}/\text{cm}^2$  and the total applied light energy was 480  $\text{J}/\text{cm}^2$ . Figure 4.17 (b) shows a millimeter-scale SU-8 tripod structure. 1.5-mm thick SU-8 was coated on the chromium glass for the backside exposure. The tilt-rotational sample holder was programmed as follows. The tilt angle was fixed at 70°, and the UV exposure was performed at the stationary rotation angles of 0°, 120°, and 240°. The exposure dose was 360  $\text{J}/\text{cm}^2$ . The inclined angle of each pillar was measured as 67° from the ground.



**Figure 4.17** Unique 3D SU-8 structures (a) an array of ‘chained triangular slab,’ (b) millimeter-tall SU-8 tripod array, (c) large (1.5 mm tall) and small (200  $\mu\text{m}$  tall) 3D petal SU-8 structure on a single structure.

The value is well-aligned with Snell’s law’s prediction with a refractive index of 1.67 for SU-8. The length of the inclined pillar was measured at 2.2 mm. Figure 4.17 (c) shows 3D SU-8 petal structures with different sizes on the same process. The size differences were caused by the different sizes of the photomask patterns, differentiating the applied UV exposure energy. The height of the large petal SU-8 structures shown in Figure 4.17 (c, left) was 1.5 mm, while the height of the small petal SU-8 structure was 200  $\mu\text{m}$ .

#### **4.6.4 High production yield**

Production yield is yet another important feature of a lithography system. The higher the number of uniform microstructures it can produce at a time, the higher its production yield is. The batch production depends on the uniformity of the light source. Figure 4.18 shows an array of SU-8 micropillars standing on one square inch Chromium glass sample. The SU-8 pillars with a diameter of 30- $\mu\text{m}$  and a height of 400  $\mu\text{m}$  were uniformly fabricated to show a batch production.

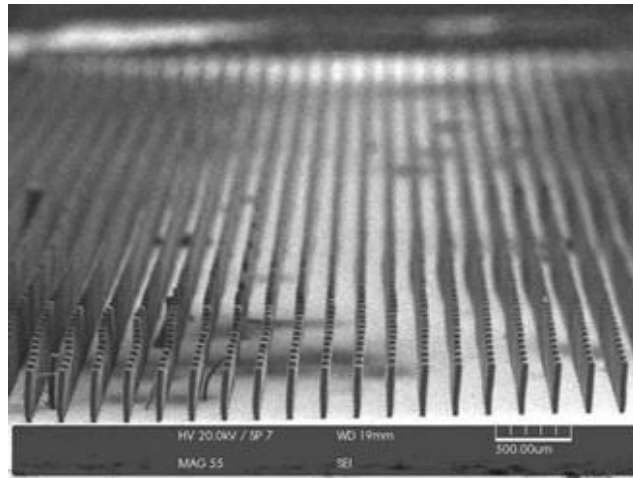


**Figure 4.18** More than 2000 micropillar array in a one-inch glass.

More than 2000 pillars are presented in the SEM image. The light source can cover an area of slightly bigger than  $5.5 \text{ cm}^2$ , and the sample holder has a diameter of 10 cm. Therefore, a bigger sample size can be targeted and patterned successfully for future applications.

#### **4.7 Summary**

A high-intensity UV-LED lithography system has been presented to fabricate millimeter tall 3-D microstructures. The presented light intensity is around  $452 \text{ mW/cm}^2$ , which enables UV light to propagate through millimeter thick SU-8 photoresist, and thereby millimeter-scale tall 3-D microstructures can be fabricated. The matrix of the 5-by-5 UV-LED array light source has individual collimating lenses with the advanced light waveguide design. The light source has high intensity and homogeneity has been ensured with an orbital rotation. Regional light on-off/intensity control for the UV-LEDs is one of the novel features that give it various photopatterning capabilities. The microcontroller-controlled tilt-rotational sample holder creates 3-D light traces into the photoresist for 3-D microfabrication. Small feature size SU-8 patterns in a few microns, high aspect ratio SU-8 structures, and millimeter tall SU-8 structures were successfully fabricated. The micro fabrications demonstrate the capability of the introduced UV-

LED system for both the conventional and the advanced millimeter thick and complex SU-8 process. These unique 3-D microstructures with expanded height in millimeter-scale have great potentiality in device fabrication of RF- and Bio-MEMS. The findings of this lithography system can be modified and improvised for a large-scale and advanced tool for UV lithography for future applications.

# **Chapter 5 - Developing an advanced programmable multidirectional UV-LED lithography system for large scale microfabrication**

## **5.1 Introduction: Programmable UV-LED lithography system for large scale production**

The first laboratory setup with a UV-LED light source was presented in 2012 [88], several other UV-LED light sources have been used for microfabrication since then [89] [90]. In addition to the research setups, mask aligner manufacturing companies are changing to UV-LED light sources. The first commercial UV-LED light source for mask alignment was developed by a company named Kloe in France [12] for mask alignment applications. The prominent commercial companies like Idonus and Quintel are using UV-LED as their lights sources in their recent models [91], [92]. Most of the commercial companies chose to replace the UV mercury vapor lamps with UV-LEDs to minimize the maintenance, cost, and environmental hazards. Other optical features and exposure capabilities were kept similar as compared to the mercury vapor lamps. While the UV-LED lithography system discussed in this research was not only characterized for the general parameters like collimation, homogeneity, resolution but was also equipped with advanced features like dual wavelength for different microfabrication ranges, adaptive light intensity control, regional control of the light source, multidirectional exposure, programmable operations, and large-scale commercial setup. On the other hand, this system can give the highest intensity so far among the existing lithography light sources by utilizing a simple collimating scheme with single lens and 3D printed waveguides. The UV-LED lithography setup presented here in this research is a complete system comprising of the unique features of UV-LEDs, highly precise tilt-rotational stage with standard mask alignment setup, integrated microscope for observation, integrated

computer control and advanced programming, adaptive control of the light source intensity and customized UV-LED pattern. A wide range of intensities with multidirectional exposure capabilities along with the user defined programming make this system an advanced tool for future generation micro-fabrications.

The previous chapter shows a high-intensity ( $452 \text{ mW/cm}^2$ ) 5-by-5 UV-LED light source with a commercial collimation lens that enabled the fabrication of millimeter tall microstructures (3 mm) [62]. A customized light waveguide and an orbital rotation structure have been introduced for improved light collimation and uniform distribution. This small prototype showed the possibility of adaptive light control and automatic control of the tilt rotational sample holder for complex microstructures with microcontroller commands.

In this age of computer-based technology, the lithography process can have significant advancements using different programming features for easier control over complex operations and large-scale productions. The use of Computer Numerical Control (CNC) is prevalent for light-motion synchronized 3D microfabrication [93], [94] for several years now. In addition to that, selective light source pattern control and adaptive light intensity control can open the opportunity for new micro-fabrication which can be hard to fabricate using the existing lithography systems.

Based on the successful implementation of UV-LEDs' novel features in developing the multidirectional lithography systems in the previous works [87], [62]; a fully programmable UV-LED mask aligner system has been presented in this chapter with large scale setup. The adjustable intensity feature with the change of current and distance has been made programmable using C++ programming software. The programmable light exposure feature resolves the non-uniform exposure issue caused by the tilting angle of the sample holder, where one end of the sample holder is closer to the light source while the other end has further distance. On the other hand, because of

having individual control over the UV-LEDs, the exposure can be customized, and varieties of microfabrication can be achieved on a single sample with a single exposure.

The system has been rescaled for large-scale production with large illumination and target areas. The motion of the sample is made fully programmable to synchronize with the adaptive light source. The tilt-rotational sample holder has a standard mask alignment setup with an integrated microscope. Therefore, this system is suitable for both traditional mask aligners and an advanced tool for 3D microlithography.

The advancement of the system resulted in a commercial setup in collaboration with Samil Tech Co. Ltd, South Korea. The design, characterization of the standard parameters, and the improvements to make an advanced UV-LED lithography system have been discussed in this chapter.

## **5.2 Concept of the programmable multidirectional UV-LED lithography**

A multidirectional UV-LED lithography system has been developed with fully programmable features, and a large-scale setup. The light source has been arranged with an alternate combination of both 405 nm and 365 nm UV-LEDs in a single PCB, customized collimating structures, programmable light intensity, programmable tilt rotational sample holder for creating multidirectional exposure. The original working principle is inspired by the 5 by 5 UV-LED lithography system prototype as discussed in chapter 4, where the size has been extended to 8 square inches with dual wavelength UV-LEDs and all the functionalities like the variable intensity, light source regional control, multidirectional operations are made programmable.

Since 365 nm is the recommended wavelength for thinner SU8 micropatterning, and 405 nm wavelength is good for millimeter tall microfabrication, a combination of both 405 nm and 365 nm UV-LEDs has been made in the light source. Utilizing the independent LED control, UV-LEDs

can be selected regionally for different microfabrication. Any combination of the UV-LEDs like only the i-line (365 nm), only the h-line (405 nm), or a combination of both can be assigned. The intensity can be adapted with the movement of the sample holder to get uniformity for the microfabrication. Figure 5.1 illustrates the concept of the programmable multidirectional UV-LED lithography system. The light source is a combination of 407 UV-LEDs in an arrangement like a compact honeycomb. The tilt-rotational sample holder is also scaled up to 9 inches diameter to match with the bigger exposure area. With the programmable operations, the ability to make varieties of complex microstructure is increased to a greater extent.

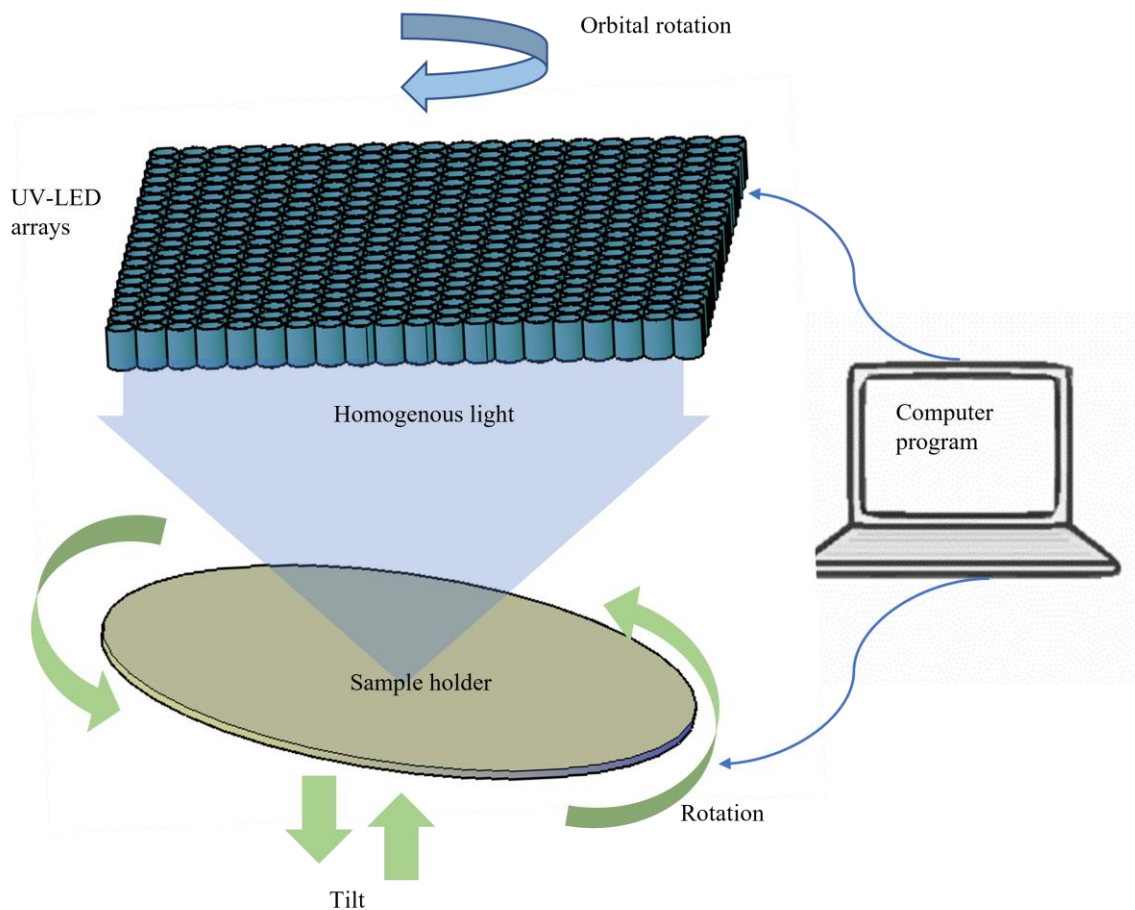


**Figure 5.1** Concept of the programmable multidirectional UV-LED lithography system.

The light source has an additional up and down movement control along the z-axis which is another unique feature of this system that makes the system able to adjust the distance for different types of microfabrication. One optical microscope and a mask alignment system is integrated for which the system works both as a mask aligner and an advanced 3D microlithography tool.

### 5.3 System design

The light source arrangement follows a regular matrix setup where the UV-LEDs with different wavelengths are arranged in alternate rows and columns. A total of 400 UV-LEDs are arranged in 20 rows and 20 columns.

#### 5.3.1 Dual-wavelength light source

The conventional lithography light sources contain multiple wavelengths including 365 nm, 405 nm, and 436 nm peaks on the broad spectrum. Different wavelengths need to be filtered out for different applications since the light source is a combination of all.

This system adopts a mix and match of both 365 nm and 405 nm UV-LEDs (LG-CUN04-BIA, LG Innotek) for facilitating both traditional and modern micro-fabrications. The two different kinds of UV-LEDs are alternately placed side by side which can be regionally controlled.

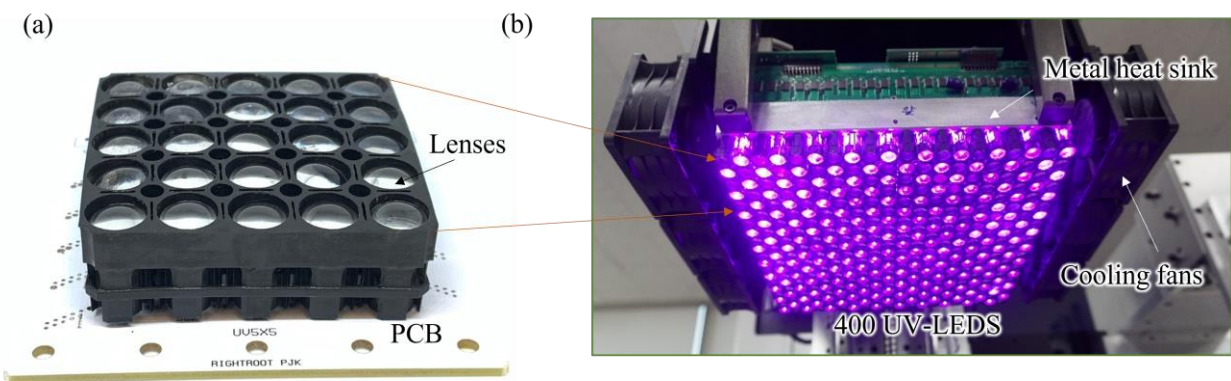


**Figure 5.2** Light source matrix (a) 5×5 matrix of the waveguide with lenses, (b) 20×20 matrix of the light source.

The system is programmed in such a way where the light source pattern can be chosen by the user. Either the 365 nm LEDs only, or 405 nm LEDs only, or altogether can be selected to eliminate the need for a filter. Every UV-LED's intensity can be individually controlled using either an integrated microcontroller or C++ programming.

### ***5.3.2 Large scale light source***

The waveguide's design is like the one shown in chapter 4. The 5 by 5 matrix setup of the waveguide has been used as the unit of the 8 square inch light source. Figure 5.2 (a) shows the unit of the waveguide matrix and Figure 5.2 (b) shows the assembly of 16 such waveguide units to make the 8 inch<sup>2</sup> light source. The single layered Aluminum PCB has a metal heat sink attached to the back for heat dissipation. Since, 400 UV-LEDs produce a lot of heat, 6 small cooling fans are integrated along the side of the light source. The power supplies are arranged above the light source to avoid long wired connections and a microcontroller unit is also incorporated for an additional semi-automated control of the light source. The whole setup is connected to a servo motor for making the orbital motion of the light source for getting homogeneity.

### ***5.3.3 Integrated programmable tilt-rotational sample holder***

A tilt-rotational sample holder was integrated with the UV-LED lithography light source to rotate and tilt in 3D spaces like the one discussed in chapter 4. However, since the UV-LED light source has been rescaled to cover a significant area of 8 square inches, the exposure area has also been expanded. Figure 5.3 shows the tilt-rotational sample holder where the diameter of the circular disc is around 9 inches which is larger than the light source.

Since the light source rotates orbitally, the overall size increases sidewise corresponding to the orbital distance of 9.8 mm. This bigger size of the circular disc compensates for the expansion in size due to rotation.

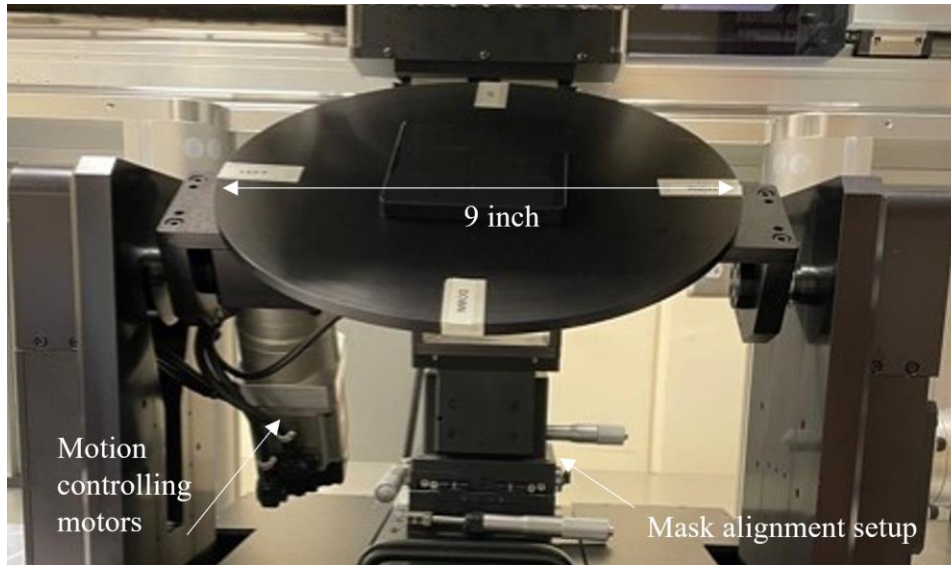


**Figure 5.3** Tilt-rotational sample holder.

The circular disc is designed to rotate around  $0^\circ$  to  $360^\circ$  in X-axis. It is attached to a flat metal bar capable of tilting around  $-180^\circ$  to  $180^\circ$  in the Y-axis. Both the rotational disc and the tilting bar are connected to two different servo motors, where the motor movements are computer program controlled.

#### ***5.3.4 Software and programs***

A significant feature of this lithography system is that the whole system is controlled by programming. The light source, the tilt-rotational system, the power connections, and the computer system are all integrated. A C++ program controls the orbital movement, timing, and position of the light source. The program also controls the movement of the sample holder and adjusts the distance between the light source and the target. Since the light source is a combination of both 365 nm and 405 nm UV-LEDs, the software can select which LEDs to turn on. Figure 5.4 shows a screenshot of the sample programs that it uses for microfabrication. An intensity value setting section selects the intensity level between 0 to 255, where 0 indicates the lowest intensity and 255 indicates the highest. The job processing part controls the linear and dynamic movement of the

light and controls the light height from the sample, the light source rotational speed, the starting angle for tilt function, and the final tilting angle. The user can assign different rotation and tilting angles and the corresponding speed values to synchronize between the tilting and rotational movements and save the operation with user-defined names. There are auto homing and emergency detection functions for ensuring perfect calibration and safety. The advantage of this programmable system is that the simultaneous rotations and tilting can be made at variable speeds, which was challenging with microcontroller commands. The programs help to keep the movements well-calibrated and precise which might not be achieved accurately by manual settings. Figure 5.4 shows a screenshot of the sample program used to fabricate complex 3D microstructure.

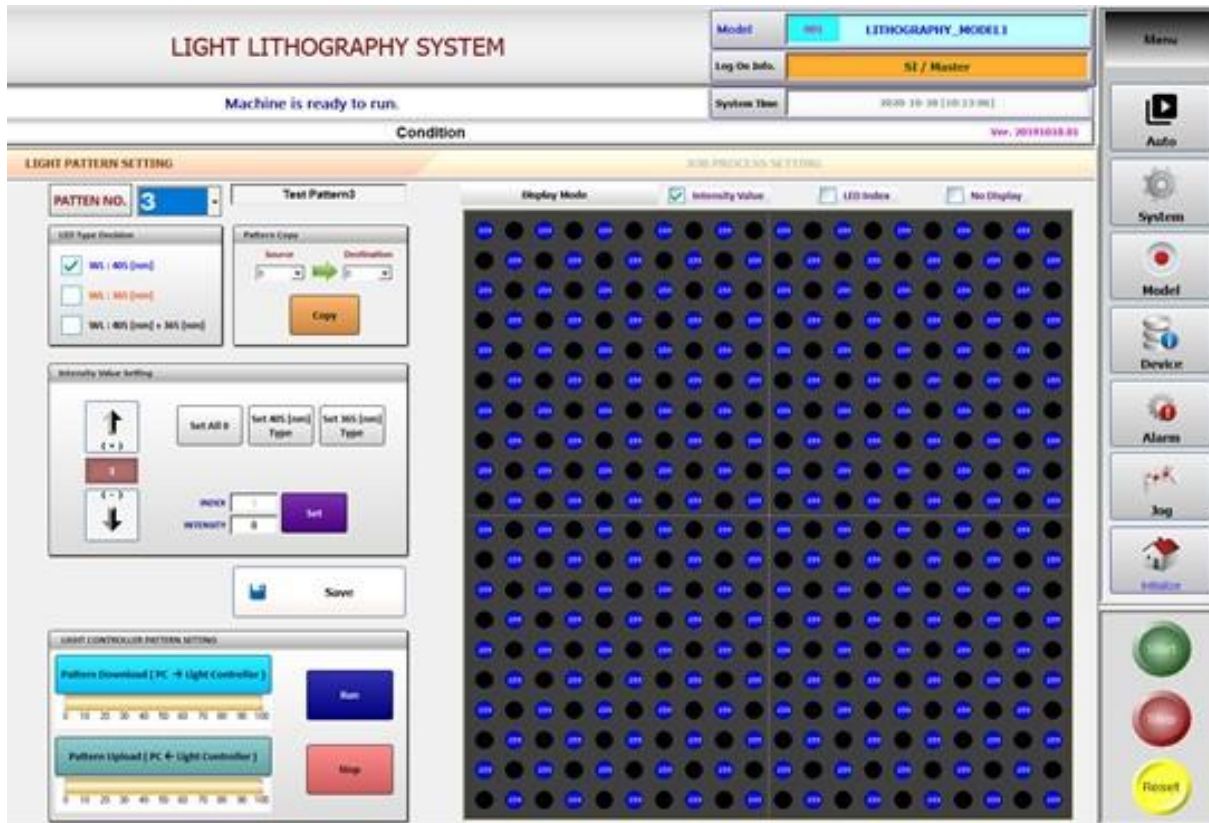
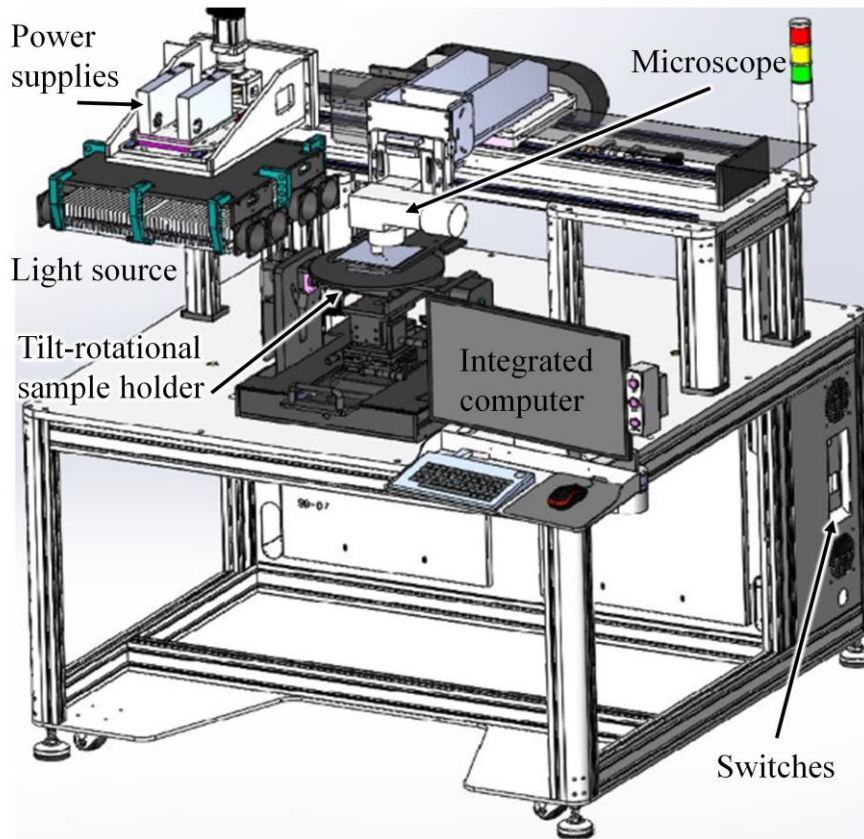


**Figure 5.4** Program controlled operations.

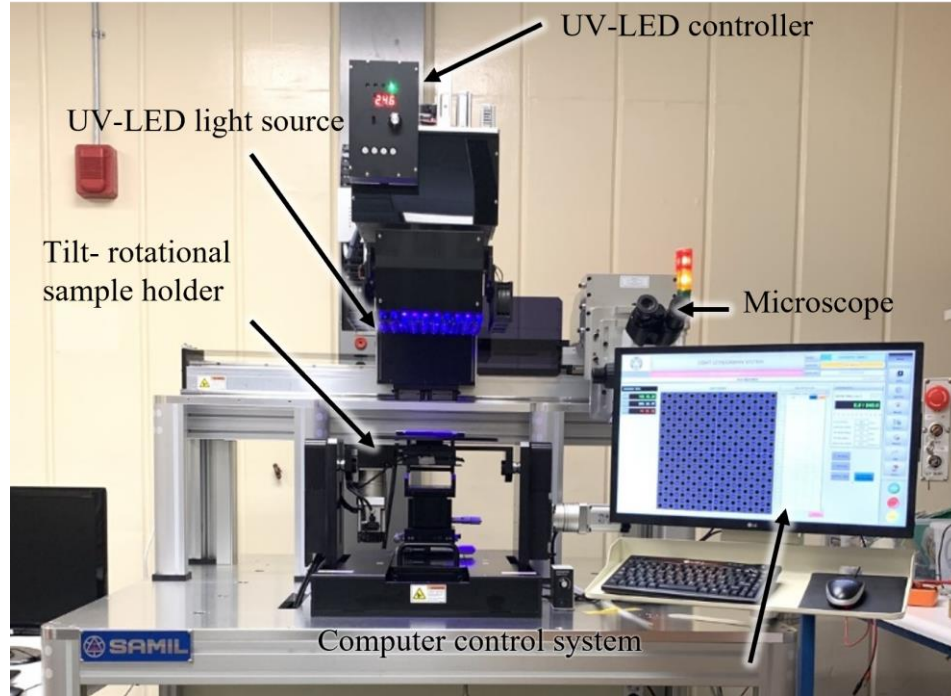
### 5.3.5 Completed integrated system

Figure 5.5 shows the schematic of the overall system. The light source is shown to be moved to the left to make space for an integrated microscope. After checking the alignment of the mask and the sample with the integrated microscope, the light source is moved back to its default position above the sample holder. The microscope is kept aside while not in use. A computer is placed on the same table as the other parts.

The power supplies for the light source are placed above the light source itself. The metal heat sinks, and 6 small fans are attached to the light source for controlling the temperature. Other power supplies are placed inside a metal casing towards the back of the machine, and the corresponding switches are placed on the metal casings.



**Figure 5.5** Illustration of the programmable UV-LED lithography system.



**Figure 5.6** Programmable multidirectional UV-LED lithography system.

All the necessary parts are placed in a benchtop setup where there are spare spaces for storing other equipment on the bottom of it. Figure 5.6 shows the overall machine after assembling. The machine is shown in its operating condition. The light source is on, and a program is set on the computer. There is a mask alignment arrangement stage where the  $x$ ,  $y$ ,  $z$  and  $\Theta$  can be adjusted. This mask stage is mimicked from the sample holder as described in chapter 3. This mask alignment stage is moveable along the  $Y$ -axis and moved under the light source when mask alignment is required. When not in use, it is kept behind the tilt-rotational sample holder.

#### **5.4 Characterization**

A lithography system deals with micro/nano-level fabrications. Therefore, different parameters associated with the system need to be precisely optimized and characterized. The important parameters of the programmable multidirectional lithography system have been characterized in the following sections.

### 5.4.1 Programmable light intensity with individual control

The surface-mounted UV-LEDs used in this system emit high-intensity lights without visible complex wiring. The UV-LEDs were chosen considering the diverging angles, the compatibility with the compact arrangements, and highest intensity. As, the collimating structure is straightforward with just a single lens, not a significant amount of light is compromised, unlike the other bulk systems where multiple integrators and condenser lenses are used. There is a threshold amount of energy required for crosslinking a definite thickness of the photoresist which is again a function of the intensity. However, the intensity fluctuates with the change of linear distance and current. Figure 5.7 shows the change of intensity with the change of linear distance corresponding to different currents for 405 nm. To be noted, the intensity for the LEDs used even at a linear distance of 15 centimeters is around 48 mW/cm<sup>2</sup> for a DC of 300 milli-Amperes, which is still very high compared to the conventional light sources and is enough for a millimeter range exposure. As the microstructures range can vary from several micrometers to several millimeters, the exposure dose also varies with the requirements.

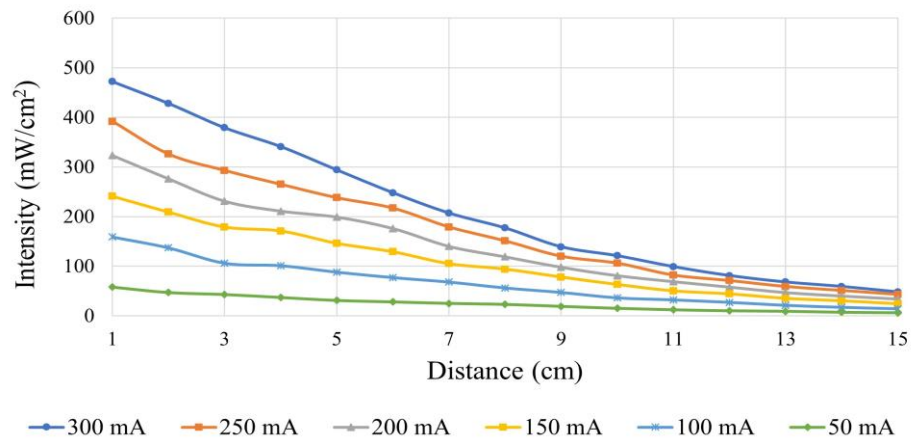


**Figure 5.7** The change of intensity with the change of distance and current (With lens and waveguide).

This exposure dose is the product of the intensity of the UV light and the exposure time. The conventional UV lithography systems have low intensities, which requires a long exposure time to cross-link thicker photoresists. High intensity available in this system compensates for the time required, allowing the fabrication of many taller microstructures with shorter exposures. The intensity of this light source varies with distance and current.

The intensity varies from 48 mW/cm<sup>2</sup> to 472 mW/cm<sup>2</sup> with the current range between 50 mA to 300 mA. The distance was varied between 1 cm to 15 cm. This adjustable nature of the UV-LED intensity has been programmed within the range of 0 to 255. Figure 5.8 (a) shows the change of intensities with brightness levels set by the program. This has been measured without lens and waveguide. It shows that, the intensity obtained from the brightness level of 170 is around 0.8 W/cm<sup>2</sup>. On the other hand, the graph is shown in Figure 5.8 (b) gives a representation of the power consumption in Watts for different brightness levels since the power consumption is a function of the current applied. It shows that power of around 1200 W is needed for getting a brightness of the level 170.

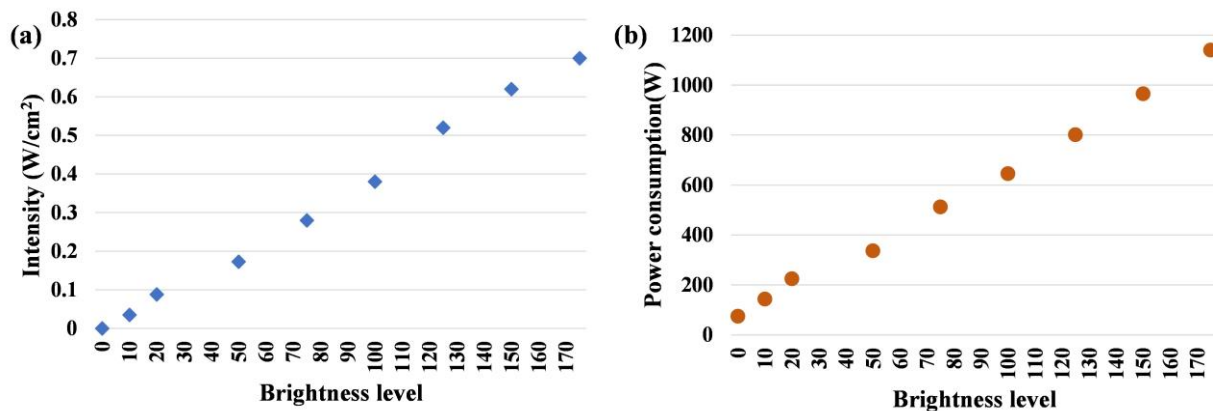


**Figure 5.8** Brightness test (a) Graphical representation of the relationship between the brightness level and the intensity, (b) Graphical representation of the relationship between the brightness level and energy consumption.

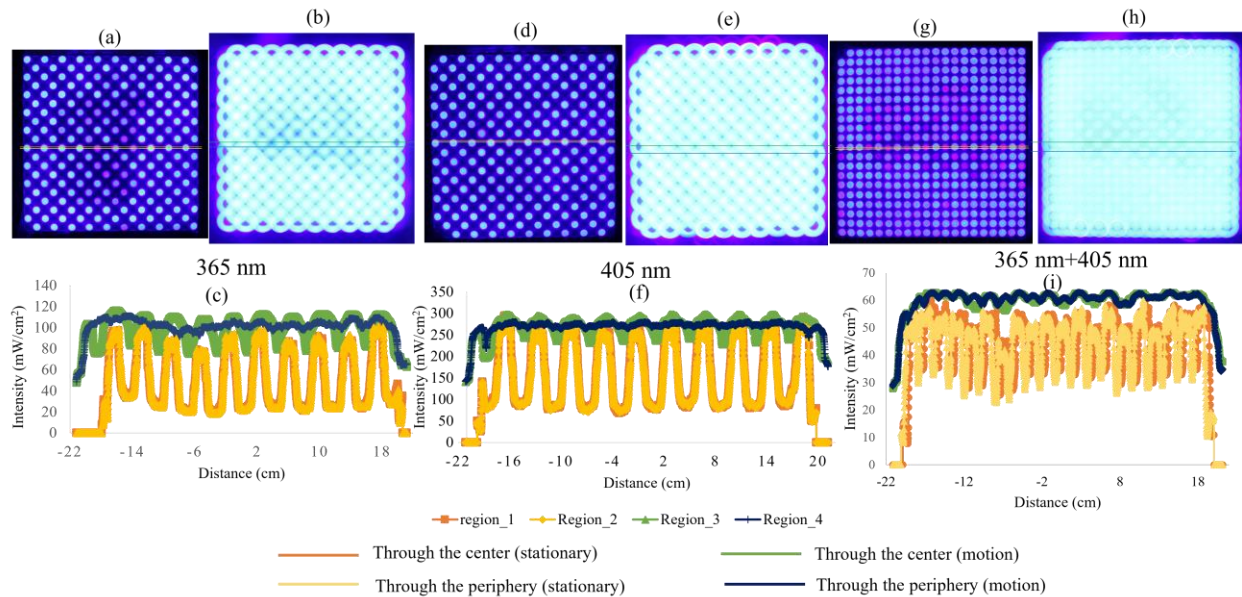
### 5.4.2 Homogeneity with dual-wavelength light source

Figure 5.9 shows the homogeneity test for the UV-LEDs system. The UV-LEDs used here are not point sources and due to the use of a plano-convex lens, the light distribution is similar to a gaussian curve, which in the practical sense means that the center of each UV-LED is brighter than the periphery of the lens. Therefore, the uniformity has been measured in four different regions as shown in Figure 5.9. Region 1 line is drawn through the center of the stationary light source, region 2 passes through the periphery of the stationary light source. Region 3 passes through the center of the light source while in motion. Figure 5.9 (a) and (b) shows the setup for the 365 nm UV-LEDs without and with rotation. These images were taken with a digital camera (Canon, Rebel EOS). Since the camera placed a distance so that the whole light source can be captured, the lights might get scattered and the image would not show the original size of the beam. To block the scattering a white paper was tightly placed on top of the light source and the actual diameter of the light (10 mm) was captured. For using the paper as a scattering blocker, some of the original intensity is sacrificed. The graphs are obtained from the ImageJ (2020) analysis of the captured photos. Figure 5.9 (c) shows the graphical comparison of the intensity at the four different regions.

The highest intensity achieved at the center is  $97 \text{ mW/cm}^2$  and the lowest at the gap is around  $20 \text{ mW/cm}^2$ . The contrast in the region 1 is around 65% and in region 2 it is around 57%. With the rotation of the light source, the intensity achieved at the center is around  $116 \text{ mW/cm}^2$  and the intensity at the gaps created caused by the long gap between the adjacent UV-LEDs is around  $77 \text{ mW/cm}^2$ . The contrast is minimized to around 18% at the gaps and around the periphery this contrast is minimized to around 8%. Although certain small gaps remain even after the orbital rotation, the intensity at those points is good enough for millimeter tall microfabrication. Some of

the UV-LEDs have dimmer intensities due to the manufacturing problem which has caused some increased amount of contrast.

Figure 5.9 (d) shows the light source without rotation, Figure 5.9 (e) shows the light source with rotation and 5.9 (f) shows the graphical comparison of the two setups using ImageJ analysis. Since the similar UV-LEDs are arranged in alternate rows and columns they have a huge gap in between the adjacent LED. In this design, the gap is around 23 mm. the highest intensity achieved from an individual UV-LED is around  $277 \text{ mW/cm}^2$  and the lowest intensity around the gap is only  $77 \text{ mW/cm}^2$ . In this setup, the contrast is around 56% at region 1 and region 2. After the orbital rotation, the light covers most the gaps, but some small gaps remain. However, these small gaps are surrounded by high intensity lights and these gaps also receive a high intensity.



**Figure 5.9** Homogeneity test for the light source (a) 365 nm LEDs (stationary), (b) 365 nm LEDs (motion), (c) Graphical analysis of the intensity profile for 405 nm LEDs with and without motion, (d) 405 nm LEDs (stationary), (e) 405 nm LEDs (motion), (f) Graphical analysis of the intensity profile for 405 nm LEDs with and without motion, (g) Combined LEDs (stationary), (h) combined LEDs (motion), (i) Graphical analysis of the intensity profile for the whole light source with and without motion

Here, in this setup, the highest intensity achieved along the LED is around  $293 \text{ mW/cm}^2$  and the intensity at the gaps is around  $243 \text{ mW/cm}^2$ . This intensity is still higher than most of the commercial UV lithography systems and a lot of microfabrication can be done using this intensity. The contrast is minimized to around 9% at region 3 which reduces further to 1.47% at the region 4. The homogeneity test shown in Figure 5.9 (g) and (h) represents the light source comprising 400 UV-LEDs at stationary and orbital rotation. The light source is arranged with alternate rows and columns of 405 nm and 365 nm UV-LEDs. Each row is 11.5 mm apart from each other and the orbital rotation is controlled with central motor movement. Figure 5.9 (g) shows the light source when all of the UV-LEDs are ON. Figure 5.9 (i) shows the graphical comparison of the light source with and without rotation. Since there are two types of UV-LEDs, there is a difference of the intensity level in this graph. The blue line shows the highest intensity of around  $66 \text{ mW/cm}^2$  at the center and  $24 \text{ mW/cm}^2$  around the gaps. The contrast is 45%. With the rotation, the overall contrast is reduced to around 3% at the center and around the periphery the contrast is reduced to around 2.5%. Since there are no gaps due to the compact arrangement of the UV-LED arrays, similar level of homogeneity is achieved all over the exposure area. The amount of contrast in this setup is mostly contributed by the difference of the wavelength and intensity between the adjacent rows and columns. This test is presented only to show the phenomenon of homogeneity using the orbital motion of the light source. The intensities of the light source when in motion shows slightly higher intensity than the original. The reason behind this is that the picture was taken with as much as exposure time as it takes for completing one rotation. The longer exposure slightly increases the intensity. On the other hand, the images show the overlapping of the LED paths. These overlaps also increase the intensity at those points. However, in the real scenario these paths do not overlap, so the homogeneity is supposed to be better than the one demonstrated here.

### 5.4.3 Uniformity with dual-wavelength light source

The light source discussed in this chapter covers up an area of 8 square inches with a total of 400 UV-LEDs. Since all the LEDs have individual control and the internal circuitry might differ to some extent as supplied by the manufacturer, their intensity might not have the same value. However, the intensity of all the UV-LEDs should maintain uniformity at an optimum extent so that the exposure is almost uniform all over the target area, adjustable intensity can be utilized to compensate for the rest. Again, since the light source has two different UV-LEDs as- 365 nm and 405 nm, their intensity will be different by default because of their optical characteristics. Therefore, when uniformity is calculated, it should be noted that the two types of LEDs will have different intensities, and that is okay for adaptive lithography applications. The LEDs are also equipped with customized waveguides and lenses. As seen in the previous sections, the intensity of the UV-LEDs decreases exponentially with the increase of the distance.

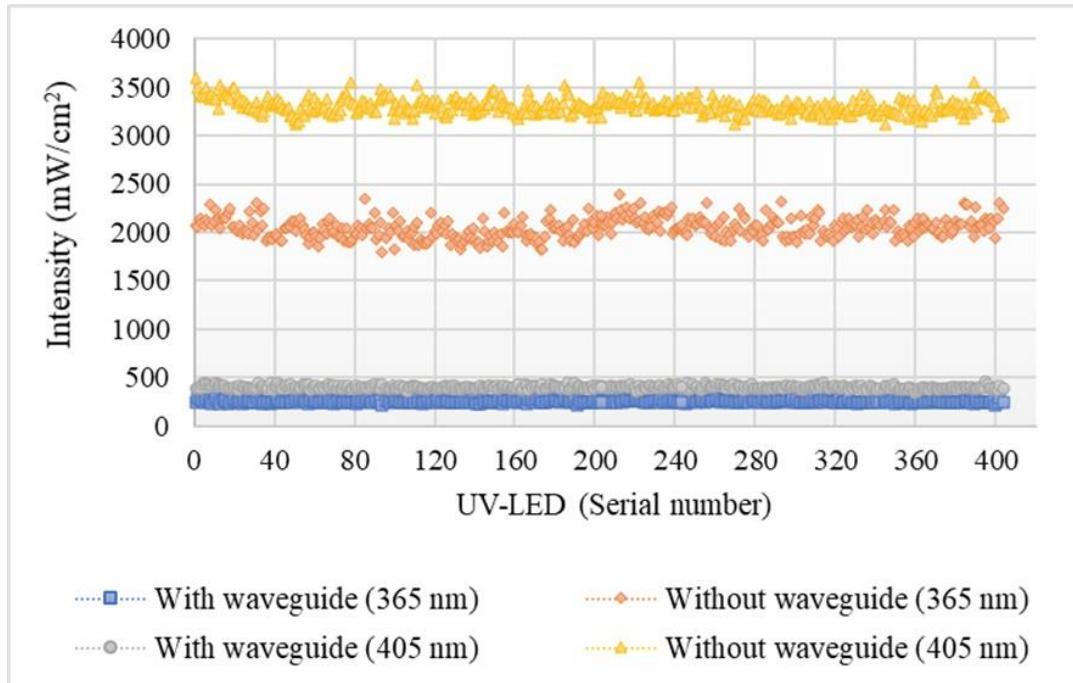


**Figure 5.10** Light source uniformity.

The lens is situated at a focal length distance for the standard optical design. As a result, the intensity differs from the original when the lens and the waveguide are added. Here in figure 5.10, the intensity distribution for all the UV-LEDs has been shown with and without waveguides.

The yellow and the orange lines show the intensity distribution without waveguides and lenses whereas the blue and the ash lines show the intensity distribution with the waveguide and the lens.

The X-axis shows the LED numbers from 1-400 except for some errors while measuring the intensity. The 405 nm UV-LEDs show a highest of 3600 mW/cm<sup>2</sup> and a lowest of 3160 mW/cm<sup>2</sup> without waveguides and lenses, giving uniformity of 6.5%. When equipped with waveguides and lenses, the same UV-LED gives the highest intensity at 452 mW/cm<sup>2</sup> and a lowest of 380 mW/cm<sup>2</sup>. The uniformity obtained in the second case is around 8.65%.

The uniformity of the light source calculated using the equation-

$$Uniformity (\%) = \frac{Highest\ intensity - Lowest\ intensity}{Highest\ intensity + Lowest\ intensity} \times 100 \quad (5.2)$$

On the other hand, the 365 nm UV LEDs give intensity in the range of 1900-2300 mW/cm<sup>2</sup> without waveguides and lenses. The uniformity is around 9.65%. These LEDs give intensity in the range between 281-237 mW/cm<sup>2</sup> with waveguides and lenses; the uniformity obtained is about 8.5%. The standard uniformity deviation for the UV lithography system should be within 10%, where these UV-LEDs maintain a good amount of uniformity with high enough intensity for lithographic applications.

#### 5.4.4 Light source stability over longer time periods

The light source stability indicates the characteristic that determines whether this lithography system gives stable performance for all kinds of lithography applications or not. Since lithography exposure is the product of the intensity and the time. For tall microstructure fabrications, the light source is in operation indefinitely as high aspect ratio structures and 3D complex structures take a long time to get cross-linked. On the other hand, batch productions or continuous production needs the light source to be ON for a long time.

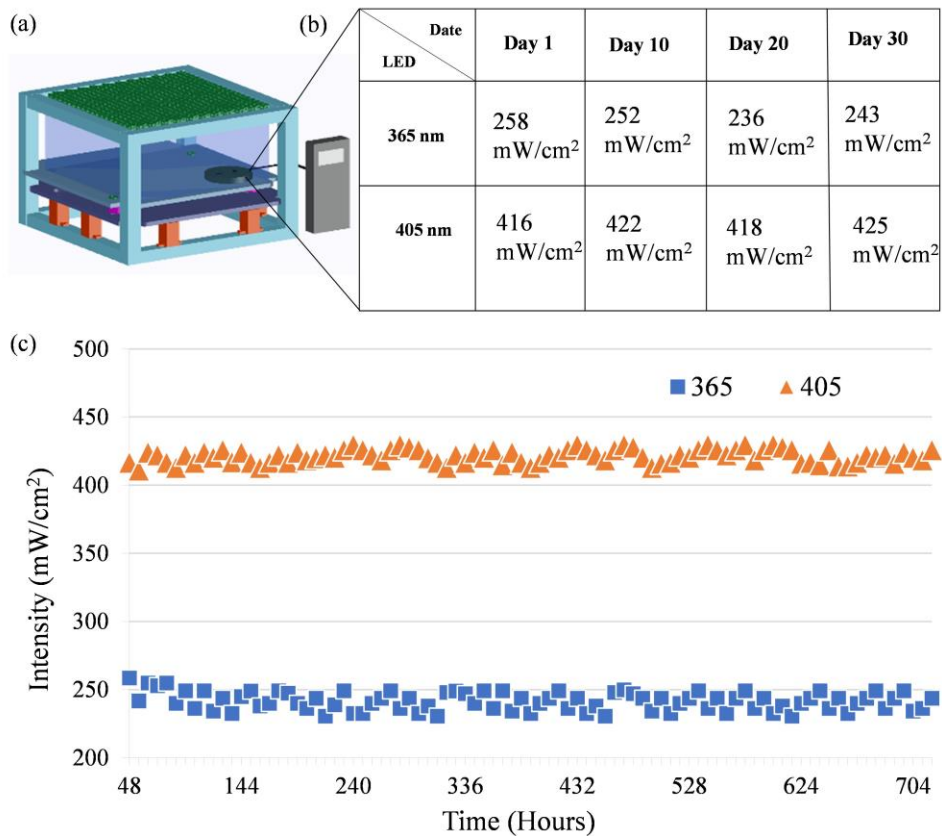


**Figure 5.11** Uniformity test (a) Test setup, (b) Table showing intensity measured at different days, (c) Graph showing the deviations of stability measurements.

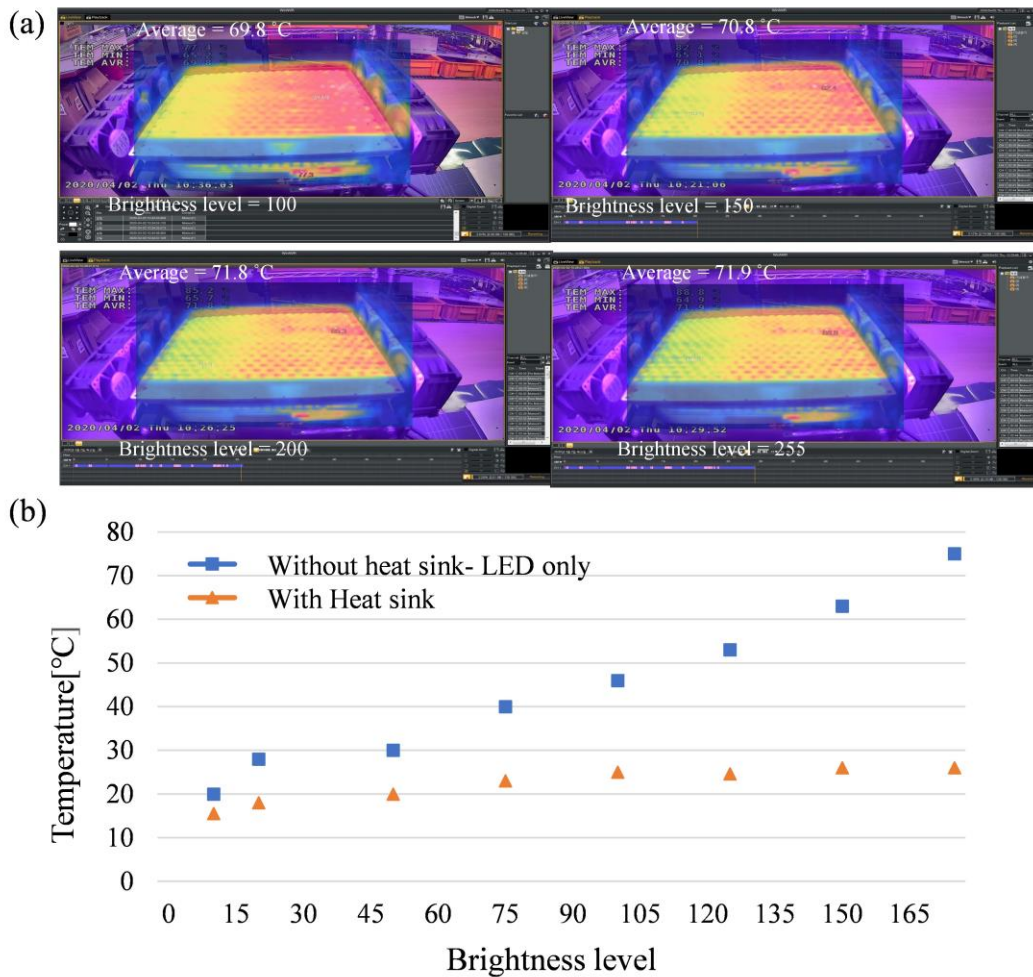
Therefore, this system needs to be characterized for long and continuous uses. Since there are no other factors like warming up, the light source should maintain a constant intensity throughout the operation time. The light source system was kept turned ON and monitored for 704 hours at a stretch, and the system's compatibility with the long hour and continuous operations was checked. Figure 5.11 (a) shows the setup of the experiment.

Figure 5.11 (b) shows the intensity readings at different days for both 405 nm LEDs and 365 nm LEDs. The graph in Fig 5.11 (c) shows a plot of the intensity with respect to time. The intensity for 405 nm LEDs varies from around 411 mW/cm<sup>2</sup> to 430 mW/cm<sup>2</sup>. The intensity for 365 nm LEDs varies from around 236 mW/cm<sup>2</sup> to 258 mW/cm<sup>2</sup>. The 405 nm UV-LED shows a deviation of around 4.41% from the perfect condition and the 365 nm UV-LED shows a deviation of around 8.52%. The characterization results show that the system is stable with 4.41% and 8.52% tolerance for the 405 nm and 365 nm UV-LEDs respectively.

#### ***5.4.5 Thermal stability for large scale setup***

Each LED used for this system can handle around 3-3.5 Watts of power. The light source comprises of 407 such high-intensity UV-LEDs. These UV-LEDs consume a huge amount of energy and produce a large amount of heat during the operation. The PCB, the waveguides, and the lenses absorb the heat from the LED by conduction and convections. Overheating can damage the 3D printed waveguides as well as the wiring materials. Therefore, temperature control is yet another vital factor for this lithography system. The ventilators provided on the waveguide walls and the Aluminum PCB board help dissipate the heat and make it flow outwards. However, the additional cooling system is required for this big setup. Therefore, a metal heat sink is provided beneath the PCB. The heat produced by the UV-LEDs can be drained out to the metal sink instead of confining inside the waveguide. Figure 5.12 (a) shows the temperature reading of the light

source at different intensity levels. The first image shows the temperature at a level of brightness level 100 where an average of 69.8° temperature is obtained, and the second image shows the temperature at a level of 150 giving an average temperature of 70.8°, the third image shows an average temperature of 71.8° at a level of 200, and the fourth image shows the temperature reading of 71.9° at the level of 255. The temperature readings were taken using a thermal camera. Figure 5.12 (b) shows the temperature changes with the brightness level change for the 405 nm UV LEDs. The blue dots in the graph show the UV-LED temperature without a heat sink.



**Figure 5.12** Thermal test (a) Temperature checked at different brightness levels, (b) Graph showing the changes of temperature with and without the heat sink.

The red dots show the temperature of LEDs after installing the metal heat sink. Around 75 degrees is observed for LEDs without a heat sink. It drops to only around 27 degrees with the help of a heat sink at a brightness level of 170. As the brightness level increases, the UV-LEDs consume more power, which increases the temperature. The use of a heat sink helps to keep the temperature under control. Even after setting the heat sink, some other small fans are also added for safe operations.

### 5.5 Second version of the light source

In the light source setup demonstrated with 400 UV-LEDs, a regular matrix arrangement was followed. This arrangement is good for getting a high intensity light source with a standard homogeneity. Since similar UV-LEDs are arranged in alternate rows and columns, a big gap remains after turning ON the similar LEDs only causing an additional contrast. This gap can be minimized, and the contrast can be further improved by using a more compact arrangement of the UV-LEDs. In this section, a second version of the light source setup has been discussed here where a more compact hexagonal honeycomb arrangement is demonstrated with the waveguide design, lens design and the collimation and homogeneity characterization.

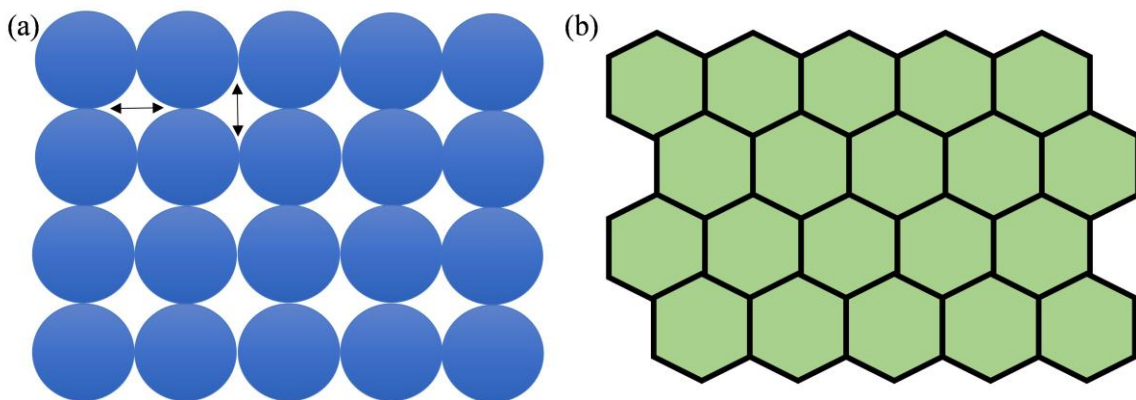


**Figure 5.13** Light source arrangements (a) Matrix arrangement of UV-LEDs in parallel rows and columns, (b) Honeycomb arrangement of UV-LEDs.

### 5.5.1 Compact honeycomb arrangement

With the aim of minimizing the contrast of the light source, the UV-LEDs have been arranged in alternate rows and columns in a zigzag pattern. The compact hexagonal arrangement has been inspired by the natural honeycomb structure. A honeycomb structure is such that each hexagonal unit connects to the adjacent units keeping no visible void in between them. Since a homogenous light source with minimum contrast is required for microlithography, the system has been adapted for hexagonal arrangement. Figure 5.13 (a) shows the regular arrangement of UV-LEDs with circular waveguides in parallel rows and columns, where a gap remains in between the neighboring UV-LEDs. On the other hand, Figure 5.13 (b) shows the honeycomb arrangement of the UV-LEDs with hexagonal waveguides. Each alternate row compensates for the gap created by the previous row and thus keeps all the UV-LEDs close and minimizes the high contrast created by the voids. On the other hand, this arrangement facilitates the accommodation of a maximum number of UV-LEDs by minimizing the unused space in between the arrays.

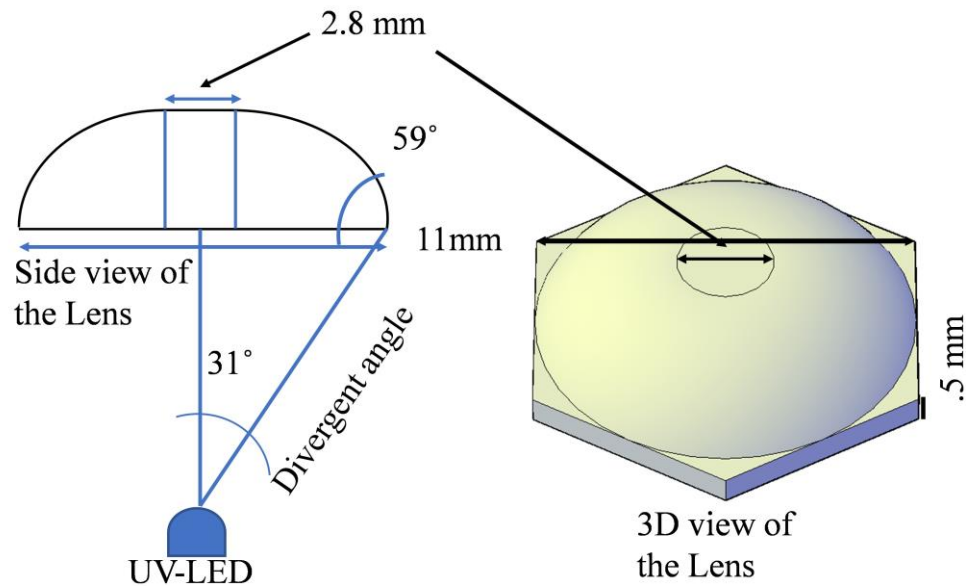


**Figure 5.14** Lens design considerations and an illustration of the hexagonal lens.

### 5.5.2 Advanced hexagonal collimating structures

Since a honeycomb arrangement has been considered for the light source, the collimating structures were designed to be hexagonal. The waveguides have been designed to mimic the honeycomb unit shape, and the corresponding lens is designed to fit inside the hexagonal waveguide perfectly.

Figure 5.14 shows the design considerations of a hexagonal lens suitable for a honeycomb UV-LED light source. The diverging UV-LED beam hits the lens with a divergence angle of  $62^\circ$  which is shown in the image as the half angle of  $31^\circ$  for lens designing.

PDMS (Polydimethylsiloxane) has been chosen as the lens material because of its high transparency to UV light [95], [96], convenience with fabrication process [97] flexibility with customization, and good collimation capability. Its angle of refraction inside the PDMS, which is  $59^\circ$  has been taken as the lens curvature angle. The middle portion of the lens was made flat in correspondence with the UV-LED chip size to ensure better collimation. The diameter of the flat center and the width of the UV-LED chip both are 2.8 mm. As circular lenses leave a particular gap with the adjacent lenses in an array structure, a hexagonal offset with a height of only 500 microns was added at the bottom so that the lenses can be arranged in a honeycomb structure with a minimum gap in between. The offset was made only  $500\ \mu\text{m}$  thin allowing the standard PDMS fabrication and minimizing the offset loss. The diameter of the lens has been taken considering the maximum distance in between the adjacent UV-LEDs.

Equation (5.2) shows the calculation that has been used for determining the focal length-

$$\frac{1}{f} = \frac{(n-1)}{r} \quad (5.3)$$

Where  $f$  is the focal length,  $n$  is the refractive index and  $r$  is the radius of curvature for the convex part of the lens.

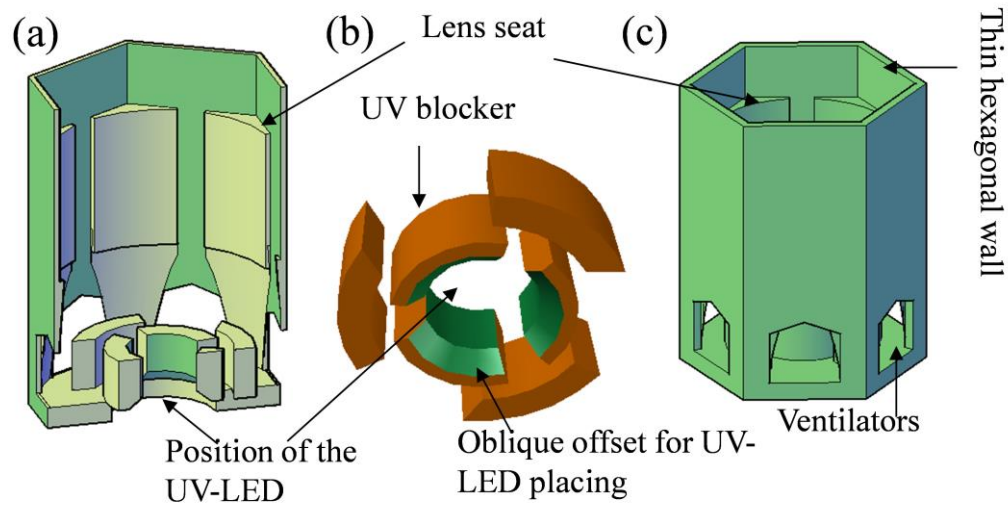


**Figure 5.15** Waveguide (a) Cross-section of the waveguide with lens seat and UV-blocker, (b) UV- blocker, (c) Waveguide unit.

The diverging light hits the lens on its focal point and is converted to collimated light beams. The radius of curvature has been determined considering the overall height and width of the lens as shown in equation (5.3).

$$r = \frac{H}{2} + \frac{W^2}{8H} \quad (5.4)$$

Where H is the height of the convex part of the lens and W is the width of the convex part. Since these lenses are not available commercially, they were made with PDMS in the lab following the standard molding procedure.

Here, in this design, a hexagonal waveguide was used to guide the light towards the lens and block any interference with the neighboring LEDs. Due to the hexagonal structure, each waveguide side was attached to another hexagonal waveguide.

The waveguide covers the LED and holds the collimating lens at its focal length. Figure 5.15 (a) shows the cross-sectional view of the waveguide where the lens seat is extended up to the bottom to make the seat robust and make enough support while printing with the 3D printer. The lens seat was made with small extensions from the waveguide wall on the six corners only so that the illuminating area is minimally sacrificed. The UV blocker is placed at the bottom and is integrated with waveguide walls. The UV-LED light has some secondary diffractions along the width.

Figure 5.15 (b) shows the design of the UV blocker to surround the UV-LED and block the unwanted diffractions. The UV blocker was made tapered from the bottom to perfectly fit the spherical LED shape. Figure 5.15 (c) shows a complete unit of the waveguide. The sidewalls of the waveguide comprise of 6 window like ventilators; these windows, along with the UV blocker gaps, create the path for airflow and prevent overheating internally. The waveguide walls are thick enough to print successfully but thin enough to minimize high contrast illumination. The optimized wall thickness between adjacent waveguides is only 500 microns. This gap between two adjacent collimated beams creates contrast in the light illumination. However, the high contrast illumination caused by these gaps gets homogenized due to the orbital rotation of the light source.

### ***5.5.3 Advanced collimation with customized lenses***

The lens is the primary collimating structure. Since a honeycomb structure was adopted, no commercial lenses met the requirements of the structure and the applications. As a result, a customized hexagonal lens was designed and fabricated in the lab. The lens parameters were calculated from equations 5.3 and 5.4 and a model was designed using AutoCAD 3D modeling. However, making a proper mold was quite challenging since the surface quality and precise control over the parameters are required.

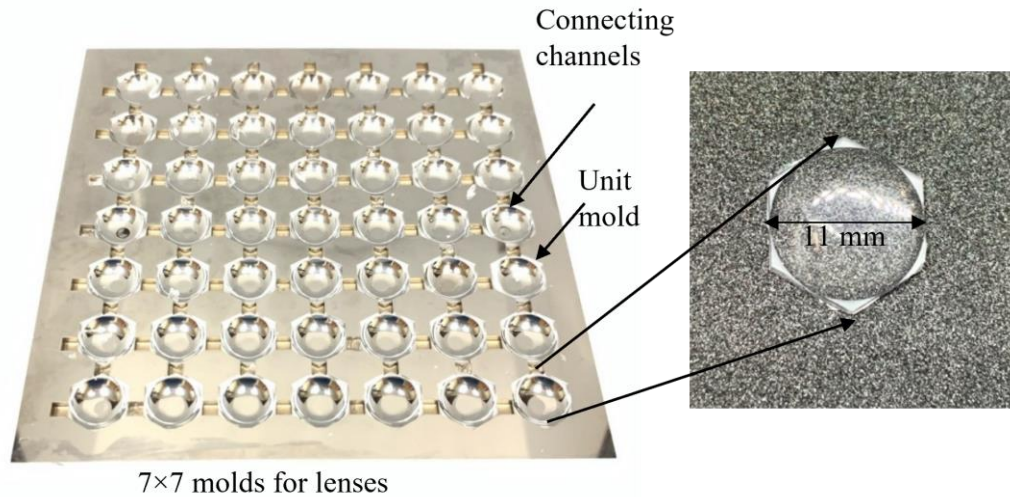


**Figure 5.16** Micromachined stainless steel lens mold, (inset- the fabricated hexagonal lens).

Therefore a customized stainless steel mold was designed and was micromachined in collaboration with Samil Tech Inc. South Korea. This mold was used for the batch fabrication of lenses. Figure 5.16 shows the lens mold, which can fabricate 49 hexagonal lenses at a time. The inset of the image shows the fabricated hexagonal lens made with PDMS.

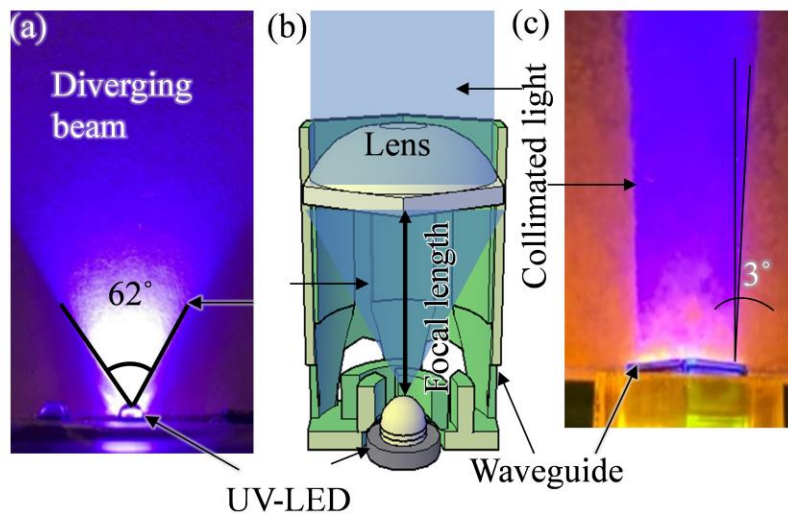


**Figure 5.17** collimation with hexagonal design (a) Divergent beam, (b) Illustration of the collimation with lens, (c) Collimation result.

Both the UV-LEDs used here in this system have a divergent beam that spreads out in the air medium with an angle of  $62^\circ$ , and some diffracted beams are seen on the lateral sides of the UV-LED tip. A UV blocker was designed slightly taller than the UV-LED itself that surrounds the UV-LED, and the diffractions are blocked from affecting the main light beam.

The actual value of the divergence was also measured utilizing the image analysis software tool ImageJ (2019) which is shown in Figure 5.17 (a). The measurement shows a divergence of  $62^\circ$ . The narrow waveguide path directs each light beam towards the respective lens, avoiding interference with other LED beams and accommodating the lens as shown in the illustration Figure 5.17 (b). Figure 5.17 (c) shows the collimation achieved by using the hexagonal lens. The deviation was measured to be  $3^\circ$  only.

#### 5.5.4 Homogeneity with the honeycomb arrangement

This version of the lithography system adopts a hexagonal honeycomb arrangement of the waveguides, and the gaps and the unusable voids created due to the matrix arrangement have been minimized. However, each waveguide separates the light emitted from its associated LED from the others. Also, since the waveguides are 3D printed, a minimum wall thickness of the waveguide is required for getting a feasible and robust structure to hold the lenses.

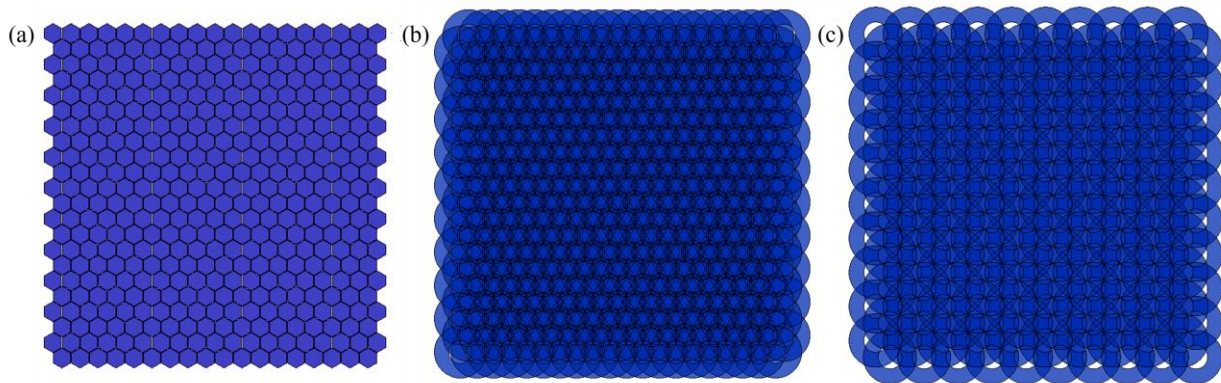


**Figure 5.18** Honeycomb light source (a) Hexagonal honeycomb arrangement, (b) All UV-LEDs on while rotating, (c) Alternate arrays are on while rotating.

The waveguides are made around 500  $\mu\text{m}$  thick, considering all these factors. These walls create dark regions on the light source. These gaps again create high contrast illumination on the substrate. As a result, the target gets exposed non-uniformly. For getting rid of that contrast, an orbital rotation is used. Figure 5.18 shows the AutoCAD drawing of the hexagonal light source at different operating states. Figure 5.18 (a) shows the light source when all the UV-LEDs are ON and there is no orbital rotation involved. Figure 5.18 (b) shows light source with the LEDs on and there is orbital rotation involved. Figure 5.18 (c) shows the light source when only the alternate UV-LEDs are on, and the light source is in orbital rotation. It seems that, even when the alternate UV-LEDs are in operation, all the gaps are covered by the motion due to the compact arrangement.

Even after changing the LED orientation and using customized lenses, a rotational movement is required for obtaining homogeneity without compromising other optics. The matrix of the LEDs is made to rotate in continuous motion so that the gaps between adjacent collimated lights are covered.

Figure 5.19 (a) shows the LEDs without rotation, Figure 5.19 (b) shows the distribution of light all over the area when kept in orbital motion. Both these images were captured with a digital camera (EOS Rebel T3i, Canon). A thin screen was placed in front of the light source to make the intensity suitable for a good image. A 6-second-long exposure was used to take the picture in Figure 5.19 (b) to complete one rotation. Figure 5.19 (c) shows the intensity distribution analyzed using ImageJ (2019) over the intensity lines drawn on the images shown in Figure 5.19 (a) (b). This uniformity test data has been taken by plotting a line through the central axis of the images. The graph for a stationary condition shows fluctuating values of the intensity, whereas the graph for the rotational movement shows almost a flat line over the target area. At stationary conditions, the highest intensity of around  $277 \text{ mW/cm}^2$  was achieved on the illuminated parts.

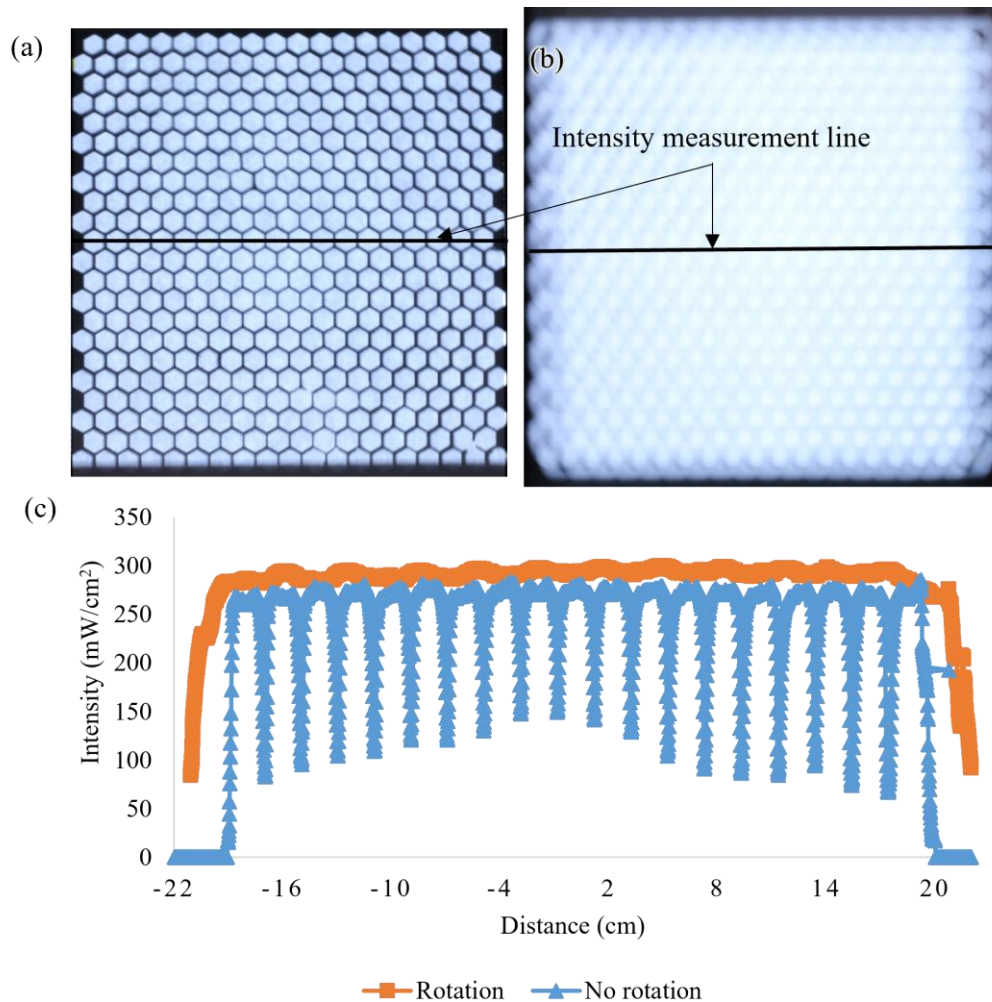


**Figure 5.19** Homogeneity with honeycomb setup (a) Light source at a stationary position, (b) Light source with orbital movement, (c) Graphical analysis of the two states of the light source.

The lowest intensity of around  $90 \text{ mW/cm}^2$  was achieved in the gaps giving a contrast of around 50%. The highest intensity measured at rotational movement is around  $294 \text{ mW/cm}^2$ , and the lowest recorded intensity was around  $284 \text{ mW/cm}^2$  on the surfaces of LEDs and the gaps respectively giving a contrast of around 1.7% only. Here, the intensity around the central axis is more while in rotation in comparison with the stationary setup, which is caused due to the overlapping of the compact UV-LEDs. Since the UV-LEDs are alternately and compactly arranged

in hexagonal form, each illuminated hexagon overlaps with all the adjacent ones while in rotation.

The contrast was measured using the formula given below-

$$\text{Contrast (\%)} = \frac{\text{Highest intensity} - \text{Lowest intensity}}{\text{Highest intensity} + \text{Lowest intensity}} \times 100 \quad (5.5)$$

Therefore, the contrast is reduced to almost 1.7% with the orbital rotation. Including some measurement errors, the homogeneity obtained can be  $1.7\pm\%$ . Thus, the system is made homogenous, and other optical parameters are undisturbed. This homogeneity helps to get uniform microstructure all over the target area and a batch production of a similar structure is facilitated as well.

## 5.6 Results

### 5.6.1 Improved resolution with 365 nm UV-LEDs and high aspect ratio microfabrication

Micro-patterning and 3D microstructure fabrications are the main functions of this multidirectional UV-LED lithography system. Resolution is one prime evaluating factor for a lithography system.

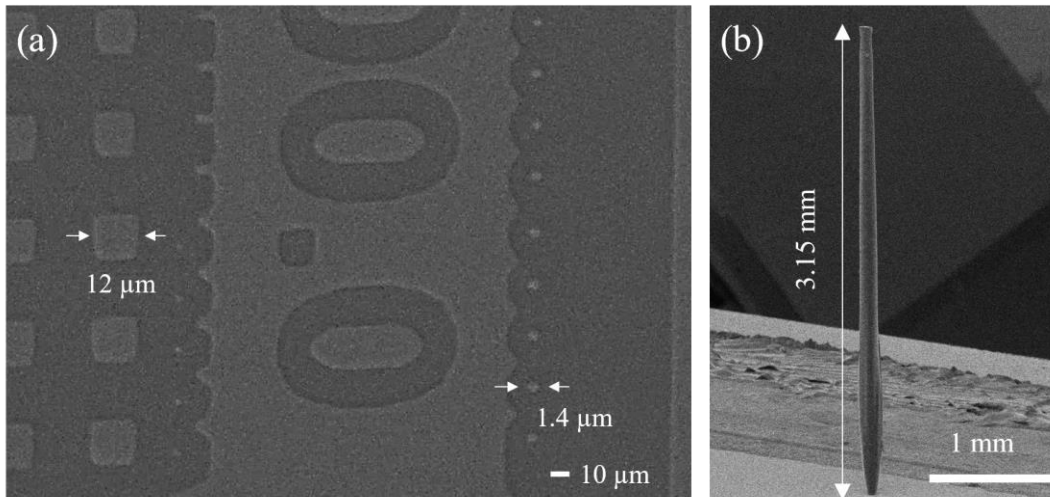


**Figure 5.20** Microfabrication (a) High-resolution patterning, (b) High aspect ratio micro tower fabrication.

Resolution is defined by the UV lithography's smallest pattern size that can be transferred on a mask. Since the wavelength, lenses and the collimating structures have been modified, an evaluation of the system has been represented again with a similar type of structures as the previous system. Figure 5.20 (a) shows high-resolution patterning as small as  $1.4\ \mu\text{m}$ . The same sample shows other sizes of patterns like  $12\ \mu\text{m}$  as well. This sample was spun at a speed of 3000 rpm on the spin coater and was baked for 5 minutes, later exposed under the UV-LED light source with an intensity of  $15\ \text{mW}/\text{cm}^2$  for 10 seconds. Figure 5.20 (b) shows the high aspect ratio micro-towers as tall as 3.15 mm with an aspect ratio of 1:10. This sample was exposed with an intensity of  $200\ \text{mW}/\text{cm}^2$  for 15 minutes only.

A resolution as high as  $1.4\ \mu\text{m}$  was achieved, and a high aspect ratio micro-tower as tall as 3.15 mm has been shown here. However, the resolution and the aspect ratio are not limited to the displayed values only, it is possible to get better resolutions and taller structures as well with modifying some fabrication parameters.

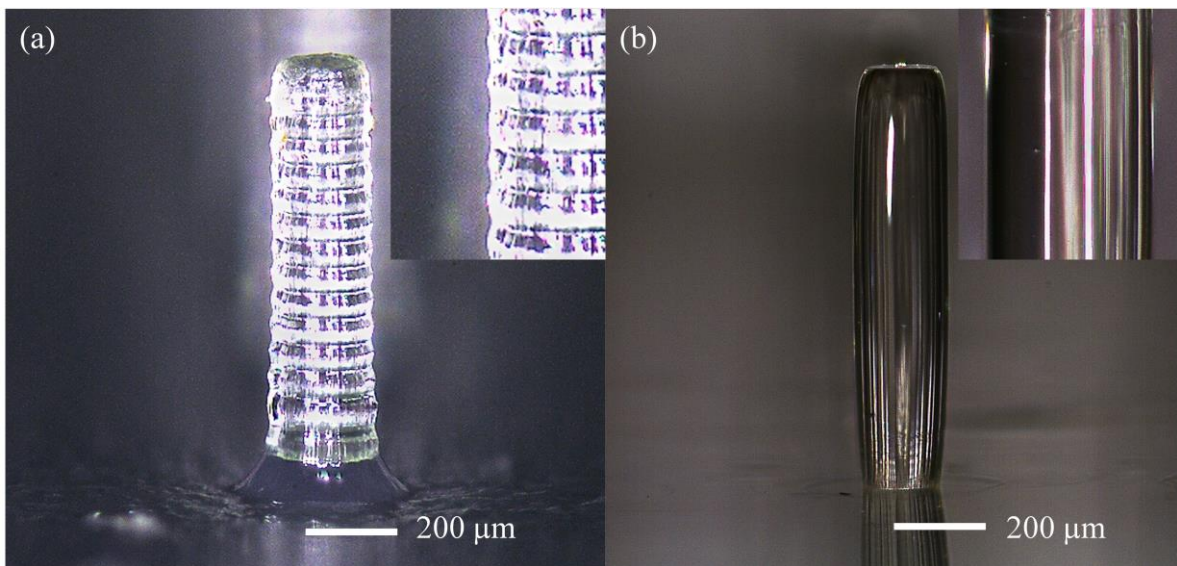


**Figure 5.21** Surface quality (a) 3D vertical pillar printed using SLA printer (Formlabs), (b) Microfabricated pillar using multidirectional UV-LED lithography system.

### ***5.6.2 Surface quality comparison with the existing 3D printing system***

3D printing technology is one prominent microfabrication field that can produce 3D structures with high resolutions and high aspect ratios using similar technology as lithography. 3D printing technology has advanced in terms of optics and 3D modeling designs and stereolithography (SLA) printers can give up to 25 microns resolution. However, the method of printing is layer by layer deposition, which gives nonuniform sidewalls on a vertical structure. Applied fields of microstructures like RF antennas, optoelectronic devices need uniformity of the structure and good surface quality to serve the purpose. In such cases, UV-LED lithography can be used to make microstructures without creating layers and with smooth sidewalls.

Figure 5.21 shows a comparative study of the printing quality for a commercial 3D printer (SLA, Formlabs) and the programmable UV-LED lithography system discussed in this chapter. Figure 5.21 (a) shows one vertical pillar printed with the commercial 3D printer where the inset shows the layering effect on the sidewall. Figure 5.21 (b) shows the vertical pillar fabricated with the same parameters using the programmable UV-LED lithography. The inset shows the smooth finishing of the sidewall. The sidewall profile shows smooth quality, and these structures are more suitable for surface-sensitive applications.

### ***5.6.3 Large scale productions***

Lithography is popular in MEMS fabrication techniques because of its repeatability and mass production ability. Thousands of microstructures can be fabricated in a single substrate with a minimum amount of time. The system discussed in this chapter has 8 square inches of exposure area, which significantly benefits the batch production without repeating the exposure session. The homogenous exposure obtained through the orbital rotation of the light source gives uniformity in the shape and size of the microstructures fabricated and the bigger size of the light source gives

the ability to fabricate thousands of microstructures simultaneously with a single exposure. For example, figure 5.22 (a) shows a section of 10000 micropillars fabricated on a single substrate with a single exposure where the diameter was preserved to be at 20~22 microns, and the height was preserved to be at 197~203 microns.

The system yielded around 90% of the pillars corresponding to the original design. Figure 5.22 (b) compares the production of the stereolithography printers (SLA) and the UV-LED lithography system discussed here. The horizontal axis gives the number of pillars obtained, and the vertical axis gives the corresponding time required. The graph shows that for getting 1089 pillars, the SLA printer requires around 114 minutes, the FDM printer requires around 60 minutes, and the UV-LED system requires only around 10 minutes. The time increases linearly with the numbers of pillars for the FDM and SLA printers, but the fabrication time remains constant for the UV-LED lithography system. In addition to that, there is no heating time required for lithography, unlike the SLA printer. Therefore, this lithography system is way faster than the 3D printers.

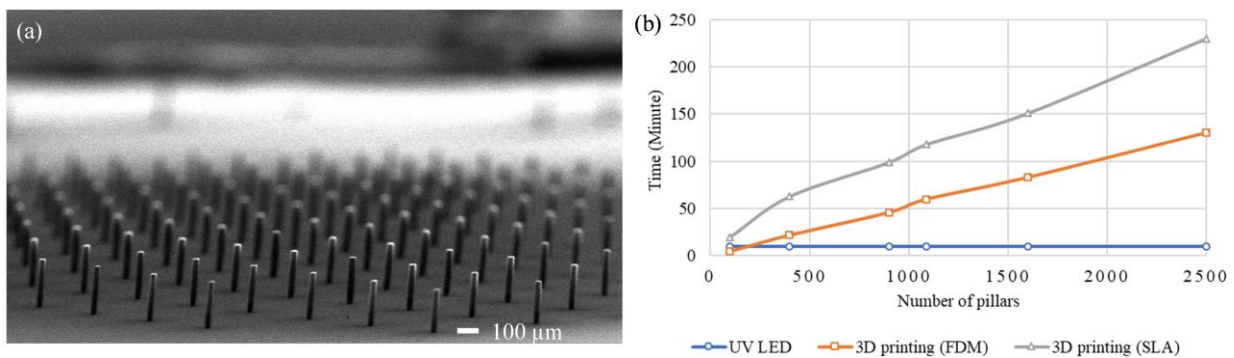


**Figure 5.22** Production yield (a) Batch production of 3D vertical microstructures, (b) Graph showing a comparison of the production yield of microstructures with time for 3D printers and the UV-LED lithography system.

#### 5.6.4 Versatility of the system

The programmable multidirectional UV-LED lithography system can fabricate complex 3D microstructure by combining different commands for tilting and rotations. For fabrications, the standard SU8 2025 procedure has been followed. Initially, Chromium coated glass samples were micropatterned with a diameter of 30 microns for all the structures shown in Figure 5.23. SU8 2025 was poured with a thickness of 500  $\mu\text{m}$  to 700  $\mu\text{m}$ . Depending on the thickness, the soft baking time was 3-5 hours. Backside exposure was performed on the samples, placing them on the tilt rotational sample holder disc. Post-exposure baking was done after exposing the samples from various angles.

Finally, the samples were developed using SU8 developer and cleaned for observation.

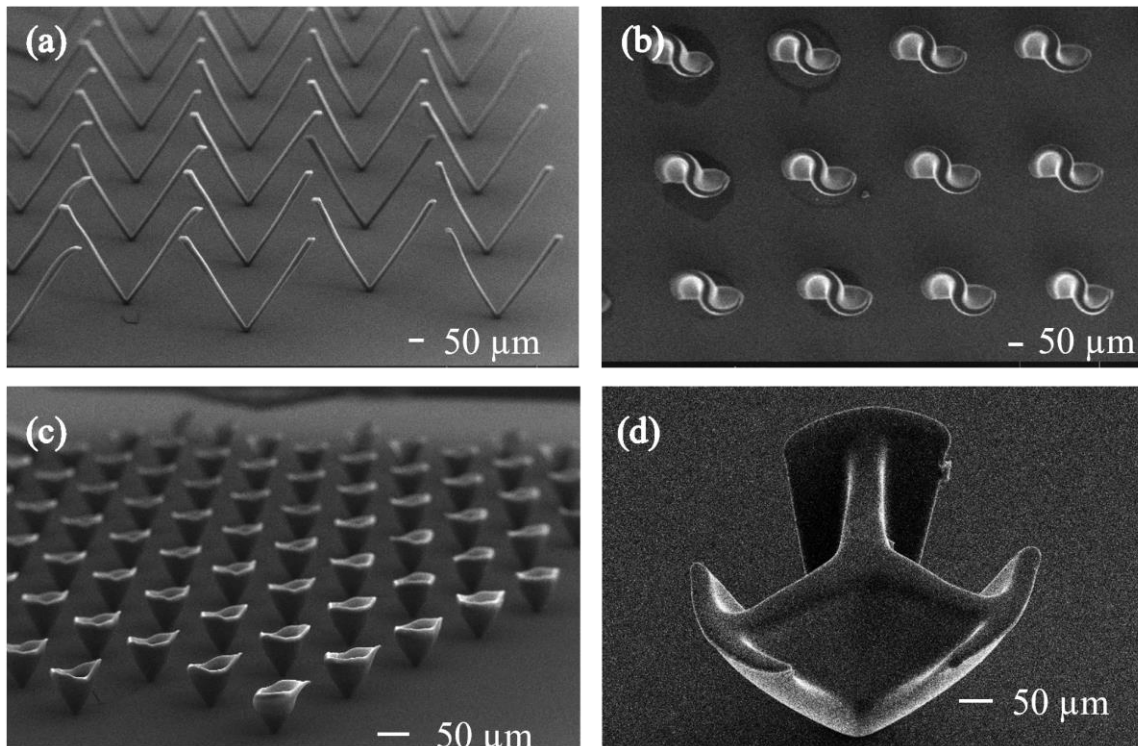


**Figure 5.23** Versatile microfabrication (a) Double inclined pillars, (b) Screwed vane structure, (c) 3D horn structure, (d) Quarter circle, (e) Double arrow, (f) 3 petal structures.

Figure 5.23 (a) shows the double inclined pillar structure, where two exposure was done at a tilting of  $70^\circ$  with a phase difference of  $180^\circ$ . Fig 5.23 (b) shows the screwed vane structures which need simultaneous rotation and tilting, which is challenging to fabricate using motor controller commands, Figure 5.23 (c) shows a tapered horn-like structure that also needs simultaneous tilting and rotation, Figure 5.23 (d) shows a 3 petalled flower structure. The complex structures need precise control over the tilting angles and the rotation angles, and swift, smooth movement to ensure the structures' finishing. The programmable functions ensure these precise movements, are not achieved from a microcontroller or manual movements. Also, the uniformity and the batch production show this system's ability for higher production yields and repeatability.

Complex 3D microstructures are getting popularity in prominent sectors like microelectromechanical systems (MEMS), RF devices, biomedical devices. The 3D structures with different geometries can be useful for different applications. For example, the vertical straight microstructures with very high aspect ratios can be used as microfluidic devices [98] and bio-inspired hair-like sensors [99] or band-specific frequency-selective devices depending on the parameters [100]. Tissue engineering is one major bioMEMS field where 3D tissue scaffolds are made mimicking the micro or nano-architecture of different tissues [40]. Since these tissues have complex and intricate shapes, it is hard to fabricate them without the help of precise and controlled technology. Another important field is the material engineering where complex and intricate geometric designs are utilized for tailoring targeted material properties [101]. The structuring flexibilities of the complex 3D structures highly benefit the mechanical properties and photonic as well as plasmonic responses. RF devices have strict performances based on their sizes and shapes. Therefore, the different shapes can be utilized for getting the desired filtering responses and antenna applications [65]. However, the complex and intricate designs demonstrated here only

represent the ability of this lithography tool to fabricate microstructures as per the user's requirement for different applications in the future. Since the scopes of microfabrication are expanding, this advanced lithography tool with versatile fabrication ability can be utilized for a wide range of applications with its customizable operations.

With higher intensity, the energy required for a microfabrication can be achieved with a very short amount of time. The integrated tilt- rotational sample holder and automatic programmable operations make time efficient fabrications negating the need of additional equipment. The regional control of the wavelength and the intensity allows the fabrication of variety of microstructures with a single operation. With large area setup, maximum production yield is achieved with minimum amount of time.

### **5.7 Performance analysis**

The programmable multidirectional UV-LED lithography system is an advanced 2D and 3D microfabrication tool. The system has been designed and customized for a wide range of traditional and modern complex 3D microfabrication with simple optics and user-friendly functionality. This system has been designed for batch productions with high repeatability and is characterized for narrow bandwidth, collimation, homogeneity, and adjustable intensity.

This dissertation focusses on the development of the UV-LED lithography system. This project started with an aim of replacing the hazardous mercury vapor lamps for lithography applications and using unique features of the UV-LEDs for making an advanced tool for lithography. Starting from the theoretical considerations and design of the single lens collimating structures all the way to the integration of the programmable multidirectional tilt-rotational system, this project made significant improvements in all the prototypes. The primary prototype with 100 UV-LEDs had only one directional exposure system, where the system was optimized for standard

intensity, collimation, and homogeneity. The system was characterized for fundamental micro patterning and 3D microfabrication. The following prototype improvised significantly in terms of waveguide design, thermal control, regional control, and multidirectional exposure system. The final version of the multidirectional UV-LED lithography system has been established with all programmable functions, dual wavelength, adaptive intensity and integrated mask alignment and 3D exposure system. Table 5.1 shows the comparative study of the improvisations achieved from different prototypes discussed so far.

**Table 5.1 comparison of the improvements on different UV-LED lithography systems discussed**

Setups	Adjustable Intensity	Wavelength	Regional control	Size	Multidirectional exposure system	Method of operation
UV-LED lithography light source [87]	Adjustable with dimmer switch	405 nm	Absent	5"×4"	Absent	Manual
The UV-LED lithography system with tilt rotational sample holder [62]	Changing current and distance	405 nm	Present	2"×2"	Separately added	Microcontroller operations
The UV-LED lithography system with computer programmable functions [102]	Programmed	405 nm+365 nm	Present	8"×8"	Integrated	C++ programmable

There are other research and commercial setups for lithography. Here, a comparative study has been presented in Table 5.2 where it shows the comparison of the size and intensity obtained from different UV-LED lithography setups.

**Table 5.2 Comparison of different UV lithography systems**

Number	Light source	Intensity (mW/cm <sup>2</sup> )	Exposure area	Reference
1	Q. L. Pham et al.	2 @ 365 nm	4"	[103]
2	H. Takahashi et al. (UV-LED)	7 @380 nm	40×40 mm <sup>2</sup>	[52]
3	M. K. Yapici et al. (UV-LED)	20 @380 nm	3"×3"	[104]
4	Midas-MDE-200SC (UV lamp)	25 @365 nm	12"	[105]
5	SPS-MDA400M (Mercury lamp)	30 @365 nm	4"	[106]
6	Kloe-UV KUB 2 (UV-LED)	35 @365 nm	4" or 6"	[107]
7	J. W. Huang et al. (UV-LED)	35.6 @365 nm	8"× 8"	[108]
8	Tamarak 152 (UV lamp)	45 @405 nm, 25 @365 nm	4"	[109]
9	Idonus- EXP 100 (UV-LED)	50 @ 365 nm	100×100 mm <sup>2</sup>	[110]
10	Quintel-NXQ200 (UV-LED)	75 @ 405 nm, 31 @ 365 nm	200 mm	[92]
11	E. D. Kurniawan et al. (UV-LED)	82 @394 nm	2×2 cm <sup>2</sup>	[111]
12	Suss-MA300 Gen 2 (UV lamp)	90 @ 405 nm	12"	[112]
13	This work (UVLED)	425@405 nm	8"× 8"	
14	This work (UVLED)	258@365 nm	8"× 8"	

Figure 5.24 shows a graph comparing the sizes and the intensities of the discussed lithography systems. Where the X-axis shows the serial number presented in the table, the primary Y axis shows the intensity expressed in  $\text{mW}/\text{cm}^2$  and the secondary Y axis shows the size of the presented lithography systems. It is seen that the intensity of the programmable multidirectional UV-LED lithography system is more than five times of the highest intensity presented so far. And the size of the light source demonstrated here the second largest among the existing setups. However, this size can be increased by adding up similar UV-LED matrices. The table and the graph show a direct comparison of the parameters that are in common with existing lithography systems. However, there are additional features of the UV-LED lithography system that are not common among the commercial lithography and haven't been compared directly.

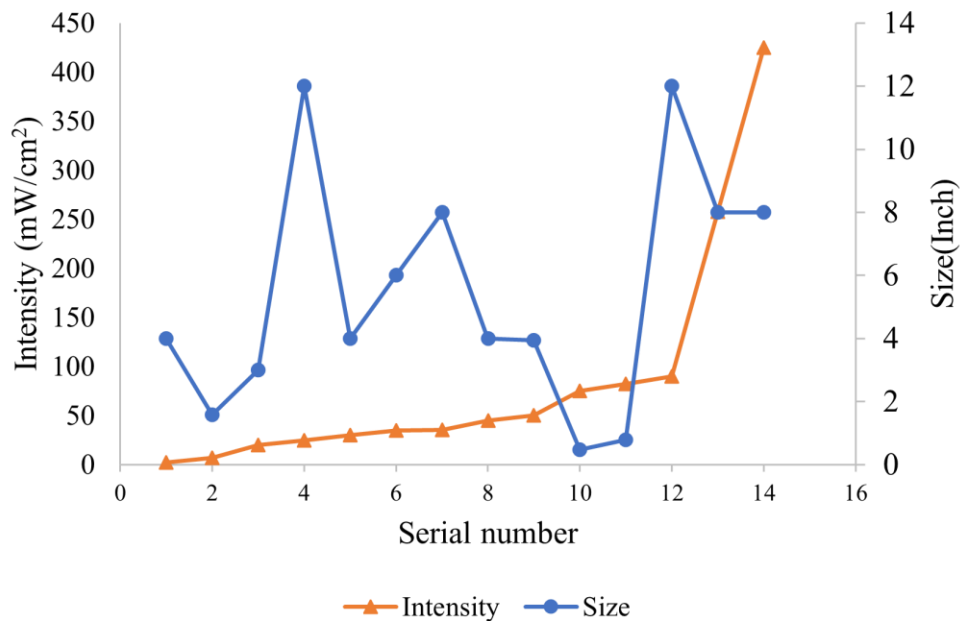


**Figure 5.24** Performance analysis of some of the prominent lithography systems.

## 5.8 Summary

An advanced UV-LED lithography system has been represented in this article. Alternative arrays of very high-intensity UV-LEDs have been used here as the exposure system. It has been characterized for high and programmable intensity, collimation, homogeneity, light source reliability, thermal stability. The system has been compared to the commercial lithography systems to show its compatibility for microfabrication. The highest intensity recorded for this system using 405 nm LEDs is  $472 \text{ mW/cm}^2$  and for 365 nm LEDs is  $258 \text{ mW/cm}^2$ . The collimation obtained is within  $\pm 3^\circ$ , whereas the standard collimation for lithography is  $< 5^\circ$ . The light source achieved around 1.5% homogeneity with an exposure area of 8 square inches. The UV-LED lithography system is unique because of its high-intensity exposure, simple and customized collimating lenses, huge exposure area with very high uniformity, high repeatability, tilt rotational sample holder with mask aligning functions, and computer control over each UV-LED. The overall system setup is simple yet capable of the most advanced 3D microfabrication. The system can fabricate traditionally fabricated several microns thin micropatterns and several millimeter-thick advanced 3D microstructures. The highest resolution and tallest structures are shown to be  $1.4 \mu\text{m}$  and 3.15 millimeters but are not restricted to these values. It is possible to get batch production of microstructures within a small period with smooth surfaces and primordial parameters. The high aspect ratio vertical micropillars shown in different examples can be used as RF monopole antennas. Other 3D structures shown in the examples can be used as microfluidic devices, microturbines, RF devices, biosensors, and actuators.

Considering the fabrication quality and design simplicity, the discussed UV-LED lithography system can replace the existing UV lithography systems with additional advanced performance. There are scopes for getting more advanced results in future fabrications as well.

These microstructures have potential uses in RF (Radio- Frequency) devices, bioMEMS devices, actuators, wearable devices, and many other vital sectors as they have smoother surfaces with higher aspect ratios.

# Chapter 6 - Tilttable UV-LED lithography system for 3D microfabrication for solid and liquid photoresists<sup>3</sup>

## 6.1 Introduction to tilttable UV-LED lithography

This chapter presents the future direction of the research with the multidirectional UV-LED lithography system. Most of the microstructures demonstrated so far are fabricated using negative tone photoresist SU8. With the development of new materials for 3D printing, many photopolymers are available nowadays to create different 3D structures. Photopolymer resins are used for stereolithography (SLA) 3D printing. Since stereolithography is the closest technology to photolithography, recent studies show the compatibility of such photopolymer resins for photolithography applications [114] [115] where the diffraction of UV light is utilized to form microneedles for bio applications. These resins are also chosen for their biocompatibility and higher young's modulus value [116], [117]. Stable microstructures can be fabricated using only one-step exposure. This fabrication process is devoid of soft baking and post-exposure baking steps, requiring minimum time and equipment for 3D microfabrication. However, for the non-baked photopolymer, the use of the tilt-rotational sample holder system can be inefficient since the sample is moved around in 3D spaces. The prevention of leaking or spilling of liquid resin is the primary challenge for this fabrication. Sugimoto *et al.* proposed the use of a rotated or inclined mirror instead of moving the sample itself for liquid resin exposure [118]. However, the reflection caused by these mirrors doesn't ensure uniform illumination over the target area which causes less production yield. Rotating prism-assisted exposure has also been for similar microfabrication [119], [120] which needs the prism to be replaced every time for a change of the angle. Due to the

---

<sup>3</sup> This article is a reformatted and slightly modified version of our article [113]

use of additional optical aids, these methods are complicated, and it is hard to maintain accuracy. Although the multidirectional sample holder can also be used for liquid-state resin exposure [121], secured locking of the sample is challenging. Since the photo polymeric resins seem very promising for bio applications like drug delivery microneedles [122], microfluidic devices [123], RF antenna [124] with time-efficient fabrication procedure, a lithography system has been discussed here, making the liquid state exposure possible in multiple directions, keeping the sample at a stationary position [113]. The independent control feature of the UV-LEDs has been utilized here. UV-LEDs can be operated without being embedded into a PCB; it can be customized to be movable in 3D spaces. On the other hand, as the sample remains stationary, the non-uniformity of the exposure due to the inclination is solved as well.

## **6.2 Concept of the tiltable UV-LED lithography system**

The principle of this system is that the light source is made to tilt at different angles instead of making the sample to be tilted at multiple angles. The tiltable UV-LED lithography system prototype comprises a 7-by-7 array of 405-nm UV-LEDs. An orbital rotation of the UV-LED array provides a uniform light intensity. The fundamental advantage of the discussed system is to create 3D light traces without the sample's tilt-rotational movement, which can cause non-uniformity of the exposure over the target area and sample instability. The discussed tiltable UV-LED light source can directly pattern on a liquid photosensitive resin (SLA 3D printing resin) saving several hours per microfabrication process.

A prototype has been designed with a simple 3D printed waveguide and a commercial 12-mm diameter glass lens. The waveguides were customized to be tiltable using extended 3D printed rods to create light inclination between  $-70^\circ$  to  $+70^\circ$ . The extended waveguide is connected to a pivot joint creating tilting angles along the  $\pm X$  and  $\pm Y$  directions.

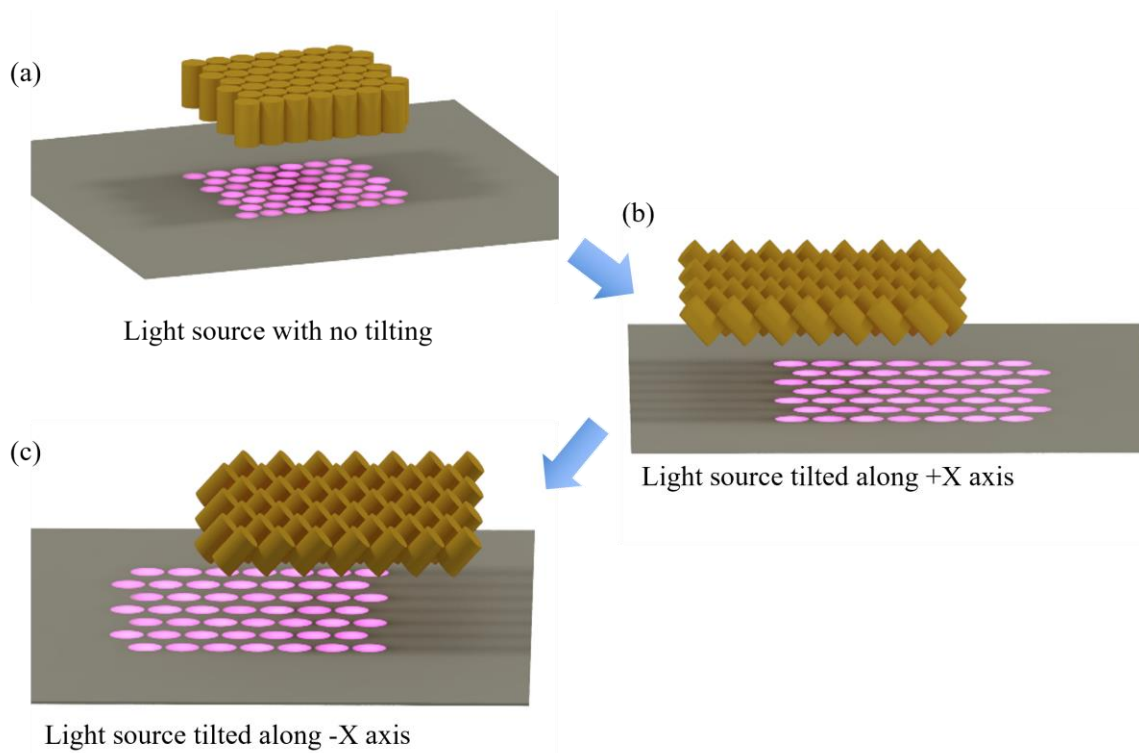


**Figure 6.1** Concept of the tiltable UV-LED lithography system.

All the movements are motorized and controlled with a microcontroller. A schematic of the working principle of the tiltable UV-LED lithography system has been shown in Figure 6.1.

Figure 6.1 (a) shows the array of 7 by 7 UV-LEDs to be stationary with zero-degree inclination. Figure 6.1 (b) shows the light source tilted on the +X axis, and Figure 6.1(c) shows the tilting in the -X-direction. The design considerations of the system are shown in the sections of this chapter and the system has been characterized for collimation, adjustable intensity, homogeneity, and uniformity. Examples of microfabrication capability have been shown with vertical pillars, inclined pillars, triangular slabs using traditional photoresist SU8, single and dual microneedles, and multi-angled petals using photo polymeric liquid resin (Surgical guide resin, Formlabs). The prototype has shown the unique ability to fabricate microstructures in both baked

and non-baked photoresists, which opens up the possibility to fabricate a lot more range of microstructures.

### 6.3 Tiltable UV-LED lithography system design

#### 6.3.1 Optical setup

A prototype of the tiltable UV-LED lithography system has been shown that can cover an exposure area of 3-inch<sup>2</sup>. A 3W high power UV-LED (Chanzon,10DGL-DZ-3W-405) was chosen as a light source with 405 nm wavelength since the 405 nm is suitable for thick photoresist processing. Since each LED must be set individually inside the waveguide for tilttable movements, the commercial (Chanzon) UV-LED was used instead of the PCB embedded LEDs. Each UV-LED is collimated using a single lens and a conical 3D printed waveguide. Figure 6.2 (a) shows the side view of the waveguide designed in AutoCAD (2021), Figure 6.2 (b) shows the inside, and Figure 6.2 (c) illustrates the integrated lens collimating structure. For light collimation, a 12-mm base-diameter glass was positioned at the lens focal length distance above the LED.

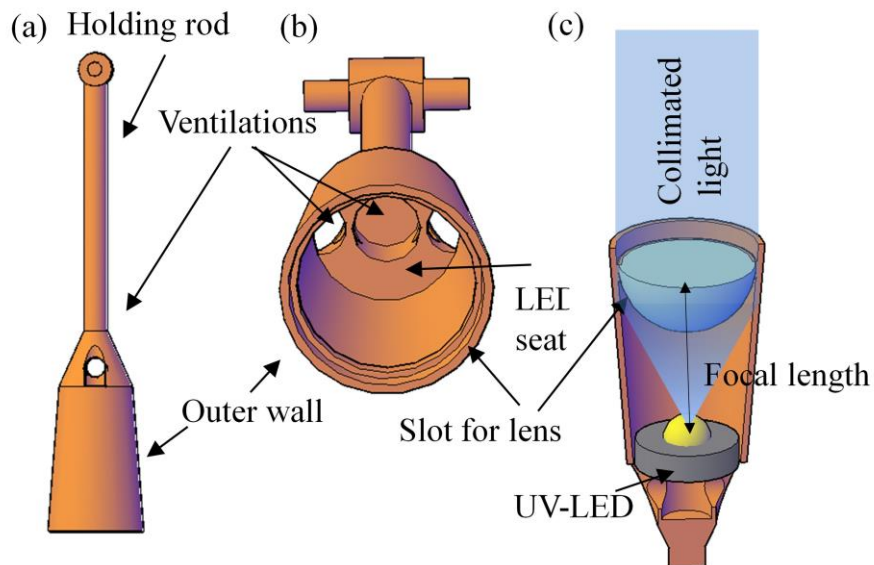


**Figure 6.2** Waveguide design with lens housing (a) Side view, (b) Inside, (c) Lens and LED integrated.

The customized waveguide was designed to locate the LED inside with ventilation holes considering heat dissipation, wiring, and lens positioning. The sidewall of the waveguide is made tapered and slightly conical to mimic the path of the primary light propagation. A seat for placing the collimating lens was made on the waveguide by creating an extension on the inner wall of the waveguide. The waveguide was coated with an anti-reflection black color to block unnecessary light leaking. The waveguide is then extended to a holding rod for creating room for tilting movement up to 70 degrees. The overall waveguide is 3D printed using an SLA printer (Form 2) with a high-temperature bearable resin (FLHTAM01, Formlabs) which has a heat deflection temperature (HDT) of 238 °C at 0.45 MPa.

### 6.3.2 Mechanical and electric setup

The preciseness of the mechanical setup is as important as the optical setup since the tilting of the light source discussed here is controlled mechanically. Figure 6.3 shows the overall design of the tiltable UV-LED lithography system where the inset shows the unit of the waveguide and the pivot joint.

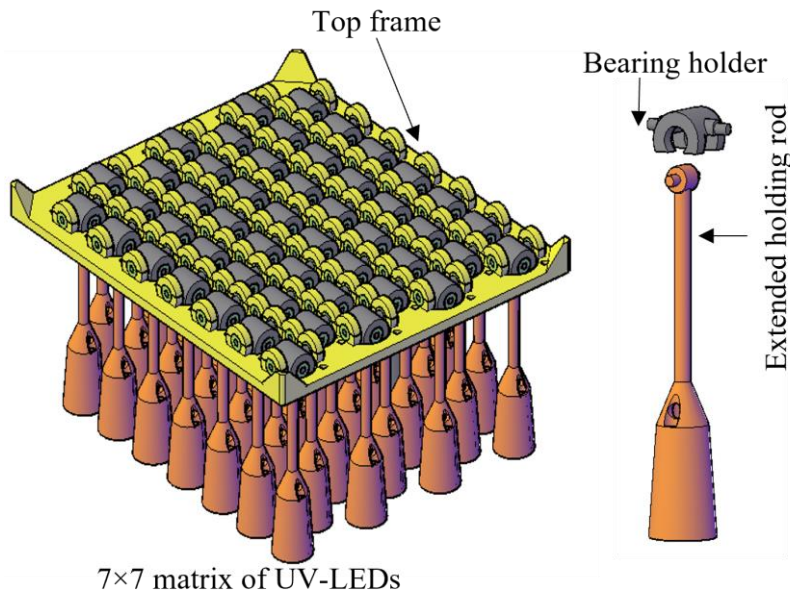


**Figure 6.3** The light source with the tilting arrangement (inset- Unit waveguide with pivot joint).

Each waveguide has a long rod, extended to have a horizontal bar at the end for holding two small bearings. This bar and the bearings are placed inside another 3D printed housing forming a pivot joint. Again, this housing is connected to a slotted frame with two more small bearings. These bearings enable x-axis and y-axis movement. The top which is also 3D printed provides the housing for all the LEDs, waveguides, and the electric wires. The electrical connections are provided with 38-gauge wires, which are convenient for this application because of their thinner diameter and flexibility. The wires are soldered on the metal legs of the UV-LED that extends up to the end of the top frame. The wires travel through the wire slots printed on the waveguides. The wires are channeled from the frame connecting to the power supply. Since the waveguides tilt in X-Y directions, the straight wires can create friction while moving. Therefore, the wires were draped spirally along the long holding rod to create some spring effect with the help of heat treatment. The LEDs were arranged in a 7 by 7 matrix. Each row was connected in series, and all the columns were connected in parallel. Each LED was rated to be operated in the range of 400-500 mA and 3-3.4 V. Two small cooling fans were integrated alongside the light source for keeping the temperature under control while in operation.

The prototype was successfully built, as shown in Figure 6.4. The light source was housed inside a 3D-printed frame. The light source and the frame were suspended from an Aluminum extrusion. The light source is supported by a slider that is free to move along the X-axis when connected to a stepper motor and the tension is created by using a pulley and a belt. The Y-axis movement is controlled with the help of another stepper motor. A laser-cut acrylic frame is placed under the 3D printed frame with holes to hold the waveguides in their respective holes while in motion; this is named the fixed frame. The fixed frame is designed so that the tilting restricts within  $\pm 70^\circ$ .

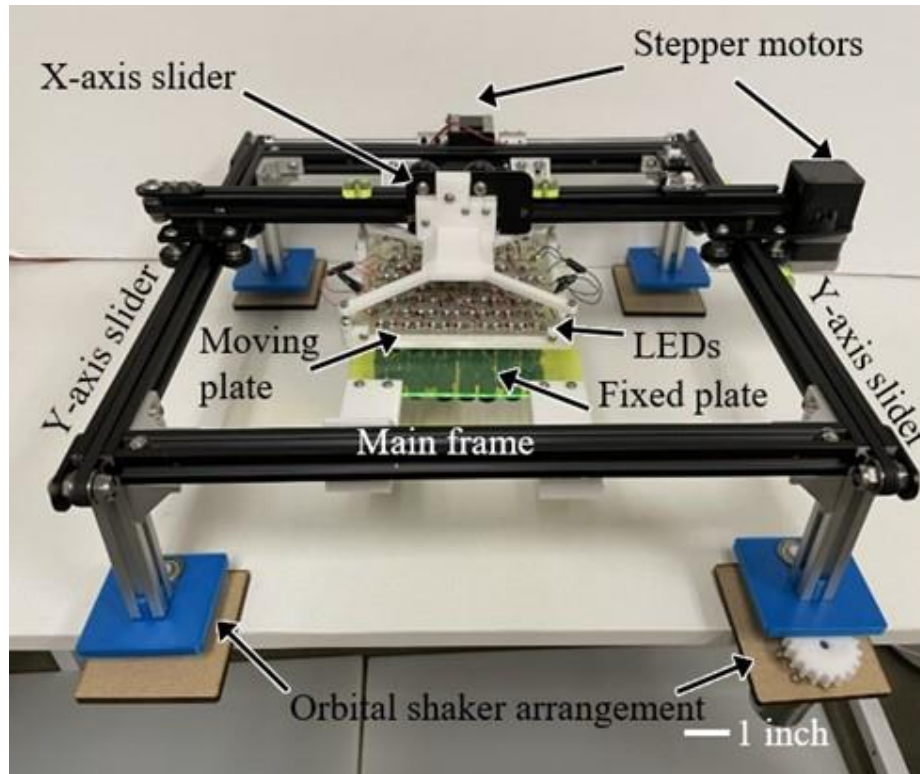


**Figure 6.4** Tiltable UV lithography system setup.

All the motions are controlled using a microcontroller (EZaxis, Allmotion Inc.), and the software for controlling these commands was made in AllMotion (2020) software. Since this source is designed to be tilting, a direct orbital motion can not be applied for getting homogeneity. For creating the homogenous illumination, the whole setup including all the parts was made to rotate in orbital motion so that the gap between the adjacent UV illumination is covered up. A high torque 12 Volt DC motor was connected to one leg of the frame and the rotating connectors and bearings were connected to all the legs which helped the orbital rotation creating homogeneous light distribution over the target area. Depending on the weight of the overall setup, a stronger motor and a larger number of bearings might be added. For this prototype, the power supply was connected externally which can be integrated later with the system.

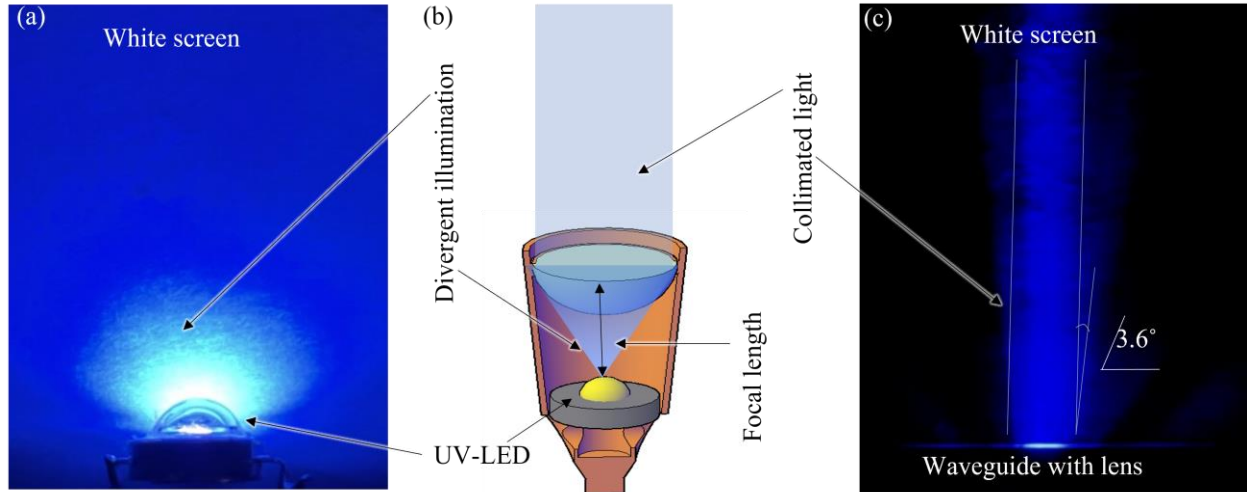


**Figure 6.5** Collimation test result (a) Divergent illumination by the UV-LED, (b) Collimated light with lens and waveguide.

## 6.4 Characterization

For building, this unique prototype of the tiltable UV-LED lithography system, the type and the design of the light source is very different from the previously discussed lithography systems. Therefore, all the standard characterizations have been thoroughly performed. This prototype has been characterized for single-lens collimation, Adjustable intensity, homogenous light distribution, and uniform light distribution all over the target.

### 6.4.1 Collimation with bigger lens and conical waveguide

The surface-mounted device (SMD) type UV-LED has been used as the light source and 12 mm convex glass cabochons (PendaHall) has been used as the collimating aid. Figure 6.5 shows the light collimation result, where Figure 6.5 (a) shows the light propagation from the LED chip without the waveguide and the lens, and Figure 6.5 (b) shows the collimated light after having the single lens on top of the LED chip seated inside the 3D printed waveguide. The original light beam shows propagation with an angle of around  $120^\circ$ .

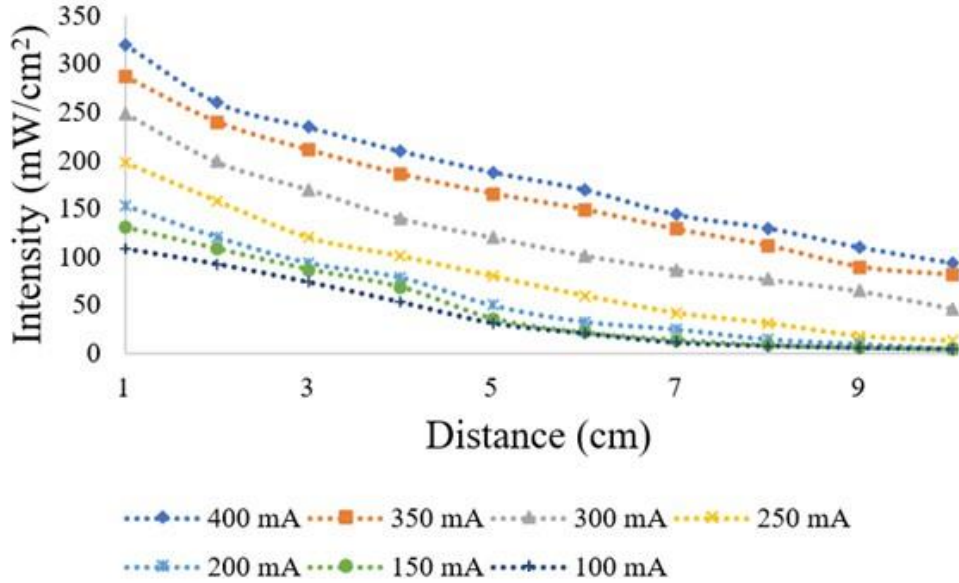


**Figure 6.6** Change of intensity with the change of distance and direct current.

The degree of the light propagation angle was analyzed using ImageJ (2020) software which shows a deviation of  $3.6^\circ$  after the addition of the lens and waveguide, which is suitable for the typical microlithography.

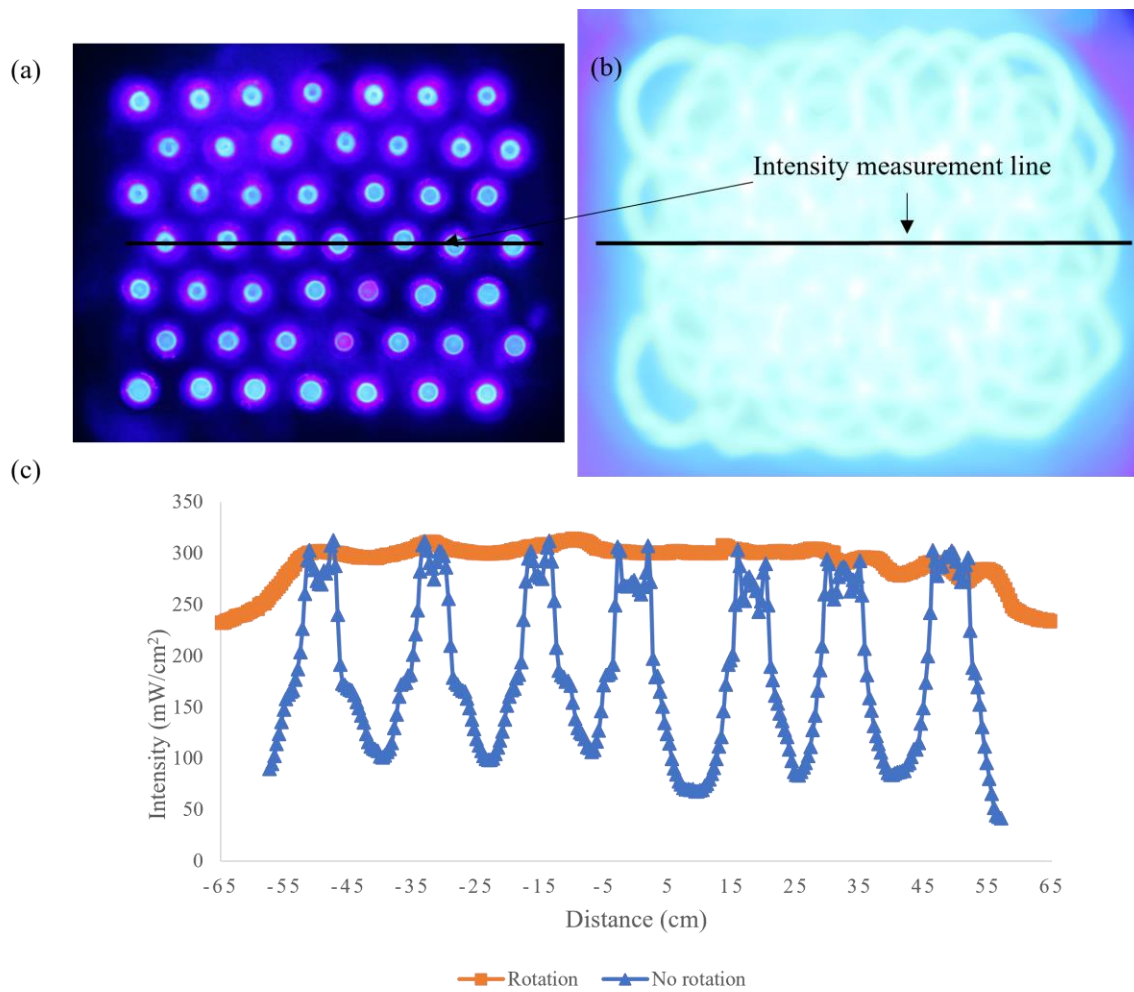
#### 6.4.2 Variable intensity with tilt functions

Figure 6.6 shows the intensity variation caused by the linear distance between the light source and the target and the variation of the driving current. The highest light intensity of  $320 \text{ mW/cm}^2$  was observed at the 400 mA/LED while the intensity was decreased linearly with the increase of the distance. Also, the driving current showed the variable intensity for a programmable UV exposure. The graph in Figure 6.6 shows the variation of intensity from  $6 \text{ mW/cm}^2$  to  $320 \text{ mW/cm}^2$  with the change of current in between 100-400 mA per UV-LED and linear distance of 1 to 10 cm.

#### 6.4.3 Homogeneity keeping the tilts intact

The gap between the adjacent UV-LEDs was 17.5 mm, which was calculated to accommodate the 12 mm lens for collimation and a room for 70 degrees tilting on both sides. This

gap creates a contrast with the illuminated parts of the light source. An orbital movement was introduced on the whole setup instead of just the light source, as the light source is already set for tilting. Therefore, the Aluminum extrusions of the frame were set for the orbital motion with the help of a high torque DC motor. The motor torque is important since only one motor is responsible for creating the movement on this heavy arrangement, unlike the previous setups where only the light source was rotated.



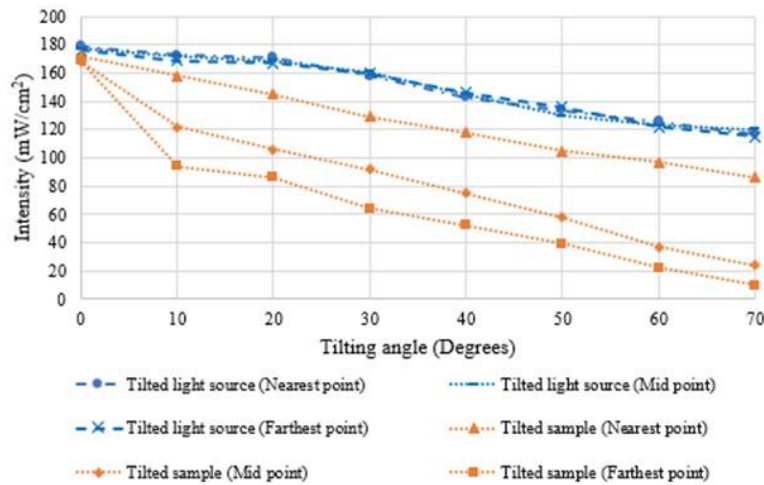
**Figure 6.7** (a) Light source without rotation, (b) Light source with rotation, (c) Graphical comparison of intensity profile with and without rotation.

Figure 6.7 (a) shows the light source at its stationary condition, Figure 6.7 (b) shows the light source at its rotating condition, and Figure 6.7 (c) graphically explains the comparison between ‘no rotation’ and ‘with rotation,’ resulting in high-intensity contrast in Figure 6.7 (a) and uniform intensity in Figure 6.7 (b). The light source without rotation gives a highest of 307 mW/cm<sup>2</sup> and a lowest of 69 mW/cm<sup>2</sup> giving a contrast of 63%. On the other hand, the light source with motion gives a contrast of around 5%.

This analysis was done using ImageJ software by drawing a line through the center of the images, and the images used in Figures 6.7 (a) and 6.7 (b) were captured using a digital camera (EOS Rebel T3i, Canon).

#### 6.4.4 Comparison of uniformity with the existing tiltable systems

Since most of the multidirectional UV lithography systems utilize the tilting of the sample, it becomes a significant concern to keep the sample secured with the movements. Significantly, the liquid resins have the ultimate risk of spilling and leaking if kept unsecured. Therefore, this system has adapted the self-tilting function keeping the sample stationary.



**Figure 6.8** Comparison of intensity distribution for an inclined light source with the tiltable sample holder.

Figure 6.8 shows a graph comparing the intensity distribution for the two different setups. The plots in orange dots show how the intensity variation at the nearest point, the mid-point, and the farthest point for a definite tilting angle when the sample is placed on a tilting sample holder.

On the other hand, blue color lines show how the intensity drop is significantly less for the nearest, mid-point, and farthest points with the tiltable light source arrangement. Compared to the sample tilting method, the overall intensity is well preserved in the tilting light source. The deviation for the intensity between the nearest and the farthest point for tiltable sample holder is around 88% whereas, the deviation for the discussed system is around 4% only. This is the most unique characteristic observed in the discussed tiltable UV-LED lithography system and it gives a lot of opportunities to fabricate complex 3D microstructures in a non-complex manner with higher fabrication possibilities.

## **6.5 Fabrication method**

### ***6.5.1 Solid photoresist microfabrication***

The solid-photoresist fabrication here means the fabrication done with soft-baked photoresists. This procedure follows the standard steps of organic cleaning, soft baking, UV exposure, post-exposure baking, and developing. An example fabrication process of a dual inclined pillar or 'V' 3D microstructure using SU-8 is as shown in Figure 6.9 (a-e). Here the viscous negative photoresist SU8 2025 was poured on the sample by following a pre-measured weight vs. thickness ratio. The samples were soft baked on a hotplate at a temperature of 95° for a few hours Figure 6.9 (a). Then, the sample was placed upside down under the exposure system, and the light was tilted to +70°. It was exposed for 10 minutes with an intensity of 120 mW/cm<sup>2</sup> for a thickness of around 300 μm as shown in Figure 6.9 (b). Similarly, the light was tilted to -70° and exposed for another 10 minutes as shown in Figure 6.9 (c).

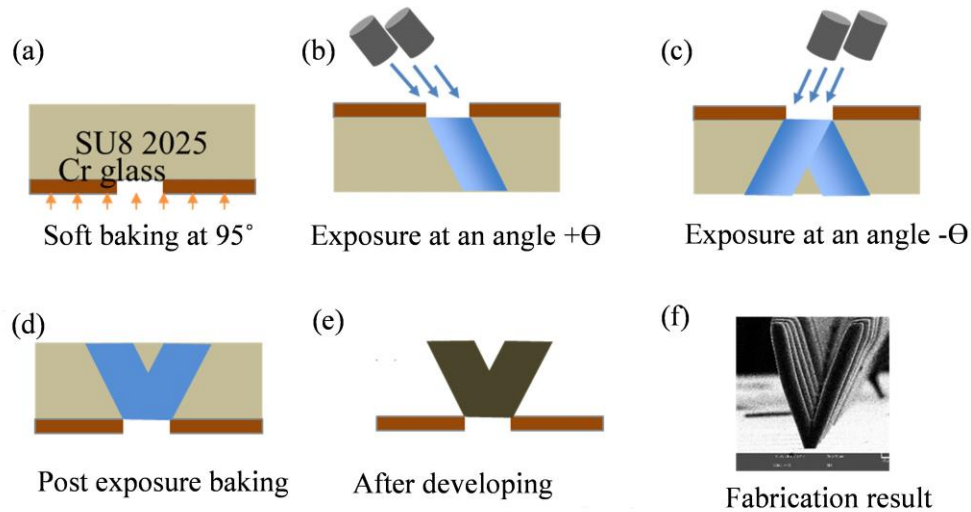


**Figure 6.9** Fabrication of SU8 structure: (a) Soft bake, (b) Inclined UV exposure at  $+\Theta$ , (c) Inclined UV exposure at  $-\Theta$ , (d) post-exposure bake, (e) Developing, (f) Fabrication result.

After exposure, the sample was done post-exposure baking at a temperature of 95° for 30 minutes as shown in Figure 6.9 (d) followed by developing for 15 minutes in fresh SU8 developer with mild agitation, Figure 6.9 (e). After developing, the sample was dried with airflow carefully.

A scanning electron microscope (SEM) image of the fabricated ‘V’ 3D microstructure has been shown in Figure 6.9 (f). This microfabrication takes several hours of soft baking depending on the photoresist thickness, and around 1 hour of post-exposure baking is done for completing the cross-linking. This method is time-consuming but is the standard method of SU8 microfabrication.

### 6.5.2 Liquid State microfabrication

For the liquid resin exposure, commercial 3D printing resin (Surgical guide, Formlabs) has been used instead of SU8. First, a 3D-printed rectangular reservoir was printed and filled up with clear resin until the resin reaches the reservoir wall height.

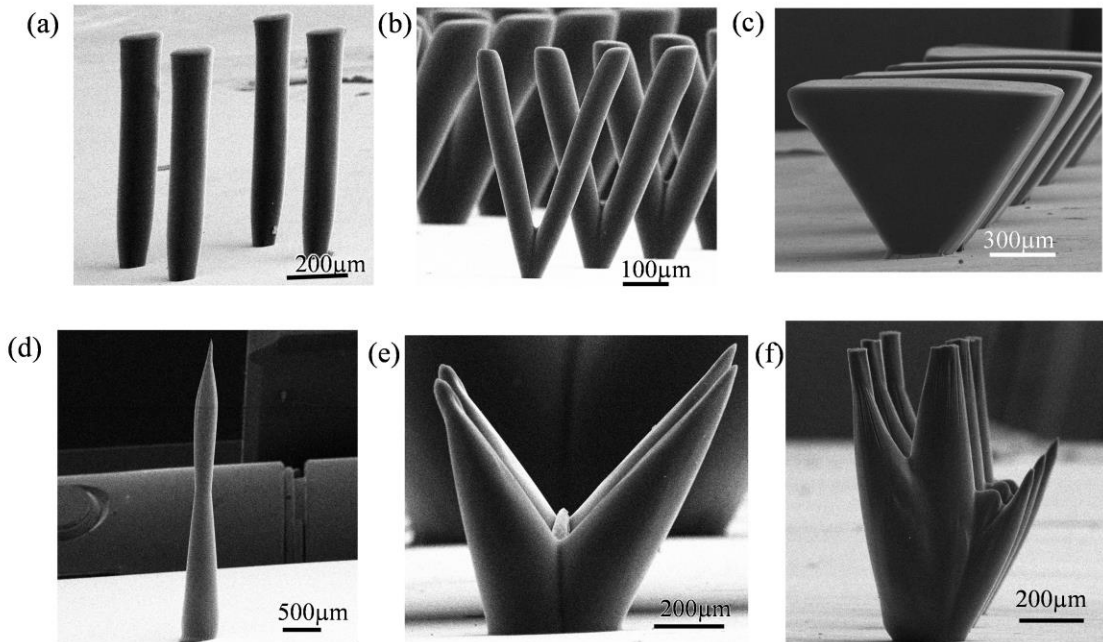


**Figure 6.10** Microfabrication results (a) SU8 vertical pillars, (b) SU8 dual Inclined pillars, (c) SU8 3D triangle, (d) Liquid resin vertical microneedle, (e) Liquid resin dual microneedle, (f) Liquid resin multi-angled petal.

Next, the photopatterned mask was placed upside down above the resin reservoir so that the patterned side of the mask touches the resin and there is no air gap between them. Then the sample was exposed for 1 min at an intensity of  $45 \text{ mW/cm}^2$  at  $+60^\circ$  and  $-60^\circ$  respectively to give a dual inclined microneedle.

After exposure, the mask was gently detached from the reservoir to form the structures on the mask. Then, the sample was developed in IPA for 5 minutes with mild agitation.

### 6.6 Microfabrication results

The fabricated results show several examples of both the solid-photoresist exposed samples and liquid photoresist exposed samples. Figure 6.10 shows the various microfabrication examples of the discussed system. Figure 6.10 (a) shows some examples of the high aspect ratio vertical

pillars. Figure 6.10 (b) shows the ‘V’ microstructures with an inclination of  $\pm 70^\circ$  with a phase difference of  $90^\circ$ . Figure 6.10 (c) shows the triangle slab which involves the continuous movement of the light source from  $-70^\circ$  to  $+70^\circ$ . Figure 6.10 (a-c) used SU8 2025 as the photoresist. Figure 6.10 (d-f) shows the examples of liquid state exposure for vertical, dual inclined, and multi-angled petal structures. 3D printer resin (Surgical guide, Formlabs) has been used as the photoresist. These structures show sharp tips instead of flatheads because the light traverses through the liquid resin in a conical way, unlike SU8 due to diffraction occurring through the liquid. If the exposure is more, then light passes through the already crosslinked structure forming secondary harmonics where the initial crosslinked structure works as a waveguide for the incoming light [125]. Figure 6.10 (d) shows a high aspect ratio vertical needle with multiple harmonics. Figure 6.10 (e) shows dual microneedles inclined at an angle of  $65^\circ$ . Figure 6.10 (f) shows how the orientation of the microneedle changes with the change of inclination and exposure dose.

These microstructures have potential uses in different fields of MEMS. For example, the vertical pillar, the inclined pillar, and the triangular slabs can be used as RF MEMS like frequency-selective devices. The microstructures made out of the liquid resin can give sharp tips and several harmonics due to the light propagation profiles through the liquid resin. These sharp needles can be used as microneedles for different kinds of sensing applications like pH sensors, Oxygen sensors for human bodies. These microneedles can also be used for skincare patches.

## **6.7 Summary**

A novel tiltable UV-LED lithography system has been demonstrated. A new approach towards complex 3D microfabrication with simpler optics and 3D printed structures has been shown as a prototype of a  $7 \times 7$  matrix of 405 nm UV-LEDs. The system has been designed as an independent tool for multi-angled lithography exposure along both X and Y axes. This system is

devoid of the complications and limitations of the 3D printing models in terms of warming up, resolution, and expensive tools. The system has been characterized for collimation and controlled tiltable movement. Good collimation was achieved with the 3D printed waveguides and commercial lenses with a deviation of  $\pm 3.6^\circ$ . Adjustable intensity option has been included for making use of a various range of intensities for versatile applications. The highest intensity as shown by the system has been recorded at  $320 \text{ mW/cm}^2$ , which is superior to typical commercial lithography systems. The uniform distribution of intensity was realized by utilizing orbital motion. The system has been shown to be suitable for both solid and liquid states of photoresist exposure. Examples of microfabrication have been shown for vertical and inclined SU8 structures. These microstructures can be applied in the fields of antenna and other RF device fabrications. The liquid resin microstructures show the potentiality to be used as microneedles which is a demanded tool for both skincare and drug delivery approaches. This system shown here only demonstrates a small prototype and the results shown here are only for demonstration purposes and will be improvised further. The findings of this system will be utilized for making an advanced tiltable UV-LED lithography system in the future.

# Chapter 7 - 5G frequency-selective device fabrication utilizing micromachined 3D microstructures<sup>4</sup>

## 7.1 Introduction

RF devices are one of the most versatile applications of MEMS. Frequency selective device (FSD) is a form of RF device that shows the reflectivity or absorption at specific resonant frequencies depending on the parameters. The major application of frequency selective devices include millimeter-wave devices [126], high-power microwave devices [127], devices made for security purposes [128]. Military communication [129] [116], miniaturized communication devices [130]. The traditional frequency-selective devices are typically 2D and the target structures are embedded in nature. This kind of structure lacks the flexibility of parameters and face significant tangent losses because of the conductive surfaces' embedded nature [131] [132].

In the early 2000s, the use of polymer core metal-coated microstructures was proposed by Yoon *et. al.* for RF device applications [133]. It is observed that the current in a metal structure is mainly confined on the outer periphery of the metal conductor due to the skin effect. Therefore, if polymer structures are coated with metal, they can act as conductors and work as RF devices. Using this principle, the application of metalized SU8 microstructures was demonstrated to be working as an RF device. Since these structures are not embedded in the substrate but rather allow air space around them, they were termed as air-lifted microstructures. This air-lifted characteristic improves the quality of the RF device by minimizing the dielectric loss caused by the embedded substrate material, and it also minimizes the coupling effect between the adjacent elements. This novel invention created a wide range of scopes for utilizing polymer-based microstructures. With

---

<sup>4</sup> This chapter is a reformatted and slightly modified version of our article [100]

the evolution of complex 3D microfabrication technology, 3D frequency-selective devices are getting more attention because of the greater flexibility of various parameters and minimum dielectric effects [134], [135]. 3D airlifted polymer pillar arrays have been demonstrated as a successful application for terahertz devices [136], [137]. Application of airlifted structures has also been demonstrated for satellite communication devices [100].

The 5G network is now dominating the industries of mobile and wireless communication. [138], [139]. 5G networks can be used in other emerging fields like energy harvesting, vehicular networks [140], [141]. 5G networks are also considered to have potential uses in the highly sensitive security sectors like military communication networks [142], [143].

This chapter highlights the application of airlifted 3D microstructures in the field of 5G (fifth generation) communication devices. Since 24-30 GHz is the most licensed and deployed 5G spectrum in the world, the 5G devices require a length or height of around 3.12 mm to 2.5 mm. These ultra-tall microstructures need very high intensity which is not available in the existing UV lithography systems. On the other hand, the UV-LED lithography system has demonstrated the ability to fabricate around 3.15 mm tall microstructures so far. Therefore, the multidirectional UV-LED lithography system has been utilized for 5G device fabrication. The 3D microstructures are metalized to be applied as the frequency-selective device.

The 3D frequency-selective devices are used in different signals based on their sizes and shapes. In this chapter, vertical pillar array has been demonstrated for frequency selective device for 5G applications.

## **7.2 Concept of 3D micromachined frequency-selective device**

A periodic array of conductive elements placed on a conductive surface is used as a frequency-selective device (FSD). The FSD either absorbs or reflects the incident signal based on

the parameters of the device. Freestanding periodic structures generally absorb some signal acting as band-stop filters while periodic apertures act like bandpass filters by reflecting certain signals. Here, the application of free-standing 3D microstructures has been demonstrated to show the practical application of the 3D microfabricated structures.

The concept is that the electric currents are stirred up on the periodic elements when an incident plane wave hits the periodic element. In the case of FSD, infinite arrays of the periodic structures are considered. Being illuminated by the plane wave, each unit of the infinite array acts like an RLC circuit. For a planar array of elements, the R, L and C are series-connected. The inductor element and the capacitor element values are a function of the frequency for which the device is targeted. And the resonant frequency is defined by the equation,

$$f = \frac{1}{2\pi\sqrt{LC}} \quad (7.1)$$

The vertical component of the incident EM wave couples with the length of the periodic structure, and the horizontal component of the EM wave couples with the period between the adjacent structures. This interaction is maximally achieved when the length is equivalent to quarter wavelength and the period is equivalent to the half-wavelength corresponding to the target frequency. Frequency selective devices are commonly designed in this way.

Here, the 5G frequency range is targeted for the frequency selective application, and 28 GHz is considered the central frequency. Therefore, the periodic structures are designed in correspondence with 28 GHz. The concept of using the 3D vertical structure as the frequency selective device has been shown in Figure 7.1. Here the transmitted signal hits the vertical pillar, and the pillar absorbs the frequency corresponding to its height and shape and reflects the other frequencies as it. Here, both the pillar and the substrate on which the pillars are standing must be electrically conductive.

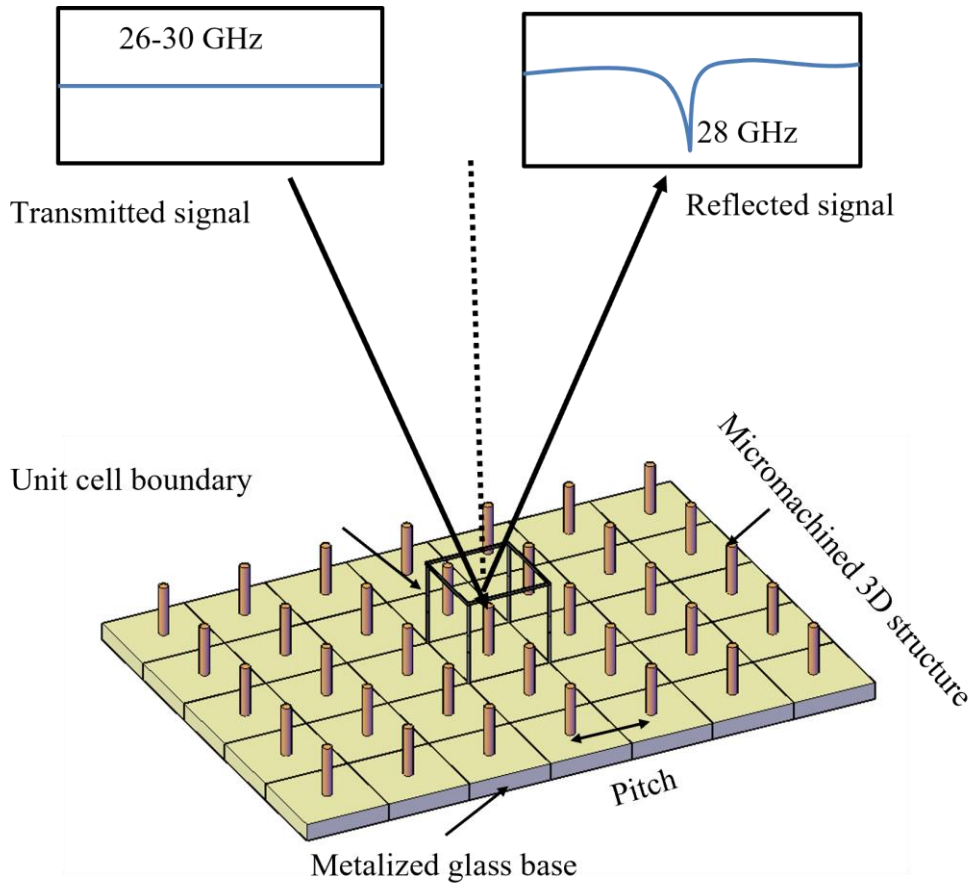


**Figure 7.1** working principle of the micromachined air-lifted 3D frequency-selective device.

The microstructures are designed with a height of one-quarter of the wavelength corresponding to the target frequency. For 28 GHz, the corresponding wavelength is 10.7 mm from the standard frequency and wavelength relationship, and the quarter of the wavelength is 2.675 mm. Therefore, the height of the 3D pillars will be 2.675 mm. The broadband signal propagates to the airlifted pillar array with a specific incident angle. The resonance frequency is also a function of the incident angle since the variation of this angle affects the real-time parameters. The vertical and horizontal electric fields are coupled with the quarter wavelength pillar structure and the half-wavelength pitch of the pillar array, respectively. The change of the incident angle affects the pillar height that results in shifts the resonant frequency.

### 7.3 Design of airlifted 3D microstructure

This study focuses on the design considerations of the frequency-selective 3D microstructure arrays tuned to different frequencies in the range of (24-30 GHz) for 5G applications. An array of high aspect ratio vertical pillars and bowties are represented as the 3D microstructure arrays for frequency-selective devices application. Implementation of polymer core 3D microstructures has been shown in RF MEMS utilizing the multidirectional lithography system [102]. The 3D microstructures need to be electrically conductive for RF application. However, metal microstructure fabrication with microscopic resolution and a high aspect ratio is complicated and expensive. On the other hand, polymer-based microstructures fabrication is time-efficient and cost-effective. If thick enough metal coating is applied corresponding to the target frequency, the metal-coated polymer acts the same way as a solid metal conductive pillar. Figure 7.2 (a) shows the concept of a solid metal pillar, and Figure 7.2 (b) shows the concept of a metal-coated polymer conductive pillar. This kind of de makes the whole process easier as well as the electric field effect increases since the resistance becomes lower due to less amount of metal.

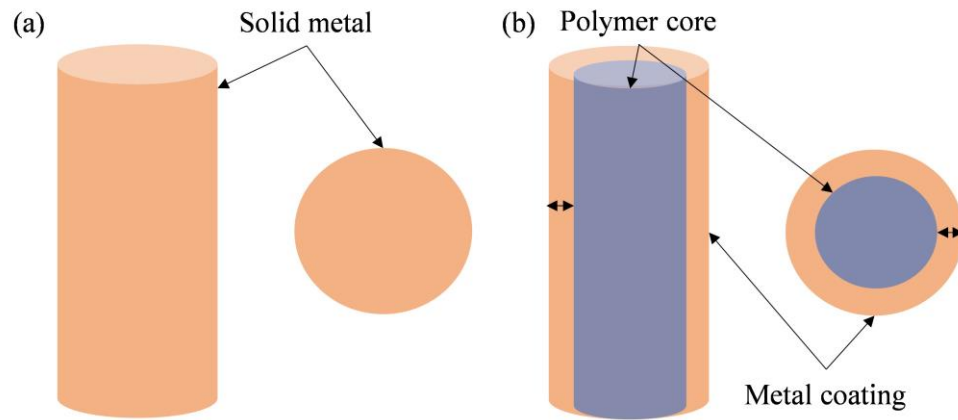


**Figure 7.2** Comparison of solid and metal coated pillars (a) Solid metal pillar, (b) Metal coated polymer pillar.

The image theory has been followed for designing the FSD here. The height of the 3D structure has been chosen to be  $\lambda/4$  which creates a mirror image from the reflection of it from the conductive base. On the other hand, the pitch/period between two adjacent 3D pillars has been decided to be  $\lambda/2$ , to complete the circuit loop. The change of height above  $\lambda/4$  reduces the power radiation and change in the design of the infinite ground affects the radiation pattern. Therefore, maintaining the parameters is important. Figure 7.3 shows the parameters considered for the FSD design.

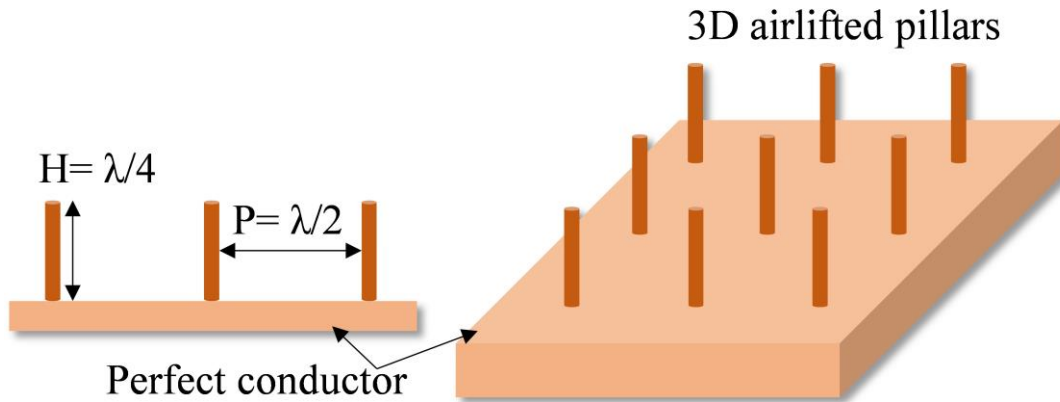


**Figure 7.3** Parameter consideration for 3D vertical pillar designing.

Another essential parameter is the thickness of the metal coating, which needs to be considerably thicker than the skin depth of the metal at the target frequency. The skin depth of any metal can be calculated using the formula-

$$\delta = \sqrt{\frac{\rho}{\pi f_0 \mu_r \mu_0}} \quad (7.2)$$

Where,

$\delta$  = Skin depth

$f_0$  = Corresponding frequency

$\rho$  = Resistivity

$\mu_r$  = Relative permeability

$\mu_0$  = Permeability of free space

Here, Copper has been chosen as the coating metal, and the target frequency for the application is 28 GHz. Therefore, using equation 1, the skin depth of copper at a frequency of 28 GHz is obtained to be 0.390  $\mu\text{m}$ . Now, to make the coating act as a solid metal, the coating thickness should be several times the skin depth. Therefore, the layer deposited by sputtering or electroless plating is not enough. Additional electroplating is required for getting enough metal thickness. After a thick metal layer is deposited on the polymer core pillar, it can function as an airlifted pillar array for FSD application.

#### **7.4 Fabrication method**

The previous chapters discussed the microfabrication with both nonbaked and baked photoresists using UV-LED photolithography. The liquid resin has been used to fabricate the airlifted microstructures considering the ease of fabrication and time efficiency.

The samples used for the microfabrication are micropatterned Chromium glasses. Standard organic cleaning with acetone, methanol, and Isopropanol is performed before fabrication. A resin repelling Teflon film is used on a non-reflecting surface so that the structures do not get stuck on the surface after crosslinking. The desired thickness of the 3D printed frame, which is 2.675 mm in this case, is placed on the Teflon to mark a boundary for the resin. The resin is then directly poured on the Teflon so that the resin reaches the height of the frame. After filling up with the resin, the patterned glass mask is placed on the frame keeping no air gap between the resin and the mask. The four sides of the mask were covered with black tape so that no light can leak through the gaps and crosslink the resin from the sides. Finally, UV light is directly exposed to the sample.

UV light creates harmonics due to diffraction effects inside liquid resin and sharp tips with instant exposures [122]. However, if the thickness is restricted and the sample is exposed for a long time with longer wavelengths, the energy gets distributed sidewise and covers up the harmonics to form cylindrical structures. Figure 7.4 shows the steps involved in the FSD fabrication. Figure 7.4 (a) shows how the resin is placed into the enclosed area of the frame on a Teflon film. Figure 7.4 (b) shows how the structure forms with continuous UV exposure. After the sample is exposed, it is gently flipped, and the Teflon film is peeled off from the surface carefully. After that, the sample is developed in fresh Isopropanol with mild agitation keeping the sample upside down to expedite the development which is shown in Figure 7.4 (c).

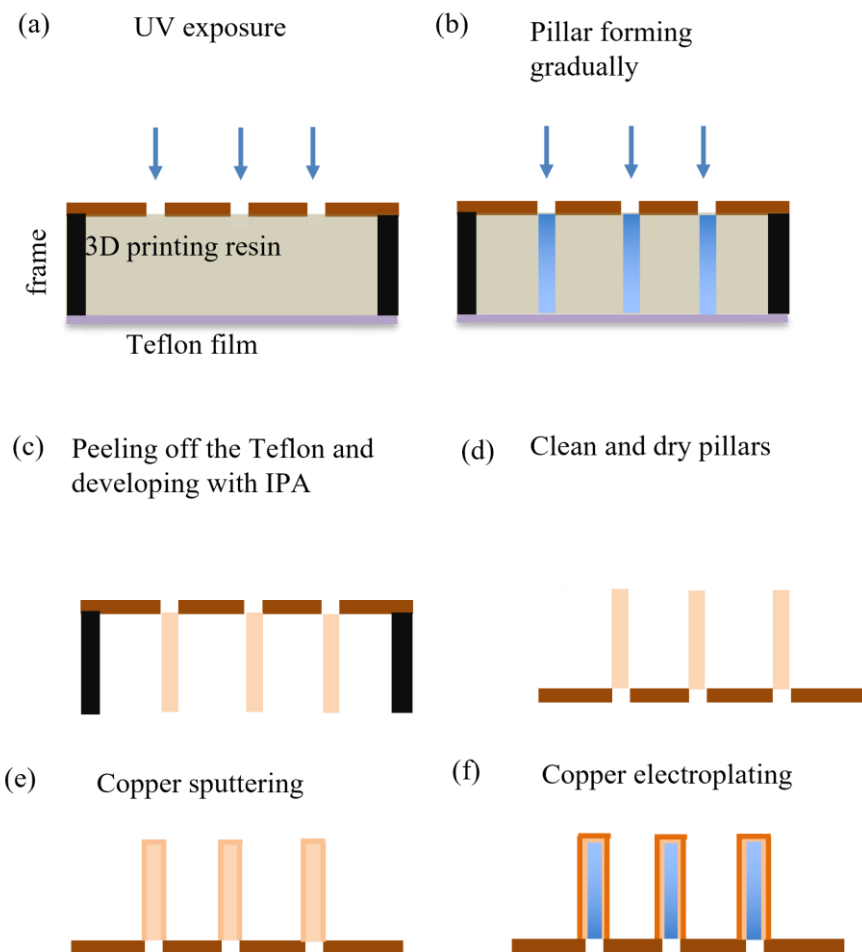


**Figure 7.4** Fabrication procedure of 3D microstructure.

After developing, the frame is removed and cleaned with fresh IPA. Next, the sample is dried and is ready for metallization, as shown in Figure 7.4 (d). For metallization, the sample is first sputtered with Titanium for obtaining good adhesion and then sputtered with copper, as shown in Figure 7.4 (e). Next, the sample is electroplated using Copper Sulphate solution to get the desired metal thickness. After electroplating, the sample is ready for analysis for frequency selective functions, as shown in Figure 7.4 (f).

## **7.5 Characterization**

5G network is the most popular cellular network in the present world. This is called the fifth-generation network for the cellular networks, which came into public use in 2019. The use of this band has spread out in most of the mobile operating networks because of more incredible download speeds and greater bandwidths. The frequency range, which falls between 24-47 GHz, has been considered the 5G frequency range. With the explosion of the 5G networks and the availability of gigabytes per second download speed, most cellular network companies are shifting their networks to 5G. However, from the wide range of frequencies between 24-47 GHz, 24 to 29.5 GHz frequencies have been chosen to be the most licensed frequency range. Therefore, this frequency range was for the frequency-selective devices, and initially, 28 GHz has been targeted. The design and the frequency selective functions are simulated first using HFSS software and later verified using a network analyzer optimized for analysis in the range of 500MHz-40 GHz. The pattern size was chosen for fabrication on a glass substrate by selecting a lithographically possible aspect ratio.

### **7.5.1 HFSS simulation**

The parameters and responses of the frequency selective device have been characterized first by simulating using Ansys HFSS software. HFSS is 3D finite element-based electromagnetic

simulation tool. A frequency-selective device is a device with an infinite array of periodic structures. It is impossible to simulate infinite numbers of elements using simulation software. Therefore, one unit cell was analyzed for frequency-selective devices to check the characteristics and behavior in a specific environment. In this case, a Floquet port simulation has been utilized for the single-cell simulation. A boundary is assigned for the unit cell, and the input signal direction is assigned.

And for getting the simulation for the Floquet port, the following differential equation is used-

$$\frac{d}{dt} \delta x(t) = \frac{\delta f(x,t)}{\delta x} |_{x = x_p} \quad (7.3)$$

$$\delta x(t) = A(t, x_p) \delta x(t) \quad (7.4)$$

Where,  $A(t, x_p) = \frac{\delta f(x,t)}{\delta x} |_{x = x_p}$  is the time varying matrix and is periodic in nature.

This theory when applied to the unit cell of the periodic structure, realizes the function for an infinite area.

For Floquet port analysis, the sweep of the frequency was set from 24 GHz-30 GHz. The target frequency was set to be 28 GHz. And the inclination of the incident angle was assigned from 1 to 10 degrees.

### 7.5.2 VNA analysis

For all these experiments done with vector network analyzer, An Anritsu (37269D) network analyzer has been used which has a frequency range of 400 MHz to 40 GHz range. 5G frequency range is chosen as the target frequency and the network analyzer has been calibrated in the range of 24 to 30 GHz. The  $S_{21}$  parameter represents the power received at port 2 relative to the port 1. Here the ports are represented as the transmitter and the receiver and has been equipped with two identical standard gain horn antennas.

These horns have been designed using the standard parameters and printed with a metal 3D printer. In this case, two standard gain WR-28 horn antennas have been used with a nominal gain of 15 dB [144]. This means each horn antenna has been designed to represent a response at around a value of 15 dB. The practical value of the gain can vary by a value of  $\pm 5$  dB. These standard gain antennas show nominal gains strictly corresponding to their designing parameters with little variations caused by surface roughness and other fabrication error [145], [146], [147]. The transmitter gain is the ability of the transmitting antenna to convert the input power into radio waves in a particular direction. On the other hand, the receiving antenna gain is the ability of the antenna to convert the radio wave coming from a particular direction into electric power. The use of identical transmitter and receiver horn antenna for measuring the transmission loss or  $S_{21}$  was demonstrated in magnetic MEMS reconfigurable frequency selective devices [148], multiband and dual polarized frequency selective devices [149]. The  $S_{21}$  response depends on the gain of the transmitter and the receiver. The mutual coupling between two antennas over an infinite ground plane placed at a separation higher than the far-field distance can be computed by using modified Friis transmission equation and  $S_{21}$  is given by-

$$S_{21}(dB) = G_t(dB) + G_r(dB) - FSPL \quad (7.5)$$

where  $G_t$  is the transmitting antenna gain,  $G_r$  the receiving antenna gain, and FSPL the free space path loss given by

$$FSPL = -27.6 + 20\log D + 20\log F \quad (7.6)$$

where  $D$  is the distance in meter, and  $F$  is the frequency in MHz [150]

Here, the distance between the two antennas is around 0.2 meter and the target frequency is around 28000 MHz. Therefore,  $FSPL = -47.37$

The gain of the antennas is 15 dB. Therefore,  $S_{21} = -17.37$  dB

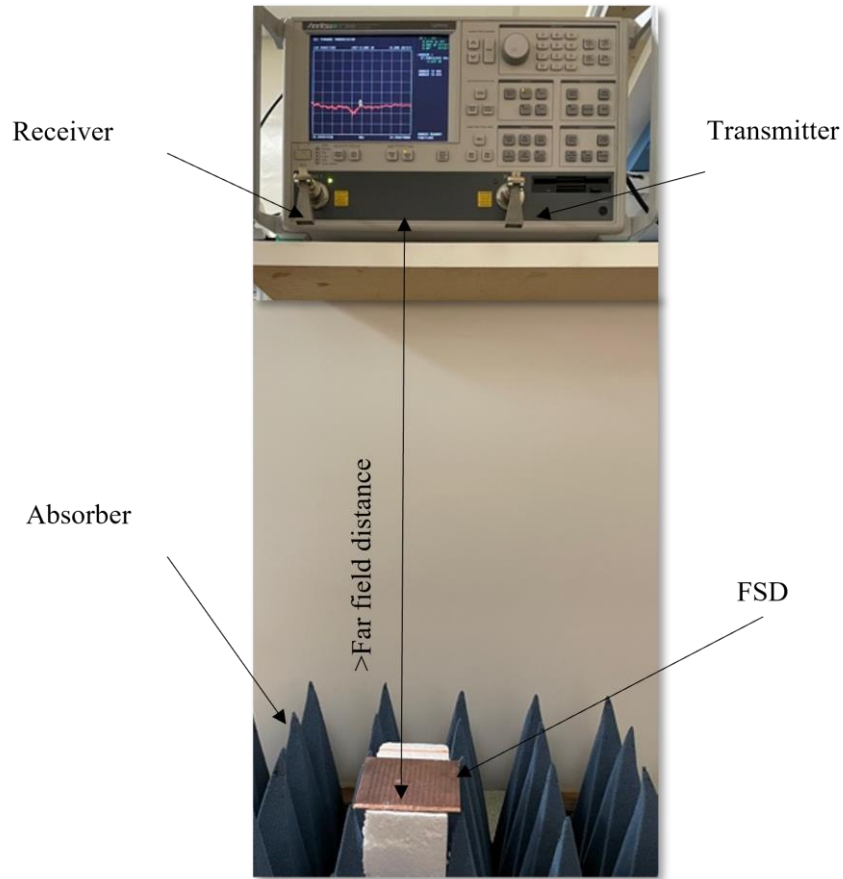


**Figure 7.5** Experimental setup for an FSD resonance testing.

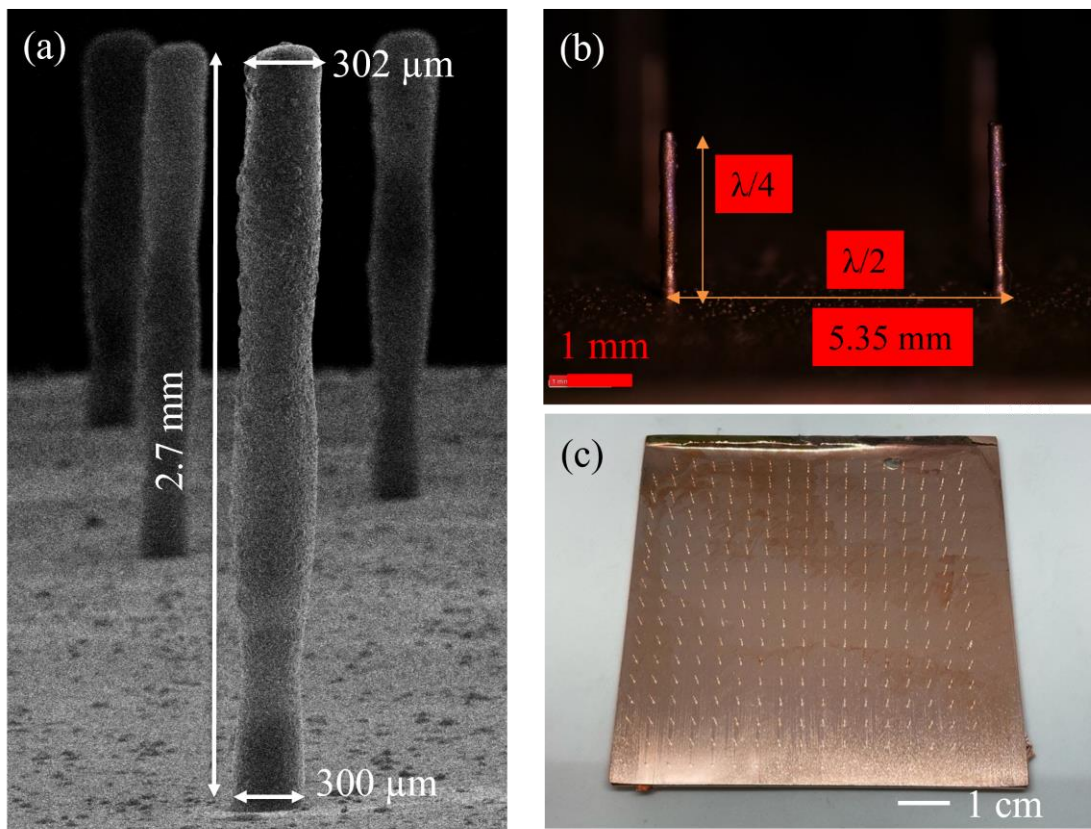
The FSD is placed in between these horn antennas as shown in Figure 7.5 and the signal sent by the transmitter is modified or changed after interacting with the FSD. This modified signal is received by the receiver in the form of the  $S_{21}$  response., therefore, the values demonstrated in the data are standard and limited by the transmitter and receiver capacity.

## 7.6 Results

The primary application of frequency selective devices is in making filters. The vertical micropillar has been demonstrated as the single frequency band-stop filter, the simulation and experimental results have been shown in the following sections.

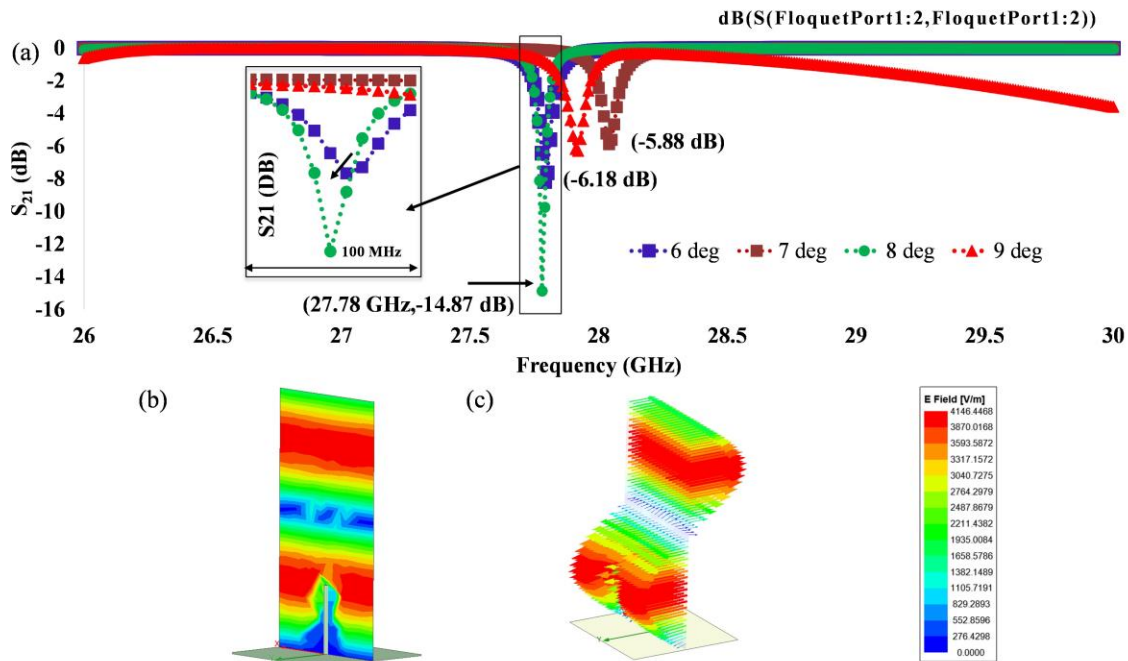
The vertical pillar has been made in a cylindrical shape with a diameter of 200 microns and a height of 2.7 mm giving an aspect ratio of 1:13. Figure 7.6 (a) shows the single unit of the vertical pillar, Figure 7.6 (b) shows two adjacent pillars with quarter-wavelength height and half-wavelength period, Figure 7.6 (c) shows one 4-inch device with arrays of vertical pillars. The floquet port was analyzed for a single unit of the vertical pillar to show the infinite array response.

Figure 7.7 Shows the Floquet port simulation where one unit of a vertical pillar has been taken for analysis. The height is taken to be equal to quarter wavelength and the boundary area is equivalent to half wavelength.



**Figure 7.6** Frequency selective device (a) Unit vertical pillar, (a) two adjacent pillars, (c) 4 -inch device.

The incident EM is directed towards the unit cell from the floquet port assigned on the top of the boundary. Since perpendicular incident wave doesn't give any resonance, the floquet port is simulated with an inclination of several degrees of inclinations. Figure 7.7 (a) shows the  $S_{21}$  parameter of the pillar at a frequency of 27.78 GHz which is slightly lower than the expected 28 GHz resonance. Here, the calculated pillar height corresponding to 28 GHz is 2.675 mm. However, due to some fabrication error, the obtained height is 2.7 mm which gives a resonance at 27.78 GHz. Several resonances are obtained i.e., at 6°, 7°, 8° and 9° incident angles, but the highest  $S_{21}$  response is obtained at 8° inclination and the value is -14.87 dB. The resonance spreads over a width of around 100 MHz, showing a narrow bandwidth filtering response. Figure 7.7 (b) shows the E-field magnitude distribution over a single pillar and Figure 7.7 (c) shows the vector of the E-field over the vertical pillar.



**Figure 7.7** HFSS simulation for the vertical pillar (a) HFSS simulation for a unit vertical pillar cell using Floquet port showing the  $S_{21}$  response, (b) The E-field distribution over the unit pillar, (c) The E-field vector over the vertical pillar.

Figure 7.8 shows the graphical representation of the frequency selective response obtained from the quarter wavelength pillar device. Here, the bandwidth ranging between 26 to 30 GHz has been shown to be sent from the transmitter end of the network analyzer. A plane copper plate was taken as the reference and the signal was normalized for every change for the incident angle. After hitting the pillar device, it gives the most attenuations in the range between 27.75 GHz to 27.85 GHz for incident angles between  $6^\circ$  to  $10^\circ$ . Here, as the incident angle increases from  $6^\circ$  to  $10^\circ$ , the resonant frequency shifts to higher values. At an incident angle of 6 degrees, it gives a resonance at 27.78 GHz corresponding to the pillar height of 2.6975 mm, at 7 degrees and 8 degrees it gives 27.8 GHz corresponding to 2.6957 mm, and at 9 and 10 degrees, it gives 27.82 GHz corresponding to a height of 2.694 mm. The band starts from around 27.75 GHz and ends at around 27.85 GHz giving a span of 100 MHz. The highest  $S_{21}$  value is achieved at 27.8 GHz, which is -16.45 dB. At 27.78 GHz and 27.82 GHz, the  $S_{21}$  achieved are -14.17 dB and -12.71 dB respectively. With some fabrication deviations, the result shows good correspondence with the calculated and the simulated data.

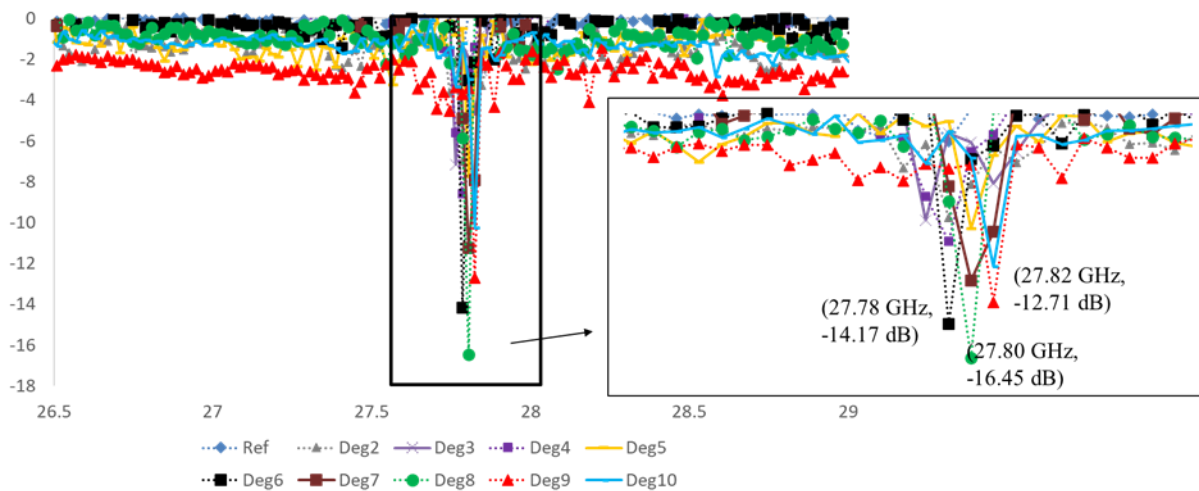


**Figure 7.8** Graph showing the response with the pillar frequency-selective device (inset-magnified view of the resonant frequencies).

**Table 7.1 Comparison between the simulated and the experimental result for the 3D vertical pillar FSD**

Parameters	Simulation	Experimental result
Resonance frequency (GHz)	27.78	27.8
Incident angle	8°	8°
S <sub>21</sub> (dB)	-14.87	-16.45
Bandwidth (MHz)	100	100

Table 7.1 shows the comparison table between the simulated and the experimental data.

Lower values of incidence didn't give any significant attenuations since the transmitted signal interferes with received ones because of the close distance between the transmitter and the receiver and doesn't interact with the pillar. As a result, most signals are reflected as it is. On the other hand, when the incident angle crosses the flare angle of the transmitter itself it doesn't respond to the FSD signal which again doesn't give any significant resonance.

### **7.7 Summary**

3D micromachined air-lifted vertical pillar arrays have been fabricated and characterized as frequency-selective devices in the 5G frequency range. The multidirectional UV-LED lithography system has been used for fabricating the microstructures. This chapter shows a good example of both the high intensity light source as well as liquid state resin microfabrication. The fabrications are both time and cost-effective and have application in the most popular 5G devices. The vertical pillar arrays have been characterized for frequency selective functions at a frequency of around 27.78 GHz with a width of 100 MHz. Where a similar conducting plate without the pillars reflected every frequency that it received. The process can be useful for monopole antenna fabrication, and other satellite communication applications. This study shows the potentiality of a variety of complex microstructures to be used for different MEMS applications

## Chapter 8 - Conclusion

The UV-LED lithography system demonstrated the highest intensity available among the commercially available lithography systems and the research setups available so far by utilizing the single-lens collimation. The 405 nm UV-LED showed an intensity of  $472 \text{ mW/cm}^2$  and the 365 nm UV-LED showed an intensity of  $258 \text{ mW/cm}^2$ . Previously the highest intensity available from a 405 nm UV lithography system was  $90 \text{ mW/cm}^2$  and for a 365 nm, it was around  $50 \text{ mW/cm}^2$ . Therefore, the demonstrated UV-LED lithography system has an intensity that is more than five times that of the available lithography systems and the mask aligners. This high intensity enables the fabrication of the high aspect ratio and tall microstructures which were not possible using the low-intensity lithography systems. Tall microstructures (1 mm or taller) and high aspect ratio microstructures (1:10 or higher) have applications in different applied fields like RF devices and microfluidic devices. High aspect ratio fabrications improve the performance of semiconductor devices by reducing the short channel effects. For RF antennas and filters, a desired height or length of the structures corresponds to a target frequency. Therefore, the physical parameters are important for a required response. Frequency-selective devices in the range of Ku- band, 5G frequency ranges, millimeter-wave ranges require structures with several millimeter heights where the airlifted tall structures help reduce the dielectric losses. In addition to that, the taller structures add up certain designing flexibilities and expand the performance capabilities in microdevices.

The combination of the high intensity and the creation of 3D traces using the tilt-rotational sample holder has added another unique feature of this system that does not exist in commercial lithography systems. The complex 3D structures have applications in cell mimicking devices, frequency, and polarization selective devices (PFSS). Complex 3D microstructures with high aspect ratios have potential uses in RF MEMS like band-specific filters

The programming function enabled this system to create 3D microstructures with one single exposure which is done in several steps or manually with additional customization in the existing lithography systems. There are no commercial systems available for complex 3D microfabrication using lithography. This UV-LED lithography system can create high-resolution patterns as small as 1.4  $\mu\text{m}$ , high aspect ratio microstructure as high as 1:40, millimeter tall microstructure as tall as 3.14 mm, and complex 3D microstructures with small diameters like a flat bowtie, bipod and tripods, circular horn and tapered horn, dual arrow, petal structures.

This research indicates the future direction of the UV-LED lithography system where the light source is made self-tiltable. This method can open up the opportunity for more versatile microfabrication with varieties of photoresists.

A practical implementation of the microstructure using lithography has been shown in the 5G frequency selective device. The parameters and the shapes of the microstructure can be customized for other frequencies as well. Following the similar fabrication method, the microstructures can be applied to other RF devices.

This research has focused on the development of a lithography system utilizing UV-LEDs. While replacing the Hg vapor lamps, this system contributes to alleviating the health hazards involved with Hg lamps and creates an environment-friendly lithography system. The combination of high intensity and multidirectional functions with customized programs enables this system for high resolution, high aspect ratio and complex 3D microfabrication which have potential uses in semiconductor devices, RF MEMS, and biomedical fields.

## Bibliography

- [1] L. Tedeschi, C. Domenici, C. Lande, A. Nannini, G. Pennelli, F. Pieri, S. Severi, “Protein patterning on polycrystalline silicon–germanium via standard UV lithography for bioMEMS applications,” *Mater. Sci. Eng. C*, vol. 30, no. 8, pp. 1221–1226, Oct. 2010.
- [2] G. Shao, "Polymer based microfabrication and its applications in optical MEMS and bioMEMS" (2011). *LSU Doctoral Dissertations*. 2925. Accessed: Nov. 12, 2021. [Online]. Available: [https://digitalcommons.lsu.edu/gradschool\\_dissertations/2925](https://digitalcommons.lsu.edu/gradschool_dissertations/2925).
- [3] V. M. Lubecke, J.-C. Chiao, “MEMS technologies for enabling high frequency communications circuits,” in *4th International Conference on Telecommunications in Modern Satellite, Cable and Broadcasting Services. TELSIKS'99 (Cat. No.99EX365)*, vol. 2, pp. 382–389 vol.2, Oct. 1999
- [4] V. K. Varadan, V. V. Varadan, “Smart electronics and MEMS for aerospace structures,” in *Micromachined Devices and Components*, Sep. 1995, vol. 2642, pp. 166–172. Accessed: Nov. 17, 2021. [Online]. Available: <https://www.spiedigitallibrary.org/conference-proceedings-of-spie/2642/0000/Smart-electronics-and-MEMS-for-aerospace-structures/10.1117/12.221165.full>
- [5] Z. Yang, Y. Zhang, T. Itoh, R. Maeda, “Flexible Implantable Microtemperature Sensor Fabricated on Polymer Capillary by Programmable UV Lithography With Multilayer Alignment for Biomedical Applications,” *J. Microelectromechanical Syst.*, vol. 23, no. 1, pp. 21–29, Feb. 2014.
- [6] M. Chattopadhyay, D. Chowdhury, “Design and performance analysis of MEMS capacitive pressure sensor array for measurement of heart rate,” *Microsyst. Technol.*, vol. 23, no. 9, pp. 4203–4209, Sep. 2017.

- [7] S. Fan, L. Meng, L. Dan, W. Zheng, X. Wang, “Polymer Microelectromechanical System-Integrated Flexible Sensors for Wearable Technologies,” *IEEE Sens. J.*, vol. 19, no. 2, pp. 443–450, Jan. 2019.
- [8] K. Hölz, J. Lietard, M. M. Somoza, “High-Power 365 nm UV LED Mercury Arc Lamp Replacement for Photochemistry and Chemical Photolithography,” *ACS Sustain. Chem. Eng.*, vol. 5, no. 1, pp. 828–834, Jan. 2017.
- [9] H. Jiang, X. Sun, R. Yang, J. Chen, L. Xie, S. Yin, “Design of UV LED illumination system for direct imaging lithography,” *Opt. Eng.*, vol. 58, no. 7, p. 075103, Jul. 2019.
- [10] K. Schindler, U. Leischner, C. Lopper, T. Striebel, P. Kaiser, “High Intensity UV-LED Mask Aligner for Applications in Industrial LED and Hg Lamp Prints Match,” pp. 672–675, 2017.
- [11] “UV-LED light engine for photolithography exposure,” Accessed: Nov 12, 2021. [Online]. Available: [https://idonus.com/downloads/idonus\\_Technical\\_note\\_UV-LED\\_light\\_engine\\_\(2020-12-14\).pdf](https://idonus.com/downloads/idonus_Technical_note_UV-LED_light_engine_(2020-12-14).pdf)
- [12] “New generation of mask aligner: UV-KUB 3,” *KLOE*, Accessed: Nov. 08, 2018. [Online] Available: <https://www.kloe-france.com/en/photolithography-equipment/masking-system/mask-aligner-uv-kub-3>.
- [13] K. Schindler, U. Leischner, C. Lopper, T. Striebel, P. Kaiser, and U. Schoembs, “High Intensity UV-LED Mask Aligner for Applications in Industrial Research,” in *MikroSystemTechnik 2017; Congress*, pp. 1–4, Oct. 2017.
- [14] C. Beuret, G.-A. Racine, J. Gobet, R. Luthier, and N. F. de Rooij, “Microfabrication of 3D multidirectional inclined structures by UV lithography and electroplating,” in *Proceedings*

- IEEE Micro Electro Mechanical Systems An Investigation of Micro Structures, Sensors, Actuators, Machines and Robotic Systems*, Oiso, Japan, pp. 81–85, 1994.
- [15] H. Lorenz, M. Despont, N. Fahrni, N. LaBianca, P. Renaud, and P. Vettiger, “SU-8: a low-cost negative resist for MEMS,” *J. Micromechanics Microengineering*, vol. 7, no. 3, pp. 121–124, Sep. 1997.
- [16] M. Despont, H. Lorenz, N. Fahrni, J. Brugger, P. Renaud, and P. Vettiger, “High-aspect-ratio, ultrathick, negative-tone near-uv photoresist for MEMS applications,” in *Proceedings IEEE The Tenth Annual International Workshop on Micro Electro Mechanical Systems. An Investigation of Micro Structures, Sensors, Actuators, Machines and Robots*, pp. 518–522, Jan. 1997.
- [17] M. Han, Woonseob Lee, Sung-Keun Lee, and S. S. Lee, “Fabrication of 3D microstructures 2003with inclined/rotated UV lithography,” in *The Sixteenth Annual International Conference on Micro Electro Mechanical Systems, 2003. MEMS-03 Kyoto. IEEE*, Kyoto, Japan, pp. 554–557, Jan. 1997.
- [18] Y.-K. Yoon, J.-H. Park, F. Cros, and M. G. Allen, “Integrated vertical screen microfilter system using inclined SU-8 structures,” in *IEEE The Sixteenth Annual International Conference on Micro Electro Mechanical Systems, 2003. MEMS-03 Kyoto*, pp. 227–230, Jan. 2003.
- [19] Y.- Yoon, J.- Park, and M. G. Allen, “Multidirectional UV Lithography for Complex 3-D MEMS Structures,” *J. Microelectromechanical Syst.*, vol. 15, no. 5, pp. 1121–1130, Oct. 2006.

- [20] J. Kim, M. Allen, and Y.-K. Yoon, "Computer-controlled dynamic mode multidirectional UV lithography for 3D microfabrication," *J Micromech Microeng J Micromech Microeng*, vol. 21, pp. 215–35003, Mar. 2011.
- [21] J. Kim, Y.-K. Yoon, and M. G. Allen, "Computer numerical control (CNC) lithography: light-motion synchronized UV-LED lithography for 3D microfabrication," *J. Micromechanics Microengineering*, vol. 26, no. 3, p. 035003, Jan. 2016.
- [22] "Mercury | NIOSH | CDC," Dec. 03, 2020. Accessed: Feb. 24, 2022. [Online]. Available: <https://www.cdc.gov/niosh/topics/mercury/default.html>.
- [23] "Argon (Ar) - Chemical properties, Health and Environmental effects." Accessed Feb. 24, 2022. [Online]. Available: <https://www.lenntech.com/periodic/elements/ar.htm>.
- [24] "SU-82000DataSheet2000\_5thru2015Ver4-2.pdf." Accessed: Jun. 22, 2021. [Online]. Available: [https://kayakuam.com/wp-content/uploads/2019/09/SU-82000DataSheet2000\\_5thru2015Ver4-2.pdf](https://kayakuam.com/wp-content/uploads/2019/09/SU-82000DataSheet2000_5thru2015Ver4-2.pdf)
- [25] J. Zhang, K. L. Tan, G. D. Hong, L. J. Yang, and H. Q. Gong, "Polymerization optimization of SU-8 photoresist and its applications in microfluidic systems and MEMS," *J. Micromech. Microeng.*, vol. 11, no. 1, pp. 20–26, Nov. 2000.
- [26] J. N. Patel, B. Kaminska, B. L. Gray, and B. D. Gates, "PDMS as a sacrificial substrate for SU-8-based biomedical and microfluidic applications," *J. Micromech. Microeng.*, vol. 18, no. 9, p. 095028, Aug. 2008.
- [27] M. Agarwal, R. A. Gunasekaran, P. Coane, and K. Varahramyan, "Scum-free patterning of SU-8 resist for electroforming applications," *J. Micromech. Microeng.*, vol. 15, no. 1, pp. 130–135, Oct. 2004.

- [28] H. Yu, O. Balogun, B. Li, T. W. Murray, and X. Zhang, "Fabrication of three-dimensional microstructures based on singled-layered SU-8 for lab-on-chip applications," *Sens. Actuators Phys.*, vol. 127, no. 2, pp. 228–234, Mar. 2006.
- [29] C.-H. Lin, G.-B. Lee, B.-W. Chang, and G.-L. Chang, "A new fabrication process for ultra-thick microfluidic microstructures utilizing SU-8 photoresist," *J. Micromech. Microeng.*, vol. 12, no. 5, pp. 590–597, Jun. 2002.
- [30] L. Dhakar, F. E. H. Tay, and C. Lee, "Development of a Broadband Triboelectric Energy Harvester With SU-8 Micropillars," *J. Microelectromechanical Syst.*, vol. 24, no. 1, pp. 91–99, Feb. 2015.
- [31] J. K. Kim, F. Herrault, X. Yu, M. Kim, R. H. Shafer, and M. G. Allen, "Microfabrication of air core power inductors with metal-encapsulated polymer vias," *J. Micromech. Microeng.*, vol. 23, no. 3, p. 035006, Jan. 2013.
- [32] D. V. Harburg, G. R. Khan, F. Herrault, J. Kim, C. G. Levey, and C. R. Sullivan, "On-chip RF power inductors with nanogranular magnetic cores using prism-assisted UV-LED lithography," in *2013 Transducers Eurosensors XXVII: The 17th International Conference on Solid-State Sensors, Actuators and Microsystems (TRANSDUCERS EUROSENSORS XXVII)*, pp. 701–704, Jun. 2013.
- [33] J. K. Kim, H. Al Thuwaini, and M. Almuslem, "Photolithography of SU-8 microtowers for a 100-turn, 3-D toroidal microinductor," *Micro Nano Syst. Lett.*, vol. 6, no. 1, p. 14, Dec. 2018.
- [34] R. Yang and W. Wang, "A numerical and experimental study on gap compensation and wavelength selection in UV-lithography of ultra-high aspect ratio SU-8 microstructures," *Sens. Actuators B Chem.*, vol. 110, no. 2, pp. 279–288, Oct. 2005.

- [35] J. K. Kim, H. Al Thuwaini, and M. Almuslem, "H-Line Transparency Analysis of Microlithography for Millimeter Scale High-Aspect Ratio SU-8 Structures," in *2019 IEEE 32nd International Conference on Micro Electro Mechanical Systems (MEMS)*, pp. 354–357, Jan. 2019.
- [36] S. Cargou, "SU-8 photolithography : UV sources," *Elveflow*, Dec. 2020, Accessed: Nov. 13, 2021. [Online]. Available: <https://www.elveflow.com/microfluidic-reviews/soft-lithography-microfabrication/su-8-photolithography-uv-sources/>
- [37] "UV LED Technology and Its Advantages," *OCIRTech*. Accessed Nov. 13, 2021. [Online]. Available: <https://www.ocirtech.com/advantages-of-uv-led-technology>.
- [38] H. Misawa and S. Juodkazis, "*3D Laser Microfabrication: Principles and Applications*." John Wiley & Sons, 2006.
- [39] T. Zandrini, O. Shan, V. Parodi, G. Cerullo, M. T. Raimondi, and R. Osellame, "Multi-foci laser microfabrication of 3D polymeric scaffolds for stem cell expansion in regenerative medicine," *Sci. Rep.*, vol. 9, no. 1, p. 11761, Aug. 2019.
- [40] R. Gauvin *et al.*, "Microfabrication of complex porous tissue engineering scaffolds using 3D projection stereolithography," *Biomaterials*, vol. 33, no. 15, pp. 3824–3834, May 2012.
- [41] D. M. Zuev, A. K. Nguyen, V. I. Putlyaev, and R. J. Narayan, "3D printing and bioprinting using multiphoton lithography," *Bioprinting*, vol. 20, p. e00090, Dec. 2020.
- [42] B. Buchroithner *et al.*, "3D multiphoton lithography using biocompatible polymers with specific mechanical properties," *Nanoscale Adv.*, vol. 2, no. 6, pp. 2422–2428, 2020.
- [43] C. Beuret, G.-A. Racine, J. Gobet, R. Luthier, and N. F. de Rooij, "Microfabrication of 3D multidirectional inclined structures by UV lithography and electroplating," in *Proceedings*

- IEEE Micro Electro Mechanical Systems An Investigation of Micro Structures, Sensors, Actuators, Machines and Robotic Systems*, Oiso, Japan, pp. 81–85, 1994.
- [44] Y.-K. Yoon, J.-H. Park, and M. G. Allen, “Multidirectional UV Lithography for Complex 3-D MEMS Structures,” *J. Microelectromechanical Syst.*, vol. 15, no. 5, pp. 1121–1130, Oct. 2006.
- [45] J-W Huang "The illumination design of UV LED array for lithography", Proc. SPIE 10587, Optical Microlithography XXXI, 105870Z, Mar. 20, 2018.
- [46] M. K. Yapici and I. Farhat, “UV-LED exposure system for low-cost photolithography,” *Opt. Microlithogr. XXVII*, vol. 9052, no. February 2014, p. 90521T, 2014.
- [47] Z. Zhang, R. Zhou, D. P. Brames, and C. Wang, “A Low-Cost Fabrication System for Manufacturing Soft-Lithography Microfluidic Master Molds,” *Micro Nanosyst.*, vol. 7, no. 1, pp. 4–12, Feb. 2015.
- [48] P. K. Challa, T. Kartanas, J. Charmet, and T. P. J. Knowles, “Microfluidic devices fabricated using fast wafer-scale LED-lithography patterning,” *Biomicrofluidics*, vol. 11, no. 1, p. 014113, Jan. 2017.
- [49] Y. Li *et al.*, “Rapid fabrication of microfluidic chips based on the simplest LED lithography,” *J. Micromech. Microeng.*, vol. 25, no. 5, p. 055020, Apr. 2015.
- [50] C. Y. Bing, A. A. Mohanan, T. Saha, R. Nagasundara Ramanan, R. Parthiban, and N. Ramakrishnan, “Microfabrication of surface acoustic wave device using UV LED photolithography technique,” *Microelectron. Eng.*, vol. 122, pp. 9–12, Jun. 2014.
- [51] S. Suzuki and Y. Matsumoto, “Lithography with UV-LED array for curved surface structure,” *Microsyst. Technol.*, vol. 14, no. 9–11, pp. 1291–1297, Oct. 2008.

- [52] H. Takahashi, I. Shimoyama, and Y. Jung Heo, “Development of a light source with a uniform intensity reinforced by a checkerboard half-mirror positioned within inverse L-shaped UV-LED arrays,” *Appl. Phys. Express*, vol. 11, no. 6, 2018.
- [53] M. Paster, T. Weichelt, “New Illumination Technology for Mask Aligner Lithography,” vol. 13, Jun. 2018.
- [54] “UV-LED light engine for photolithography exposure,” Accessed: Nov 12, 2021. [Online]. Available: [https://idonus.com/downloads/idonus\\_Technical\\_note\\_UV-LED\\_light\\_engine\\_\(2020-12-14\).pdf](https://idonus.com/downloads/idonus_Technical_note_UV-LED_light_engine_(2020-12-14).pdf).
- [55] J. Ernasconi, T. Charf, U. Ogler, and H. Erzig, “High-power modular LED-based illumination systems for mask-aligner lithography,” vol. 26, no. 9, pp. 11503–11512, Apr. 2018.
- [56] B. G. Crowther, D. G. Koch, J. M. Kunick, J. P. M. Jr, R. Harned, and R. A. Gontin, “A fly’s eye condenser system for uniform illumination,” in *International Optical Design Conference 2002*, vol. 4832, pp. 302–310. Dec. 2002.
- [57] M. Erickstad, E. Gutierrez, and A. Groisman, “A low-cost low-maintenance ultraviolet lithography light source based on light-emitting diodes,” *Lab. Chip*, vol. 15, no. 1, pp. 57–61, 2015.
- [58] J. Kim and Y.-K. Yoon, “Fabrication of three-dimensional millimeter-height structures using direct ultraviolet lithography on liquid-state photoresist for simple and fast manufacturing,” *J. MicroNanolithography MEMS MOEMS*, vol. 14, no. 3, p. 033504, Jul. 2015.

- [59] J. K. Kim, H. Al Thuwaini, and M. Almuslem, “Photolithography of SU-8 microtowers for a 100-turn, 3-D toroidal microinductor,” *Micro Nano Syst. Lett.*, vol. 6, no. 1, p. 14, Dec. 2018.
- [60] “ECE6450L7-Optical Lithography.pdf.” Accessed: Mar. 02, 2022. [Online]. Available: <https://alan.ece.gatech.edu/ECE6450/Lectures/ECE6450L7-Optical%20Lithography.pdf>
- [61] “5.pdf.” Accessed: Mar. 02, 2022. [Online]. Available: <http://www.cityu.edu.hk/phy/appkchu/AP6120/5.PDF>
- [62] S. F. Shiba, J. Y. Tan, and J. Kim, “Multidirectional UV-LED lithography using an array of high-intensity UV-LEDs and tilt-rotational sample holder for 3-D microfabrication,” *Micro Nano Syst. Lett.*, vol. 8, no. 1, p. 5, Apr. 2020.
- [63] L. P. Lee, S. A. Berger, D. Liepmann, and L. Pruitt, “High aspect ratio polymer microstructures and cantilevers for bioMEMS using low energy ion beam and photolithography,” *Sens. Actuators Phys.*, vol. 71, no. 1, pp. 144–149, Nov. 1998.
- [64] R. Yang, D. L. Feedback, and W. Wang, “Microfabrication and test of a three-dimensional polymer hydro-focusing unit for flow cytometry applications,” *Sens. Actuators Phys.*, vol. 118, no. 2, pp. 259–267, Feb. 2005.
- [65] C. Kim, “Integrated microwave antennas and passive filters using 3D microfabrication and metamaterial architectures,” Ph.D., University of Florida, United States -- Florida. Accessed: Nov. 21, 2021. [Online]. Available: <https://www.proquest.com/docview/1727121293/abstract/7583789E6EDC4F3APQ/1>
- [66] R. Yang, S. A. Soper, and W. Wang, “Microfabrication of pre-aligned fiber bundle couplers using ultraviolet lithography of SU-8,” *Sens. Actuators Phys.*, vol. 127, no. 1, pp. 123–130, Feb. 2006.

- [67] A. Bertsch, H. Lorenz, and P. Renaud, "Combining microstereolithography and thick resist UV lithography for 3D microfabrication," in *Proceedings MEMS 98. IEEE. Eleventh Annual International Workshop on Micro Electro Mechanical Systems. An Investigation of Micro Structures, Sensors, Actuators, Machines and Systems (Cat. No.98CH36176*, pp. 18–23, Jan. 1998.
- [68] S. Maruo and K. Ikuta, "Three-dimensional microfabrication by use of single-photon-absorbed polymerization," *Appl. Phys. Lett.*, vol. 76, no. 19, pp. 2656–2658, May 2000.
- [69] S. Maruo and S. Kawata, "Two-photon-absorbed near-infrared photopolymerization for three-dimensional microfabrication," *J. Microelectromechanical Syst.*, vol. 7, no. 4, pp. 411–415, Dec. 1998.
- [70] S. Maruo and K. Ikuta, "Fabrication of freely movable microstructures by using two-photon three-dimensional microfabrication," in *Micro- and Nano-photonic Materials and Devices*, vol. 3937, pp. 106–112, Apr. 2000.
- [71] J. B. Hutchison *et al.*, "Robust polymer microfluidic device fabrication via contact liquid photolithographic polymerization (CLiPP)," *Lab. Chip*, vol. 4, no. 6, p. 658, Dec. 2004.
- [72] Y. Hirai, Y. Inamoto, K. Sugano, T. Tsuchiya, and O. Tabata, "Moving mask UV lithography for three-dimensional structuring," *J. Micromechanics Microengineering*, vol. 17, no. 2, pp. 199–206, Dec. 2006.
- [73] P. Gandhi and K. Bhole, "3D Microfabrication Using Bulk Lithography," pp. 393–399, Aug. 2012.
- [74] K. Ikuta, K. Hirowatari, "Real three dimensional micro fabrication using stereo lithography and metal molding," in *[1993] Proceedings IEEE Micro Electro Mechanical Systems*, pp. 42–47, Aug. 1993.

- [75] Y. Zhang, Y. Fu, H. Wang, H. Li, S. Pan, and Y. Du, "High resolution integral imaging display by using a microstructure array," *J. Opt. Technol.*, vol. 86, no. 2, pp. 100–104, Feb. 2019.
- [76] G. Jiang, S. Baig, and M. R. Wang, "Prism-assisted inclined UV lithography for 3D microstructure fabrication," *J. Micromechanics Microengineering*, vol. 22, no. 8, p. 085022, Aug. 2012.
- [77] M. C. Peterman, P. Huie, D. M. Bloom, and H. A. Fishman, "Building thick photoresist structures from the bottom up," *J. Micromechanics Microengineering*, vol. 13, no. 3, pp. 380–382, May 2003.
- [78] K. Nakamura, H. Kubota, A. Nakada, T. Inokuchi, and K. Kosaka, "Development of reticle-free exposure method with LCD projection image," vol. 4754, p. 737, Jul. 2002.
- [79] Wenguang Yang, Haibo Yu, Y. Wang, and L. Liu, "Fabrication of microstructures using the DMD-based modulating projection printing method," in *10th IEEE International Conference on Nano/Micro Engineered and Molecular Systems*, pp. 625–629, Apr. 2015.
- [80] M. Han, Woonseob Lee, Sung-Keun Lee, S. S. Lee, "Fabrication of 3D microstructures with inclined/rotated UV lithography," in *The Sixteenth Annual International Conference on Micro Electro Mechanical Systems, 2003. MEMS-03 Kyoto. IEEE*, pp. 554–557, Jan. 2003.
- [81] J. K. Kim, M. G. Allen, and Y.-K. Yoon, "Computer-controlled dynamic mode multidirectional UV lithography for 3D microfabrication," *J. Micromechanics Microengineering*, vol. 21, no. 3, p. 035003, Mar. 2011.
- [82] J. K. Kim, "Advanced Multidirectional UV Lithography for Three Dimensional (3-D) Micro- / Nano Structures," State University of New York at Buffalo, 2010. Accessed: Sep. 2021. [Online]. Available:

<https://www.proquest.com/openview/72c90b0d803f038089718f319a57ab33/1?pq-origsite=gscholar&cbl=18750>

- [83] J. Kim, T.-S. Yun, H. Jee, and Y. K. Yoon, “Adjustable Refractive Index Method for Complex Microstructures by Automated Dynamic Mode Multidirectional UV Lithography,” in *2009 IEEE 22nd International Conference on Micro Electro Mechanical Systems*, pp. 733–736, Jan. 2009.
- [84] J.K. Kim, H. A. Thuwaini, and M. Almuslem, “Photolithography of SU-8 microtowers for a 100-turn, 3-D toroidal microinductor,” *Micro Nano Syst. Lett.*, vol. 6, no. 1, p. 14, Dec. 2018.
- [85] J. Kim, Y.-K. Yoon, and M. G. Allen, “Computer numerical control (CNC) lithography: light-motion synchronized UV-LED lithography for 3D microfabrication,” *J. Micromechanics Microengineering*, vol. 26, no. 3, p. 035003, Mar. 2016.
- [86] S. F. Shiba, H. Jeon, J.-S. Kim, J.-E. Kim, and J. Kim, “3D Microlithography Using an Integrated System of 5-mm UV-LEDs with a Tilt-Rotational Sample Holder,” *Micromachines*, vol. 11, no. 2, Art. no. 2, Feb. 2020.
- [87] S. F. Shiba *et al.*, “UV-LED Lithography System and Characterization,” in *2020 IEEE 15th International Conference on Nano/Micro Engineered and Molecular System (NEMS)*, pp. 73–76, Sep. 2020.
- [88] J. K. Kim, S. J. Paik, M. G. Allen, and F. Herrault, “UV-LED LITHOGRAPHY FOR 3-D HIGH ASPECT RATIO MICROSTRUCTURE PATTERNING,” in *2012 Solid-State, Actuators, and Microsystems Workshop Technical Digest*, Hilton Head, South Carolina, USA, pp. 481–484, May 2012.

- [89] Q. L. Pham, N. Tong, A. Mathew, S. Basuray, R. S. Vonorov “A compact low-cost low-maintenance open architecture mask aligner for fabrication of multilayer microfluidics devices.” Jul. 2018.
- [90] C.-K. Huang and J.-G. Sung, “The Application of UV-LEDs to Microlithography,” Jun. 2009, pp. 579–582. doi: 10.1115/MicroNano2008-70055.
- [91] “UV LED Exposure System.” Accessed: Jul. 01, 2021. [Online]. Available: <https://www.idonus.com/products-sub/uv-exposure-system.html>.
- [92] “NXQ200 UV-LED Flood Exposure System,” *Neutronix Quintel*." Accessed: Nov. 15, 2021. [Online]. Available: <http://neutronixinc.com/products/mask-aligner-products/nxq200-uv-led-flood-exposure-system/>.
- [93] H. L. Thanh, B. Q. Ta, H. L. The, V. Nguyen, K. Wang, and F. Karlsen, “Low-Cost Fabrication of Hollow Microneedle Arrays Using CNC Machining and UV Lithography,” *J. Microelectromechanical Syst.*, vol. 24, no. 5, pp. 1583–1593, Oct. 2015.
- [94] J. Kim, Y.-K. Yoon, and M. G. Allen, “Double-side exposure UV-LED CNC lithography for fine 3D microfabrication,” in *2017 IEEE 12th International Conference on Nano/Micro Engineered and Molecular Systems (NEMS)*, pp. 463–466, Apr. 2017.
- [95] K. K. Sadasivuni, M. Mohiuddin, X. Gao, A. Akther, S. Mun, and J. Kim, “Cellulose/PDMS hybrid material for actuating lens,” in *Nanosensors, Biosensors, and Info-Tech Sensors and Systems 2015*, vol. 9434, pp. 97–102, Apr. 2015.
- [96] N. Riehle *et al.*, “Influence of PDMS molecular weight on transparency and mechanical properties of soft polysiloxane-urea-elastomers for intraocular lens application,” *Eur. Polym. J.*, vol. 101, pp. 190–201, Apr. 2018.

- [97] J. Y. Tan, G. Goh, and J. Kim, “Microfabrication of Microlens by Timed-Development-and-Thermal-Reflow (TDTR) Process for Projection Lithography,” *Micromachines*, vol. 11, no. 3, Art. no. 3, Mar. 2020.
- [98] S. Natarajan, D. A. Chang-Yen, and B. K. Gale, “Large-area, high-aspect-ratio SU-8 molds for the fabrication of PDMS microfluidic devices,” *J. Micromechanics Microengineering*, vol. 18, no. 4, p. 045021, Apr. 2008.
- [99] K. Rajasekaran, H. D. Bae, S. Bergbreiter, and M. Yu, “3D Printed Bio-Inspired Hair Sensor for Directional Airflow Sensing,” in *2020 IEEE/RSJ International Conference on Intelligent Robots and Systems (IROS)*, Las Vegas, NV, USA, pp. 8945–8950, Oct. 2020.
- [100] S. F. Shiba, J. Y. Tan, C. Kim, S. J. Kim, and J. Kim, “Ku-Band Frequency Selective 3D Vertical Pillar Array,” in *2021 21st International Conference on Solid-State Sensors, Actuators and Microsystems (Transducers)*, pp. 1383–1386, Jun. 2021.
- [101] “3D Microfabrication of high-precision structures for material engineering | Nanoscribe.” Accessed: Feb. 01, 2022. [Online]. Available: <https://www.nanoscribe.com/en/applications/3d-microfabrication-of-high-precision-structures-for-material-engineering>.
- [102] S. F. Shiba, H. Jeon, J.-S. Kim, J.-E. Kim, and J. Kim, “Development of Programmable UV-LED Microlithography System for 3D Microfabrication,” *J. Microelectromechanical Syst.*, pp. 1–9, 2021.
- [103] Q. L. Pham, N. a. N. Tong, A. Mathew, S. Basuray, and R. S. Voronov, “A compact low-cost low-maintenance open architecture mask aligner for fabrication of multilayer microfluidics devices,” *Biomicrofluidics*, vol. 12, no. 4, p. 044119, Jul. 2018.

- [104] M. K. Yapici and I. Farhat, "UV-LED exposure system for low-cost photolithography," in *Optical Microlithography XXVII*, vol. 9052, pp. 523–529, Mar. 2014.
- [105] "MIDAS SYSTEM CO.,LTD.," Accessed Nov. 15, 2021. [Online]. Available: <http://www.midas-system.com>.
- [106] SPS-Europe, "4" UV Exposure System (Manual)," *www.sps-europe.com*. Accessed Nov. 15, 2021. [Online]. Available: <https://www.sps-europe.com/order/4quot-uv-exposure-system-manual/17763/>.
- [107] "UV-LED masking system: UV-KUB 2," *KLOE*, Nov. 08, 2018. Accessed: Nov. 21, 2021. [Online]. Available: <https://www.kloe-france.com/en/photolithography-equipment/masking-system/masker-uv-kub-2>
- [108] J.-W. Huang, "Design and fabrication of UVLED array aligner for proximity and soft contact exposure," in *Optical Microlithography XXXIII*, vol. 11327, pp. 256–266, Mar. 2020.
- [109] "Mask Aligner and Exposure Station." Accessed: Nov. 15, 2021. [Online]. Available: <https://www.memphis.edu/imc/materials-science/mask-aligner.php>.
- [110] "UV-EXP series of photolithography exposure systems," p. 9.
- [111] E. D. Kurniawan, M. Riswan, M. S. A. Al Ba'id, P. L. Gareso, and R. V. Manurung, "Development of Uniform Ultraviolet Light Source using Light-Emitting Diode (LED) Array for Photolithography System with Controllable Exposure Dose and Duration," in *2019 International Conference on Radar, Antenna, Microwave, Electronics, and Telecommunications (ICRAMET)*, pp. 84–88, Oct. 2019.

- [112] “Mask Aligner MA300 Gen2 | SUSS MicroTec | Production Tool.”, Accessed Nov. 15, 2021. [Online]. Available: <https://www.suss.com/en/products-solutions/mask-aligner/ma300-gen2>.
- [113] S. F. Shiba, K. Wang, and J. J. Kim, “Tilttable UV-LED Lithography for 3D Microfabrication,” in *2021 21st International Conference on Solid-State Sensors, Actuators and Microsystems (Transducers)*, pp. 517–520, Jun. 2021.
- [114] J. Y. Tan, A. Kim, and J. J. Kim, “Fabrication and Characterization of Hollow Microneedle Array Using Diffraction UV Lithography,” in *2021 21st International Conference on Solid-State Sensors, Actuators and Microsystems (Transducers)*, pp. 1150–1153, Jun. 2021.
- [115] J. Y. Tan, A. Kim, and J.K. Kim, “Modeling, characterization, and fabrication of bell-tip microneedle array by diffraction and self-aligned lens effects,” *Appl. Phys. Lett.*, vol. 119, p. 023501, Jul. 2021.
- [116] “surgical\_guide\_technical\_data\_sheet\_en.pdf.” Accessed: Nov. 14, 2021. [Online]. Available: [https://formlabs-media.formlabs.com/datasheets/surgical\\_guide\\_technical\\_data\\_sheet\\_en.pdf](https://formlabs-media.formlabs.com/datasheets/surgical_guide_technical_data_sheet_en.pdf)
- [117] J. S. Kochhar, W. J. Goh, S. Y. Chan, and L. Kang, “A simple method of microneedle array fabrication for transdermal drug delivery,” *Drug Dev. Ind. Pharm.*, vol. 39, no. 2, pp. 299–309, Feb. 2013.
- [118] T. Sugimito and H. Takahashi, “Multidirectional UV lithography via inclined/rotated mirrors for liquid materials,” *Appl. Phys. Express*, vol. 13, no. 7, p. 076502, Jun. 2020.

- [119] G. Jiang, S. Baig, and M. R. Wang, “Prism-assisted inclined UV lithography for 3D microstructure fabrication,” *J. Micromechanics Microengineering*, vol. 22, no. 8, p. 085022, Jul. 2012.
- [120] H. Takahashi, Y. J. Heo, and I. Shimoyama, “Scalable Fabrication of PEGDA Microneedles Using UV Exposure via a Rotating Prism,” *J. Microelectromechanical Syst.*, vol. 26, no. 5, pp. 990–992, Oct. 2017.
- [121] J. Kim and Y.-K. Yoon, “Fabrication of three-dimensional millimeter-height structures using direct ultraviolet lithography on liquid-state photoresist for simple and fast manufacturing,” *J. MicroNanolithography MEMS MOEMS*, vol. 14, no. 3, p. 033504, Jul. 2015.
- [122] J. Y. Tan, M. Ahn, H. Al-Thuwaini, S.-O. Choi, and J. J. K. Kim, “Diffraction Lithography for 3-D Microneedle Fabrication,” in *2020 IEEE 33rd International Conference on Micro Electro Mechanical Systems (MEMS)*, pp. 921–924, Jan. 2020.
- [123] J. Hansson, H. Yasuga, T. Haraldsson, and W. van der Wijngaart, “Synthetic microfluidic paper: high surface area and high porosity polymer micropillar arrays,” *Lab. Chip*, vol. 16, no. 2, pp. 298–304, 2016.
- [124] J. Kim, X. Cheng, H. Ahn, D. S. Elles, and Y. Yoon, “Lithographically defined integrable air-lifted bow-tie antennas,” in *2010 IEEE 23rd International Conference on Micro Electro Mechanical Systems (MEMS)*, pp. 791–794, Jan. 2010.
- [125] J. Y. Tan, M. Ahn, H. Al-Thuwaini, S.-O. Choi, and J. J. K. Kim, “Diffraction Lithography for 3-D Microneedle Fabrication,” in *2020 IEEE 33rd International Conference on Micro Electro Mechanical Systems (MEMS)*, pp. 921–924, Jan. 2020.

- [126] W. Mohyuddin, D. S. Woo, H. C. Choi, and K. W. Kim, "A practical double-sided frequency selective surface for millimeter-wave applications," *Rev. Sci. Instrum.*, vol. 89, no. 2, p. 024703, Feb. 2018.
- [127] J. H. Barton, C. R. Garcia, E. A. Berry, R. G. May, D. T. Gray, and R. C. Rumpf, "All-Dielectric Frequency Selective Surface for High Power Microwaves," *IEEE Trans. Antennas Propag.*, vol. 62, no. 7, pp. 3652–3656, Jul. 2014.
- [128] U. Rafique, S. Ali, M. Afzal, and M. Abdin, "Bandstop Filter Design for GSM Shielding Using Frequency Selective Surfaces," *Int. J. Electr. Comput. Eng.*, vol. 2, pp. 846–850, Dec. 2012.
- [129] "afi17-220.pdf." Accessed: Mar. 22, 2021. [Online]. Available: [https://static.e-publishing.af.mil/production/1/af\\_a2\\_6/publication/afi17-220/afi17-220.pdf](https://static.e-publishing.af.mil/production/1/af_a2_6/publication/afi17-220/afi17-220.pdf)
- [130] C. T.-C. Nguyen, "Frequency-selective MEMS for miniaturized low-power communication devices," *IEEE Trans. Microw. Theory Tech.*, vol. 47, no. 8, pp. 1486–1503, Aug. 1999.
- [131] B. A. Belyaev, S. A. Khodenkov, and V. F. Shabanov, "Investigation of frequency-selective devices based on a microstrip 2D photonic crystal," *Dokl. Phys.*, vol. 61, no. 4, pp. 155–159, Apr. 2016.
- [132] M. A. Belen, P. Mahouti, and M. Palandöken, "Design and realization of novel frequency selective surface loaded dielectric resonator antenna via 3D printing technology," *Microw. Opt. Technol. Lett.*, vol. 62, no. 5, pp. 2004–2013, 2020.
- [133] Y.-K. Yoon, J.-W. Park, and M. G. Allen, "Polymer-core conductor approaches for RF MEMS," *J. Microelectromechanical Syst.*, vol. 14, no. 5, pp. 886–894, Oct. 2005.

- [134] S. N. Azemi, K. Ghorbani, and W. Rowe, "3D Frequency Selective Surfaces," *Prog. Electromagn. Res. C*, vol. 29, pp. 191–203, 2012.
- [135] J.-J. DeLisle, "Upgrade Frequency-Selective Surface Filters From 2D To 3D," *Microwaves & RF*, Jan. 10, 2014. Accessed: Feb. 07, 2021. [Online]. Available: <https://www.mwrf.com/technologies/passive-components/article/21845452/upgrade-frequencyselective-surface-filters-from-2d-to-3d>.
- [136] C. Kim, D. J. Arenas, D. B. Tanner, and Y. Yoon, "Micromachined Air-Lifted Pillar Arrays for Terahertz Devices," *IEEE Electron Device Lett.*, vol. 35, no. 4, pp. 470–472, Apr. 2014.
- [137] C. Long, L. Yan, C. Kim, D. J. Arenas, Y.-K. Yoon, and D. B. Tanner, "Characterization of Micromachined Air-lifted Terahertz Antenna Arrays," vol. 2013, p. C22.013, Mar. 2013.
- [138] A. Osseiran, J. F. Monserrat, and P. Marsch, *5G Mobile and Wireless Communications Technology*. Cambridge University Press, 2016.
- [139] K. Kaur, S. Kumar, and A. Baliyan, "5G: a new era of wireless communication," *Int. J. Inf. Technol.*, vol. 12, no. 2, pp. 619–624, Jun. 2020.
- [140] M. Imran, L. U. Khan, I. Yaqoob, E. Ahmed, M. A. Qureshi, and A. Ahmed, "Energy Harvesting in 5G Networks: Taxonomy, Requirements, Challenges, and Future Directions," *ArXiv191000785 Cs Eess*, Oct. 2019, Accessed: Nov. 14, 2021. [Online]. Available: <http://arxiv.org/abs/1910.00785>
- [141] D. Marabissi *et al.*, "Experimental Measurements of a Joint 5G-VLC Communication for Future Vehicular Networks," *J. Sens. Actuator Netw.*, vol. 9, no. 3, Art. no. 3, Sep. 2020,.

- [142] L. Bastos, G. Capela, A. Koprulu, and G. Elzinga, "Potential of 5G technologies for military application," in *2021 International Conference on Military Communication and Information Systems (ICMCIS)*, pp. 1–8, May 2021.
- [143] P. Grønsund *et al.*, "5G Service and Slice Implementation for a Military Use Case," in *2020 IEEE International Conference on Communications Workshops (ICC Workshops)*, pp. 1–6, Jun. 2020.
- [144] T. Samuels, "SAS-588 Standard Gain Horn Antenna," Accessed: Nov. 26,2021. [Online]. Available: <https://www.ahsystems.com/catalog/SAS-588.php>
- [145] M. W. Sabri, M. K. A. Rahim, and F. Zubir, "3D printed horn antenna using direct metal laser melting technique for millimetre wave applications," *Indones. J. Electr. Eng. Inform. IJEEI*, vol. 7, no. 2, pp. 323–330, May 2019.
- [146] H. Yao, S. Sharma, R. Henderson, S. Ashrafi, and D. MacFarlane, "Ka band 3D printed horn antennas," in *2017 Texas Symposium on Wireless and Microwave Circuits and Systems (WMCS)*, pp. 1–4, Mar. 2017.
- [147] U. Armendariz, S. Rommel, S. Rodriguez, I. T. Monroy, J. J. V. Olmos, and C. B. Olsen, "Evaluation and performance analysis of 3D printing technique for Ka-band antenna production," in *2016 46th European Microwave Conference (EuMC)*, pp. 1259–1262, Oct. 2016.
- [148] J. Zendejas, J. Gianvittorio, Y. Rahmat-Samii, and J. Judy, "Magnetic MEMS Reconfigurable Frequency-Selective Surfaces," *Microelectromechanical Syst. J. Of*, vol. 15, pp. 613–623, Jul. 2006.

- [149] J. Gianvittorio, J. Romeu, S. Blanch, and Y. Rahmat-Samii, “Self-Similar Prefractal Frequency Selective Surfaces for Multiband and Dual-Polarized Applications,” *Antennas Propag. IEEE Trans. On*, vol. 51, pp. 3088–3096, Dec. 2003.
- [150] P. Martin, D. Ray, and N. Prasad, “Characterization study of mutual coupling between monopole antennas on finite ground plane at out of band resonant frequencies,” *Prog. Electromagn. Res. C*, vol. 101, pp. 247–259, Jan. 2020.